PSERC

Enhanced State Estimators

Final Project Report

Power Systems Engineering Research Center

A National Science Foundation
Industry/University Cooperative Research Center
since 1996

Power Systems Engineering Research Center

Enhanced State Estimators

Final Project Report

Report Authors

Jun Zhu, Ph.D. Student
Ali Abur, Professor
Northeastern University

Mark J. Rice, Student
G.T. Heydt, Professor
Arizona State University

Sakis Meliopoulos, Professor
Georgia Institute of Technology

PSERC Publication 06-45

November 2006

Information about this project

For information about this project contact:

Ali Abur, Ph.D.
Northeastern University
Department of Electrical and Computer Engineering
Boston, MA 02115-5000
Tel: 617-373-3051
Fax: 617-373-4431
Email: abur@ece.neu.edu

Power Systems Engineering Research Center

This is a project report from the Power Systems Engineering Research Center (PSERC). PSERC is a multi-university Center conducting research on challenges facing a restructuring electric power industry and educating the next generation of power engineers. More information about PSERC can be found at the Center's website: http://www.pserc.org.

For additional information, contact:

Power Systems Engineering Research Center
Arizona State University
577 Engineering Research Center
Box 878606
Tempe, AZ 85287-8606
Phone: 480-965-1643
FAX: 480-965-0745

Notice Concerning Copyright Material

Acknowledgments

This is the final report for the PSERC project “Enhanced State Estimators (S-22).” We express our appreciation for the support provided by PSERC's industrial members and by the National Science Foundation received under the Industry / University Cooperative Research Center program.

The authors thank all PSERC members for their technical advice on the project, especially Dale Krummen (AEP); Jay Giri (AREVA); Patrick Panciatici, Yacine Hassaine and Benoit Delourme (RTE-France), Jianzhong Tong, Kenneth Huber and Tom Kennedy (PJM Interconnection); and Ram Adapa (EPRI). Project leader was Ali Abur (Northeastern University) and co-investigators were Sakis Meliopoulos (Georgia Institute of Technology) and Gerald Heydt (Arizona State University).

Executive Summary

Power system operators need real-time information obtained from measurements and computationally efficient tools to maintain a system that can reliably deliver energy to consumers, even under the dynamically changing power flow and facility availability conditions that exist into contemporary power grids. Direct measurement of all system state variables is not done today, and even when direct measurements are available, they inevitably have errors of varying magnitude. As a result, a state estimator is an essential tool for system monitoring because it processes a redundant set of measurements to obtain the best complete estimate of the current system state. State estimators, integrated into control center energy management systems, provide estimates of unmeasured quantities by processing data collected at substations to determine the steady-state voltage phasor (that is, voltage magnitude and angle) at each bus in the system. These estimated phasors are then used to calculate other quantities needed by the system operator, such as branch currents, bus power injections, and branch power flows.

Power system operators need to be confident in the results from state estimators before they will use the information for making critical decisions. Our research sought to understand challenges for achieving that confidence, and to propose and assess possible state estimator enhancements to address those challenges. The enhancements from this research address challenges of:

1. efficient detection and identification of network parameter errors (that is, errors in representing the electrical characteristics of the underlying transmission system);
2. efficient state estimation in multi-area, regional systems;
3. effective placement of phasor measurement units to improve confidence in state estimator results; and
4. modeling assumptions about the physical electric power system that introduce inaccuracies and computational problems in state estimation.

These challenges are becoming more relevant as grid and market operation responsibilities expand to cover much greater geographic areas than experienced in the industry's history. At the same time, grids are becoming more congested with rapidly changing power flow patterns responding to market conditions. The research project final report has four parts covering the proposed and tested state estimator enhancements.

Part I: Detection and Identification of Network Parameter Errors

All energy management system applications use a network model. Examples of network model parameters include (1) transmission line resistances, reactances, and charging capacitances; (2) transformer reactances and tap values; and (3) shunt capacitor and reactor values. Errors in parameter values occur because of the lack of perfect knowledge of the network's electrical characteristics at every point in time.

To attempt to compensate for network parameter errors, the state estimation problem can be extended by specifying a suspect set of parameters and estimating them at the same time as the other system variables. Thus, once the parameter in error is identified, its correct value is estimated using an augmented state estimation method. Unfortunately, it is difficult to

confidently identify the correct set of suspect parameters, particularly in very large systems with thousands of parameters. If any erroneous parameters are excluded from the set of suspect parameters, then the estimation results will be biased (that is, the expected value is no longer the true value), which is certainly not desired.

In this research, a method is developed that allows detection and identification of network parameter errors without having to put parameters into a suspect set. This method also has the advantage of making it possible to identify errors in actual system measurements and in parameters even when both errors exist simultaneously. The method uses the state estimation solution based on the minimization of weighted least squares method, enhanced with error identification and correction procedures. Simulations illustrate the effectiveness of the method, along with the inherent limitations of error identification for certain special cases. The method can be readily implemented as a user-defined option by modifying existing state estimation code.

Part II: Efficient Regional, Multi-Area State Estimation

Solution of the state estimation problem for large multi-area systems presents several unique challenges. Individual areas may have their own state estimators that use different solution algorithms, and input data structures and formats. One way to determine a regional solution is to implement a central state estimator that collects measurements from all areas and solves a very large scale state estimation problem. An obvious computational drawback of this approach is the increase in the problem size as new areas are added to the existing system. In addition, bad measurements or topology errors in a given area will cause divergence of the regional system state estimator, even though states associated with the rest of the areas remain observable with the given measurements.

This research offers an alternative solution, where individual state estimators are used in individual control areas and these solutions are then combined with measurements at area boundaries to reach an integrated solution for the entire region. Simulations demonstrate the viability of decentralized state estimation using the developed state estimation software. Different measurement configurations for the IEEE 14 and 118 bus test systems were used in these simulations.

In the future, data from phasor measurement units could be incorporated into the multi-area state estimation approach for bad data processing and to facilitate coordination of individual area solutions. In the meantime, the proposed method does not require the use of phasor measurement unit data.

Part III: Locating Phasor Measurement Units to Increase Confidence in State Estimates

State estimation uses measured values (such as from sensors) of voltage magnitude, and active and reactive power, along with the network electrical characteristics, to determine the values of state variables that are not observed. However, measurement errors can occur that will reduce confidence in the state estimator’s results. When sensors are properly calibrated, the measurement error is not as serious a problem. On the other hand, the increasingly deployed sensorless technologies use analog to digital (A/D) converter technology to sample voltage and

current waveforms. Once the sampled waveforms are available, the required measurements can be retrieved with numerical computation. Data measurement technologies introduce measurement variability and bias. The major error sources are (a) the instrument transformers, (b) the cables connecting the instrument transformers to the sensors or A/D converters, and (c) the sensors or A/D converters.

The advent of phasor measurement unit (PMU) technology provides an opportunity to further improve confidence in state estimation results. A PMU is an instrument that provides time-synchronized phasor measurements, a feature also known as synchrophasors. A PMU provides time-stamped measurements of active power, reactive power, frequency, current, voltage magnitude, and phase angle. The time-stamped characteristic of a PMU is one of its most innovative features. The PMU 'sensor' is a Global Positioning System (GPS) technology that uses conventional active and reactive power transducers as well as conventional current and voltage transformers. The PMU technology samples the waveform from 2,000 to 10,000 times per second, and then computes phasors generally around 10 to 60 times per second.

By strategically locating PMUs, the effects of measurement errors can be reduced. The question is how to most effectively locate new PMUs to enhance the state estimator. It is possible to specify quantitative "condition indicators" that can be used to develop an algorithm for state estimator design. In this research, the condition indicators are used to assess PMU placement alternatives. With two test beds (the IEEE 57 bus test bed and a representation of a southwest power system with 180 buses and 254 lines), it is shown that PMU placement can significantly improve the condition numbers, thereby producing more confidence in the state estimation results. Examples show that use of condition analysis for PMU placement appears to be consistent with robustness analysis and other techniques for sensor placement.

The next steps in this research include examining the effects of PMU placement on condition indicators for a nonlinear state estimator, designing a full implementation procedure of the algorithm for state estimator design, and testing the procedure on a large test bed.

Part IV: Using Better System Models to Enhance State Estimation

Over the past thirty-five years, the basic structure of power system state estimation process has been based on (a) a single-phase model, (b) an active power, reactive power, and voltage magnitude measurement set, (c) non-simultaneous measurements, and (d) a single frequency model. This basic structure implies the following assumptions: (1) all current and voltage waveforms are pure sinusoids with constant frequency and magnitude; (2) the system operates under balanced, three-phase conditions; and (3) the power system is a symmetric three-phase system that is fully described by its positive sequence network. These assumptions introduce deviations between the physical system and the mathematical model, resulting in poor confidence in and bias of the state estimator. In practice, these assumptions can cause the state estimation algorithm not to reach a solution. The trend toward very large regional power systems raises important research questions about the effects of these assumptions on state estimation results.

The research explored the effects of the three assumptions and the use of sensorless technologies on state estimation results. Numerical examples showed that segregated phase measurements of voltage and power flow (instead of balanced three-phase flow) and a three-phase model with the traditional state estimation approach results in substantial improvement in state estimate quality. Numerical experiments also showed that adding GPS-synchronized measurements improves state estimator performance. The experiments indicate that system model inaccuracies tend to increase estimation errors as the system size grows. As a result, it is expected that there would be more confidence in state estimation based on three-phase measurement sets, synchronized measurements, and full three-phase models, even for highly stressed regional systems.

The effects of system assumptions on state estimation accuracy suggests that design of new state estimation systems should be tested on models that can be either based on traditional assumptions described above or a relaxed set of assumptions. This research led to the design and specification of a prototype test bed with a high fidelity power system simulation tool that could be used to better understand state estimation challenges and test possible solutions. The test bed will help to identify and quantify various error sources. The simulation tool uses a detailed system representation that, for example, models all phase conductors, shield wires, and grounding of transmission lines. The simulation model solution gives an accurate operating system condition, including imbalances and asymmetries. With the tool, a range of measurement set characteristics can be generated by appropriately injecting measurement errors, including single-phase measurements, three-phase measurements, three-phase individual measurements, traditional set of measurements, and phasor measurements. The hybrid state estimation algorithm can switch between a three-phase model or a positive sequence model. The next step in this research is to move from the prototype to a full-scale test-bed implementation.

Part I

Network Parameter Error Identification

Authors

Jun Zhu, Ph.D. Student
Ali Abur, Professor
Northeastern University

Table of Contents

List of Figures

List of Tables

1. Introduction

All the energy management system (EMS) applications make use of the network model in the mathematical formulation of their problem. Transmission line resistances, reactances and charging capacitances, transformer reactances and tap values, and shunt capacitor/reactor values are examples of network parameters that are required to build the network model. Among the EMS applications, state estimation plays an important role since it provides the network model for all other applications.

Traditionally, state estimation is carried out assuming that the correct network model is known. Therefore, any inconsistencies detected during the estimation process will be blamed on the analog measurement errors. However, the error in the parameter value, which is assumed not existing normally, will cause nearly permanent errors in the state estimation results.

Recently, a new topology error identification method [1] based on a reduced system model and the use of Lagrange multipliers is proposed. It addresses the main shortcoming of the previously proposed methods by eliminating the need to identify a suspect substation before topology error identification.

In this report, a new parameter error identification method that complements the topology error identification method mentioned above is proposed. This method is based on the Lagrange multipliers of the parameter constraints. A set of additional variables that correspond to the errors in the network parameters is introduced into the state estimation problem. However, direct estimation of these variables is avoided by the proposed formulation. Following the traditional state estimation solution, measurement residuals are used to calculate the Lagrange multipliers associated with the parameter errors. If these are found to be significant, then the associated parameter will be suspected of being in error. The main advantage of this method is that the normalized measurement residuals and parameter error Lagrange multipliers can be computed, allowing their identification even when they appear simultaneously. The first part of the proposed procedure is based only on the conventional weighted least-squares (WLS) state estimation solution; however, the subsequent error identification and correction procedures will have to be implemented and integrated into the existing code. There is no need to specify a suspect set of parameters a priori, since the method will readily identify the erroneous parameters along with any existing bad measurements.

The objective of this report is to testify the validity of the parameter identification and correction method stated above in real power system. The report is organized such that Section II presents the proposed formulation and solution of the parameter error identification problem. Section III gives the flow chart of the method. Implementation details and the results of simulations are given in Section IV. The input and output data structure is introduced in section V. Section VI concludes the report, followed by the Appendix.

2. Lagrange Multipliers Method

In this section, a brief presentation of the Lagrange multipliers method will be given. It is composed of three parts: (1) formulation of state estimation, (2) computation of the normalized Lagrange multipliers to identify bad parameter, and (3) correction of the bad parameter.

2.1 Problem Formulation

Consider the following measurement model:

$$z = h(x, p_e) + e \tag{2.1}$$

where:

z	measurement vector;
$h(x, p_e)$	nonlinear function relating the measurements to the system states and network parameter errors;
x	system state vector, including voltage magnitudes and phase angles;
p_e	vector containing network parameter errors;
e	vector of measurement errors.

Buses with no generation or load, will provide free and exact measurements as zero power injections. These can be treated as equality constraints given by:

$$c(x, p_e) = 0 \tag{2.2}$$

Network parameter vector will be modeled as:

$$p = p_t + p_e \tag{2.3}$$

where p and p_t are the assumed and true network parameter vectors. Network parameter errors are normally assumed to be zero by the state estimator. Therefore, for error free operation, the following equality constraint on network parameter errors will be used:

$$p_e = 0 \tag{2.4}$$

The weighted least squares (WLS) state estimation problem in the presence of network parameter errors and equality constraints can then be formulated as the following optimization problem:

$$\begin{aligned} \text{Minimize} \quad & J(x) = \tfrac{1}{2} r^t W r \\ \text{Subject to} \quad & c(x, p_e) = 0 \\ & p_e = 0 \end{aligned} \tag{2.5}$$

where:

$r = z - h(x, p_e)$ is the measurement residual vector,
W is the diagonal matrix whose inverse is the measurement error covariance matrix, cov(e).

Applying the method of Lagrange multipliers, the following Lagrangian can be defined for the optimization problem of (2.5):

$$L = \frac{1}{2} r^t W r - \mu^t c(x, p_e) - \lambda^t p_e \tag{2.6}$$

Applying the first order optimality conditions:

$$\frac{\partial L}{\partial x} = H_x^t W r + C_x^t \mu = 0 \tag{2.7}$$

$$\frac{\partial L}{\partial p} = H_p^t W r + C_p^t \mu + \lambda = 0 \tag{2.8}$$

$$\frac{\partial L}{\partial \mu} = c(x, p_e) = 0 \tag{2.9}$$

$$\frac{\partial L}{\partial \lambda} = p_e = 0 \tag{2.10}$$

where:

$$H_x = \frac{\partial h(x, p_e)}{\partial x} \tag{2.11}$$

$$C_x = \frac{\partial c(x, p_e)}{\partial x} \tag{2.12}$$

$$H_p = \frac{\partial h(x, p_e)}{\partial p_e} \tag{2.13}$$

$$C_p = \frac{\partial c(x, p_e)}{\partial p_e} \tag{2.14}$$

μ and λ are the Lagrange multipliers for the equality constraints (2.2) and (2.4).

Equation (2.8) can be used to express λ in terms of μ and r:

$$\lambda = S \cdot \begin{bmatrix} r \\ \mu \end{bmatrix} \tag{2.15}$$

where:

$$S = -\begin{bmatrix} WH_p \\ C_p \end{bmatrix}^t \tag{2.16}$$

is the parameter sensitivity matrix.

Equality constraint (2.4) allows substitution of p_e in (2.7)-(2.9). Denoting $h(x,0)$ and $c(x,0)$ by $h_0(x)$, $c_0(x)$ respectively, the measurement equations will take the following form:

$$z = h_0(x) + e \tag{2.17}$$

$$c_0(x) = 0 \tag{2.18}$$

Note that (2.17) and (2.18) are the conventional measurements and zero injection equations used by the state estimators. They do not include parameter errors as explicit variables. Substituting the first order Taylor approximations for $h_0(x)$ and $c_0(x)$, the following linear equations will be obtained:

$$H_x \cdot \Delta x + r = \Delta z \tag{2.19}$$

$$C_x \cdot \Delta x = -c_0(x_0) \tag{2.20}$$

where:

$\Delta x = x - x_0$, x_0 being the initial guess for the system state vector $\Delta z = z - h_0(x_0)$

Using (2.7), (2.19), and (2.20), the following equation will be obtained:

$$\begin{bmatrix} 0 & H_x^t W & C_x^t \\ H_x & I & 0 \\ C_x & 0 & 0 \end{bmatrix} \bullet \begin{bmatrix} \Delta x \\ r \\ \mu \end{bmatrix} = \begin{bmatrix} 0 \\ \Delta z \\ -c_0(x_0) \end{bmatrix} \tag{2.21}$$

This equation is the same equation used for iterative solution of the conventional WLS state estimation problem. Hence, the solution for the measurement residuals r and the Lagrange multipliers for the zero injections μ can be obtained first by iteratively solving (2.21). Once the state estimation algorithm successfully converges, (2.15) can be used to recover the Lagrange multiplier vector λ associated with the parameter errors.

2.2 Computation of Normalized Lagrange Multipliers

Since the main aim of this work is to identify parameter errors, the validity of the constraint (2.10) will have to be tested. This can be done based on the Lagrange multiplier vector λ associated with the parameter error vector p_e. In order to test the significance of a given λ_i value, it will be normalized using its covariance matrix $\mathrm{cov}(\lambda)$, which can be obtained as shown below.

Letting $u = [r \quad \mu]^T$ and using (2.15):

$$\Lambda = \mathrm{cov}(\lambda) = S \cdot \mathrm{cov}(u) \cdot S^t \tag{2.22}$$

The covariance of u, $\mathrm{cov}(u)$ can be calculated by first expressing r and μ in terms of the measurement mismatch. To do that, let the inverse of the coefficient matrix in (2.21) be given in partitioned form as follows:

$$\begin{bmatrix} 0 & H_x^t W & C_x^t \\ H_x & I & 0 \\ C_x & 0 & 0 \end{bmatrix}^{-1} = \begin{bmatrix} E_1 & E_2 & E_3 \\ E_4 & E_5 & E_6 \\ E_7 & E_8 & E_9 \end{bmatrix} \tag{2.23}$$

Noting that $c_0(x) = 0$ at the solution, (2.21) will yield the following expressions for r and μ:

$$r = E_5 \cdot \Delta z \tag{2.24}$$

$$\mu = E_8 \cdot \Delta z \tag{2.25}$$

Let $\Psi = [E_5 \quad E_8]^T$, then:

$$u = \Psi \cdot \Delta z \tag{2.26}$$

$$\mathrm{cov}(u) = \Psi \cdot W^{-1} \cdot \Psi^t \tag{2.27}$$

The Lagrange multipliers for the parameter errors can then be normalized using the diagonal elements of the covariance matrix Λ defined in (2.22):

$$\lambda_i^N = \frac{\lambda_i}{\sqrt{\Lambda(i,i)}} \tag{2.28}$$

for all i = 1…k, where k is the total number of network parameters whose errors are to be identified.

Note that the denominator in (2.28) will be zero for cases where local measurement redundancy does not allow detection of errors in parameter. One such case is when all measurements that are

functions of a parameter are critical. The other obvious one is when there are no measurements that are functions of a parameter.

2.3 Correction of the Parameter in Error

After the parameter in error is identified, this specific parameter can be corrected by estimating its true value simultaneously with the other state variables [2]. In order to accomplish this, the state vector is augmented by the suspicious parameter p, yielding the following new state vector, v:

$$v = [x_1, x_2, ..., x_n \mid p] \tag{2.29}$$

where v is the set of state variables.

$x_1, \ldots, x_n$	conventional state variables
p	parameter precisely identified as erroneous.

The solution of the state estimation problem will yield not only the state estimates but also the estimated value of the suspect parameter.

3. Parameter Identification Algorithm

3.1 Overall Process

The above formulation can be used to develop an algorithm to detect and identify network parameter errors. Such an algorithm is presented below:

Step 1. Initial State Estimation.

This is the WLS state estimation problem as currently solved by existing software. In addition to the measurement residual vector r, the solution will provide the Lagrange multiplier vector μ of zero injections if they are treated as equality constraints in the state estimation formulation. The solution involves repeated solution of (2.21) until convergence. Note that all parameter errors are assumed to be zero and therefore ignored at this step.

Step 2. Bad Data and Parameter Error Identification.

Compute the normalized residuals for the measurements, and the normalized Lagrange multipliers for the parameter errors, as in (2.28). Section 2.2 illustrates the steps leading to (2.28). Choose the larger one between the largest normalized residual and the largest normalized Lagrange multiplier.

- If the chosen value is below the identification threshold, then no bad data or parameter error will be suspected. A statistically reasonable threshold to use is 3.0, which is the one used in all simulations presented in the next section.
- Else, the measurement or the parameter corresponding to the chosen largest value will be identified as the source of the error.

Step 3. Correction of the Parameter Error

If a measurement is identified as bad, it is removed from the measurement set. Equivalently, its value can be corrected using a linear approximation for the estimated measurement error.

If a parameter is identified as erroneous, it is corrected by estimating its value by the method described in Section 2.3 using the augmented state vector defined as (2.29). Substitute the estimated parameter value for the old one and go to Step 1.

Note that bad data and parameter errors are processed simultaneously. This is possible provided that there is sufficient measurement redundancy and the parameter errors are not strongly correlated with the bad data. Since parameter errors are persistent whereas bad data usually appear in a single scan, the likelihood of simultaneously having strongly interacting bad data and parameter errors is small. Furthermore, using this approach, there is no need to specify which parameter is to be tested for errors, a priori state estimation. Those three steps are separated from each other. Step 2 uses the results of the normal state estimation done in Step 1, and the set of suspicious parameters can be easily changed in Step 2 and without requiring re-estimation of the system states.

3.2 Flow Chart

The flow chart of the algorithm is shown below.

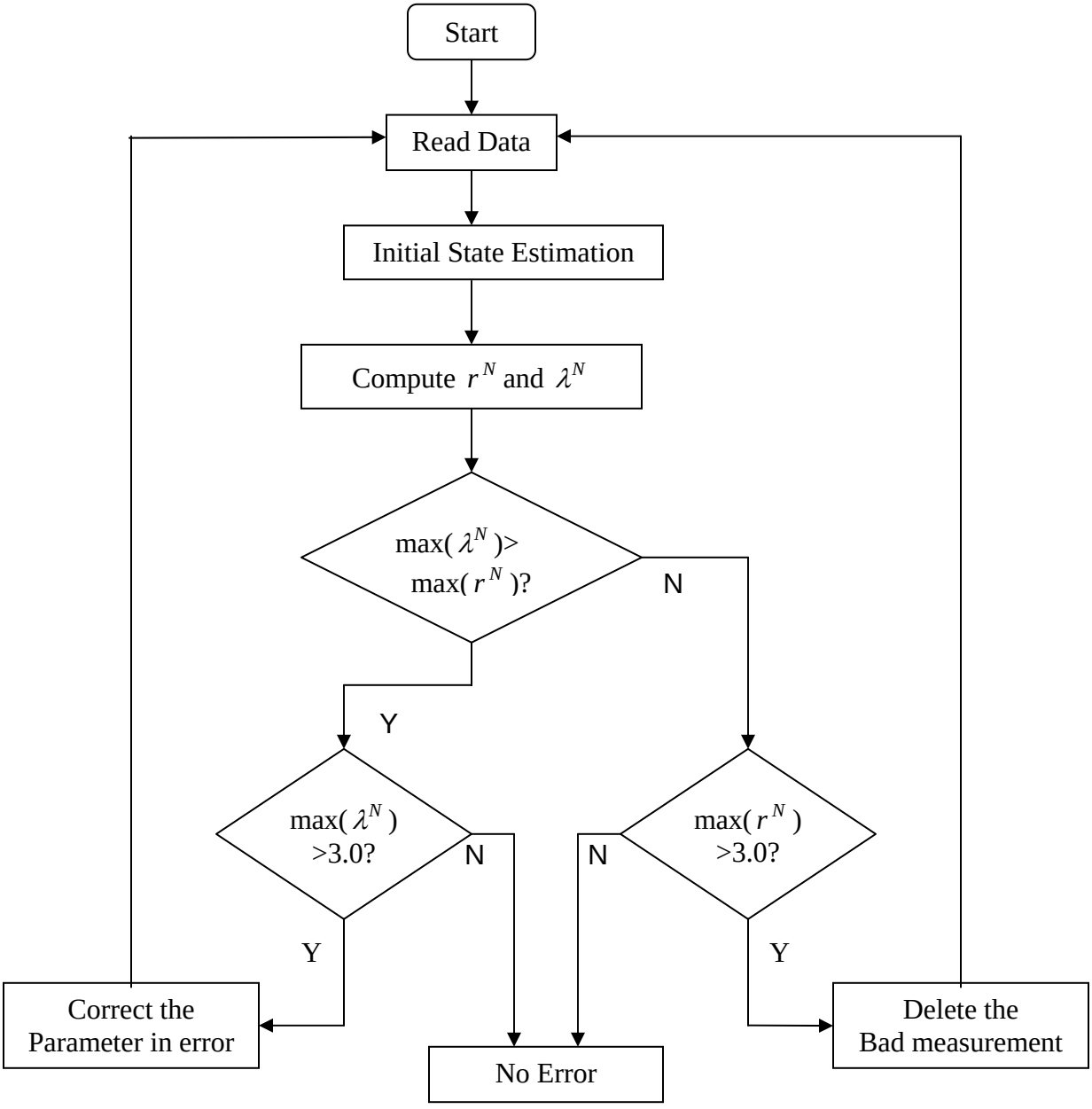

4. Simulation Results

The above-described parameter error identification procedure is implemented and tested on IEEE 14-, 30- and 57-bus test systems. Different cases are simulated where errors are introduced in transmission line parameters, transformer taps, shunt capacitors, and analog measurements. Both single errors and simultaneously occurring errors in analog measurements and parameters are simulated. The performance of the method as well as its limitations is illustrated through these examples.

4.1 Line Impedance or Measurement Error

This case presents single errors in transmission line impedances or analog measurements. The method is shown to differentiate between these different types of errors and to correctly identify the error. The simulated errors for the three test systems are listed in Table I, where tests A and B are carried out as follows.

Test A) An error is introduced in the line parameter listed in Table 4.1; all analog measurements are error free.
Test B) No parameter errors are introduced; all measurements are error free, except for the listed flow in Table 4.1.

Table 4.1 Simulated Parameter and Measurement Errors

Test System	Bad Parameter/Meas.	
	Test A	Test B
14-bus	r_{4-5}	q_{4-5}
30-bus	x_{5-7}	p_{5-7}
57-bus	r_{4-6}	q_{6-4}

Tables 4.2-4.4 show the sorted normalized residuals and normalized Lagrange multipliers, obtained during the tests of Table 4.1. The correction of the parameter error is shown in Table 4.5. As evident from the above, single line impedance errors as well as single analog measurement errors can be identified and corrected by this approach.

Table 4.2 Results of Error Identification – 14-bus System

Test A		Test B	
Measurement/ Parameter	Normalized residual / λ^N	Measurement/ Parameter	Normalized residual / λ^N
r_{4-5}	7.88	q_{4-5}	12.02
r_{2-4}	5.98	q_5	8.61
r_{2-5}	4.84	q_4	6.57
q_{4-5}	4.81	x_{4-5}	5.35
t_{5-6}	4.59	x_{2-4}	4.18

Table 4.3 Results of Error Identification – 30-bus System

Test A		Test B	
Measurement/ Parameter	Normalized residual / λ^N	Measurement/ Parameter	Normalized residual / λ^N
x_{5-7}	25.47	p_{5-7}	19.50
x_{7-6}	22.01	r_{5-7}	12.34
x_{2-5}	21.92	p_5	10.56
r_{7-6}	15.78	q_6	9.97
r_{2-5}	15.42	x_{7-6}	9.86

Table 4.4 Results of Error Identification – 57-bus System

Test A		Test B	
Measurement/ Parameter	Normalized residual / λ^N	Measurement/ Parameter	Normalized residual / λ^N
r_{4-6}	14.82	q_{4-6}	8.78
q_{4-6}	9.65	r_{4-6}	5.96
r_{3-4}	7.37	x_{5-6}	4.22
r_{4-5}	7.09	s_4	4.01
p_{4-6}	6.79	q_4	4.01

Table 4.5 Estimated and True Parameters of Line Impedances

Test system	Bad Parameter	Corrected Parameter	Parameter without error
14-bus	r_{4-5}	0.01355	0.01355
30-bus	x_{5-7}	0.11593	0.11600
57-bus	r_{4-6}	0.04295	0.04300

4.2 Transformer Tap or Measurement Error

This case presents single errors in transformer taps or analog measurements. Errors are simulated for the 57-bus test system, where tests A and B are carried out as follows:

Test A) A 1% error is introduced in the transformer tap value; all analog measurements are error free.
Test B) No parameter errors are introduced; all measurements are error free, except for the flow .

Table 4.6 shows the sorted normalized residuals and Lagrange multipliers that are obtained during Tests A and B. Again, for Test A, the estimated value of the wrong parameter is shown in Table 4.7.

Table 4.6 Tap and Measurement Error Identification

Test A		Test B	
Measurement/ Parameter	Normalized residual / λ^N	Measurement/ Parameter	Normalized residual / λ^N
t_{13-49}	63.19	p_{13-49}	18.52
q_{13-49}	53.48	x_{13-49}	6.71
x_{13-49}	48.69	r_{48-49}	6.37
x_{48-49}	25.60	p_{49}	6.17
r_{46-47}	20.03	x_{14-46}	5.58

Table 4.7 Estimated and True Parameters of Taps

Test system	Bad Parameter	Corrected Parameter	Parameter without error
57-bus	t_{13-49}	0.89502	0.89500

As in case 1, the method successfully identifies and corrects transformer tap errors while maintaining its ability to identify any errors appearing in analog measurements.

4.3 Errors in Shunt Capacitor/Reactor

Errors in the parameters of shunt devices such as capacitors or reactors can be detected but not identified. The reason is the lack of redundancy, i.e., there is only one measurement, namely, the reactive power injection at the corresponding bus, whose expression contains this parameter. Hence, when there is an error in this injection measurement or an error in the shunt device parameter, this error will be detected, but its source cannot be identified. The injection measurement and the parameter constraint constitute a critical pair. This case illustrates two examples of this limitation for 14- and 30-bus test systems.

Errors are introduced in the shunt susceptances at bus 9(s_9) and at bus 24(s_{24}) of 14- and 30-bus systems, respectively. The normalized residuals and Lagrange multipliers are given in sorted form in Table 4.8. Note that the reactive injection measurements and shunt susceptances have identical normalized values, indicating that they constitute a critical pair whose errors cannot be identified.
The estimated and true parameter values are shown in Table 4.9.

Table 4.8 Shunt Susceptance Errors

14-bus system		30-bus system	
Measurement/ Parameter	Normalized residual / λ^N	Measurement/ Parameter	Normalized residual / λ^N
s_9	5.80	s_{24}	12.72
q_9	5.80	q_{24}	12.72
q_{9-10}	3.05	q_{22-24}	5.78
t_{4-9}	2.51	q_{22}	5.23
q_{14}	2.05	q_{23-24}	4.65

Table 4.9 Estimated and True Parameters of Shunt Susceptances

Test system	Bad Parameter	Corrected Parameter	Parameter without error
14-bus	s_9	0.1900	0.1900
30-bus	s_{24}	0.0432	0.0430

4.4 Simultaneous Errors

This case shows the identification of multiple errors occurring simultaneously in the 14-bus system. Errors are simulated in the reactance of the transmission line 2–4, tap of the transformer 4–9, and the power flow measurement in line 4-2. The largest normalized value test is used to identify these errors one at a time. Results of normalized value tests for each error identification cycle are presented in Table 4.10.

Table 4.10 Multiple Error Identification Results

Error identification cycle					
1st		2nd		3rd	
z/ p	r^N / λ^N	z/ p	r^N / λ^N	z/ p	r^N / λ^N
x_{2-4}	60.56	t_{4-9}	23.87	p_{4-2}	5.07
p_{4-2}	46.48	p_{9-4}	17.99	p_3	3.75
x_{4-5}	40.49	t_{4-7}	10.00	p_4	3.02
x_{2-5}	30.24	r_{7-9}	9.78	r_{2-4}	2.86
t_{4-9}	25.00	p_4	9.68	p_{4-5}	2.25
Identified and Eliminated error					
x_{2-4}		t_{4-9}		p_{4-2}	

When corrected, the parameter values are found, as shown in Table 4.11. Notice that when there are multiple errors in the network parameters as well as analog measurements; repeated application of the largest normalized value test can identify errors one by one, as shown in Table 4.10. However, due to the interaction between multiple parameter errors, sequential correction of parameter errors may yield approximate values, as in Table 4.11. This approximation error can be minimized by executing an extra estimation solution, where all identified parameters are included simultaneously in the augmented state vector. The results for this case are shown in Table 4.12. Note that the results in Table 4.12 are more accurate than those given in Table 4.11.

Table 4.11 Estimated and True Parameters of Multiple Errors

Step	Bad Parameter	Corrected Parameter	Parameter without error
1st	x_{2-4}	0.17400	0.17632
2nd	t_{4-9}	0.96015	0.96000

Table 4.12 Simultaneous Estimation of All Identified Parameters

Bad Parameter	Estimated Parameter	True Parameter
x_{2-4}	0.17633	0.17632
t_{4-9}	0.96000	0.96000

Similar to the case of the multiple interacting and conforming bad data, there may be situations where strongly interacting parameter and analog measurement errors cannot be identified due to error masking. Such cases are, however, rare and cannot be handled by this method.

4.5 Inherent Limitation: Multiple Solutions

Identification of errors in network parameters is inherently limited by the available set of measurements as well as the system topology. The limitation is due to the possibility of multiple solutions corresponding to two or more parameter errors that affect the same subset of measurements.

Consider two network parameters p_1, p_2 and their erroneous values p_1^a, p_2^b. If two different solutions x^a, x^b yielding the same objective function value can be found such that

$$J\left(x^a, p_1^a, p_2\right) = J\left(x^b, p_1, p_2^b\right) \tag{4.1}$$

then the WLS state estimator will equally likely converge to either one of these solutions. Hence, it will not be possible to identify which of these two parameters is actually in error.

One such situation is illustrated by the following two tests that are carried out on the IEEE 14-bus system whose diagram and measurements are shown in Fig. 4.1.

Test A) The reactance x_{6-12} for line 6–12 is incorrect; all measurements are exact.

Test B) The reactance x_{12-13} for line 12–13 is incorrect; all measurements are exact.

The incorrect parameters for the two neighboring lines are chosen as shown in Table 4.13. These two parameter errors will be detectable but not identifiable. Either one of the parameters can be

identified as incorrect, depending upon the initial conditions used in the iterative solution of the state estimation problem.

Table 4.13 Objective Function Values for Tests A and B

	Erroneous Parameter	Assumed Value	True Value	$J(x)$
Test A	x_{6-12}	0.23656	0.25581	14.7064
Test B	x_{12-13}	0.29988	0.19988	14.7068

In Test A, the proposed method correctly identified x_{6-12} as the erroneous parameter, while in Test B, the same algorithm still identified the same parameter instead of the incorrect parameter x_{12-13} as bad data. The reason can be easily seen by looking at the almost identical objective function values corresponding to the two tests in Table 4.13. As shown in Table 4.14, in Test B, x_{6-12} is identified instead of the real parameter in error, x_{12-13}. The estimated states for the two test cases are shown in Table 4.15. Note that the two estimates differ very little, only at the buses incident to the branches with parameter errors, namely, buses 6, 12, and 13.

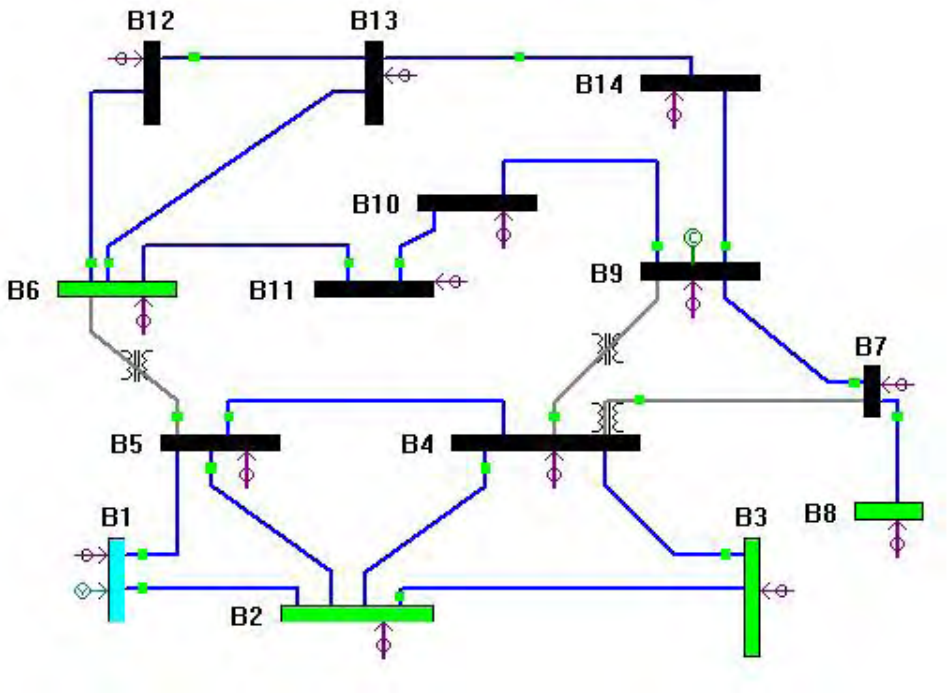

Figure 4.1 IEEE 14-Bus System

Table 4.14 Error Identification of Series Lines

Test A		Test B	
Measurement/ Parameter	Normalized residual / λ	Measurement/ Parameter	Normalized residual / λ
x_{6-12}	3.8291	x_{6-12}	3.8280
x_{12-13}	3.8250	x_{12-13}	3.8148
x_{6-13}	2.8902	x_{6-13}	2.7479
p_{6-12}	2.4126	p_{12-13}	2.5182
p_{12-13}	2.3390	p_{6-12}	2.4759

Table 4.15 Estimated States for Tests A and B

Bus No:	Test A		Test B	
	V	θ	V	θ
1	1.0600	0	1.0600	0
2	1.0450	-5.2379	1.0450	-5.2382
3	1.0100	-13.1662	1.0100	-13.1669
4	1.0159	-10.8853	1.0159	-10.8858
5	1.0180	-9.2395	1.0180	-9.2403
6	1.0700	-14.8812	1.0700	-14.8857
7	1.0679	-14.6357	1.0678	-14.6355
8	1.0900	-16.4757	1.0900	-16.4758
9	1.0606	-16.0028	1.0605	-16.0023
10	1.0547	-16.0920	1.0547	-16.0922
11	1.0588	-15.6241	1.0587	-15.6260
12	1.0558	-15.7289	1.0559	-15.7184
13	1.0510	-15.8867	1.0510	-15.8656
14	1.0384	-16.9473	1.0384	-16.9403

5. Program Data Structure

The input data files for the parameter identification program include the system network information and the power measurements. The output data files give the normalized Lagrange multipliers of parameters and the normalized residuals of measurements.

5.1 Input Data Files of Parameter Identification Program

The input data of the parameter identification are composed of three files: (1) the detailed circuit breaker topology data, (2) power flow measurement data, and (3) voltage data.

5.1.1 seinput.dat

```
9    0.1900
-99
1   1   2   0  1.00000  0.01938  0.05917  0.00000  0.05280
2   1   5   0  1.00000  0.05403  0.22304  0.00000  0.04920
3   2   5   0  1.00000  0.05695  0.17388  0.00000  0.03400
4   2   4   0  1.00000  0.05811  0.17632  0.00000  0.03740
5   2   3   0  1.00000  0.04699  0.19797  0.00000  0.04380
6   3   4   0  1.00000  0.06701  0.17103  0.00000  0.03460
7   4   5   0  1.00000  0.01335  0.04211  0.00000  0.01280
8   7   8   0  1.00000  0.10000  0.17615  0.00000  0.00000
9   7   9   0  1.00000  0.00000  0.11001  0.00000  0.00000
10   9  10   0  1.00000  0.03181  0.08450  0.00000  0.00000
11   9  14   0  1.00000  0.12711  0.27038  0.00000  0.00000
12  10  11   0  1.00000  0.08205  0.19207  0.00000  0.00000
13   6  11   0  1.00000  0.09498  0.19890  0.00000  0.00000
14   6  12   0  1.00000  0.12291  0.25581  0.00000  0.00000
15   6  13   0  1.00000  0.06615  0.13027  0.00000  0.00000
16  12  13   0  1.00000  0.22092  0.19988  0.00000  0.00000
17  13  14   0  1.00000  0.17093  0.34802  0.00000  0.00000
18   5   6   1  0.93000  0.00000  0.25202  0.00000  0.00000
19   4   7   1  0.97000  0.00000  0.20912  0.00000  0.00000
20   4   9   1  0.96000  0.00000  0.55618  0.00000  0.00000
-99
```

The file shown above is the state estimation input file for the 14 bus system. This input file includes the system network parameter data. –99 is used to flag of the end of data. It is composed of two parts, the bus parameter data and the line parameter data of the system.

1. bus parameter data
1st column: bus number.
2nd column: shunt conductance of that bus.

2. line parameter data
1st column: the branch number.
2nd to 3rd columns: the start and end bus number the line connected.
4th column: the line type. For a transformer, the value is 1 and for a normal transmission line, the value is 0.

5th column: tap value. For a transformer, it gives the tap value of that transformer. For normal transmission line it is 1.
6th to 9th columns: the resistance, reactance, conductance and susceptance of the non-zero impedance branch. For circuit breakers, the values will be all zeros.

5.1.2 measureinput.dat

```
1   16   12   13     0.01706    0.000001
1   13   11    6    -0.08318    0.000001
1    7    4    5    -0.65249    0.000001
1    3    5    2    -0.42806    0.000001
1    5    2    3     0.74916    0.000001
1    9    7    9     0.24558    0.000001
1   15    6   13     0.18251    0.000001
1    4    4    2    -0.57571    0.000001
1    1    1    2     1.64619    0.000001
1    6    3    4    -0.21709    0.000001
1    8    7    8     0.10427    0.000001
1   10    9   10     0.04214    0.000001
1   11    9   14     0.08841    0.000001
1   12   10   11    -0.04799    0.000001
1    2    1    5     0.79389    0.000001
1    1    2    1    -1.59881    0.000001
1    3    2    5     0.43813    0.000001
1   14    6   12     0.07878    0.000001
1   13    6   11     0.08380    0.000001
1   17   13   14     0.06232    0.000001
1   18    5    6     0.45700    0.000001
1   19    4    7     0.34976    0.000001
1   20    9    4    -0.17996    0.000001
1   19    7    4    -0.34976    0.000001
1    9    9    7    -0.24558    0.000001
1   18    6    5    -0.45700    0.000001
-99
3   14    -0.14900    0.000001
3   10    -0.09000    0.000001
3    7     0.00000    0.000001
3    8    -0.10000    0.000001
3    3    -0.94200    0.000001
3    2     0.18300    0.000001
3    1     2.44007    0.000001
3   11    -0.03500    0.000001
3   12    -0.06100    0.000001
3    6    -0.11200    0.000001
3   13    -0.13500    0.000001
3    9    -0.29500    0.000001
3    4    -0.47800    0.000001
3    5    -0.07600    0.000001
-99
2   16   12   13     0.00545    0.000001
2   13   11    6    -0.01979    0.000001
2    7    4    5     0.15986    0.000001
2    3    5    2    -0.02089    0.000001
2    5    2    3     0.03398    0.000001
2    9    7    9     0.07384    0.000001
2   15    6   13     0.06480    0.000001
```

```
2    4    4    2     0.03172    0.000001
2    1    1    2    -0.22194    0.000001
2    6    3    4     0.03761    0.000001
2    8    7    8    -0.19024    0.000001
2   10    9   10     0.05699    0.000001
2   11    9   14     0.04570    0.000001
2   12   10   11    -0.00139    0.000001
2    2    1    5     0.04270    0.000001
2    1    2    1     0.30810    0.000001
2    3    2    5     0.01546    0.000001
2   14    6   12     0.02296    0.000001
2   13    6   11     0.02108    0.000001
2   17   13   14     0.00792    0.000001
2   18    5    6     0.12921    0.000001
2   19    4    7    -0.09147    0.000001
2   20    9    4     0.01250    0.000001
2   19    7    4     0.11639    0.000001
2    9    9    7    -0.06750    0.000001
2   18    6    5    -0.08177    0.000001
-99
4   14    -0.05000    0.000001
4   10    -0.05800    0.000001
4    7     0.00000    0.000001
4    8     0.19746    0.000001
4    3     0.05980    0.000001
4    2     0.34330    0.000001
4    1    -0.17920    0.000001
4   11    -0.01800    0.000001
4   12    -0.01600    0.000001
4    6     0.02693    0.000001
4   13    -0.05800    0.000001
4    9    -0.16600    0.000001
4    4     0.03900    0.000001
4    5    -0.01600    0.000001
-99
0    1     1.06000    0.000001
-99
1
2
3
4
5
6
7
8
9
10
11
12
13
14
15
16
17
18
19
20
```

```
-99
```

The above shown file is the measurement file for the 14 bus system. It is composed of six parts. They are real and reactive power flow measurements, real and reactive power injection measurements, voltage magnitude measurements and suspicious line set.

Real power flow measurements
1st column: the flag of the measurement. 1 represents it is a real power flow measurement.
2nd column: the branch number of that power flow.
3rd to 4th columns: the start and end bus number of that power flow.
5th column: the real power flow measurement.
6th column: the weight of that measurement.

Real power injection measurements
1st column: the flag of the measurement. 3 represents it is a real power injection measurement.
2nd column: the bus number of that power injection.
3rd column: the real power injection measurement.
4th column: the weight of that measurement.

Reactive power flow measurements
1st column: the flag of the measurement. 2 represents it is a reactive power flow measurement.
2nd column: the branch number of that power flow.
3rd to 4th columns: the start and end bus number of that power flow.
5th column: the reactive power flow measurement.
6th column: the weight of that measurement.

Reactive power injection measurements
1st column: the flag of the measurement. 4 represents it is a reactive power injection measurement.
2nd column: the bus number of that power injection.
3rd column: the reactive power injection measurement.
4th column: the weight of that measurement.

Voltage magnitude measurements
1st column: the flag of the measurement. 0 represents it is a voltage magnitude measurement.
2nd column: the bus number of that voltage measurement.
3rd column: the voltage magnitude measurement.
4th column: the weight of that measurement.

Suspicious line set
1st column: the line number of the lines whose parameters are suspected to be in error.

5.2 Output Data Files Parameter Identification Program

There is only one output file of the parameter identification program.

5.2.1 BADDATAOTP.dat

```
Normalized lagrange multiplier

8       R           7         8       0.0793
8       X           7         8       0.0601
1       X           1         2       0.0219
17       R          13        14       0.0196
4       X           2         4       0.0188
11       R           9        14       0.0164
5       X           2         3       0.0153
14       R          6        12       0.0145
16       R         12        13       0.0144
19       X          4         7       0.0131
9       S                             0.0130
2       R           1         5       0.0120
11       X          9        14       0.0117
9       R           7         9       0.0108
20       T          4         9       0.0106
4       R           2         4       0.0104
9       X           7         9       0.0102
18       X          5         6       0.0101
20       X          4         9       0.0098
19       T          4         7       0.0090
5       R           2         3       0.0083
10       R          9        10       0.0079
3       R           2         5       0.0077
6       R           3         4       0.0073
12       X         10        11       0.0069
3       X           2         5       0.0069
13       X          6        11       0.0064
7       X           4         5       0.0058
13       R          6        11       0.0057
17       X         13        14       0.0049
12       R         10        11       0.0044
18       T          5         6       0.0040
2       X           1         5       0.0039
15       X          6        13       0.0039
6       X           3         4       0.0031
7       R           4         5       0.0030
16       X         12        13       0.0015
15       R          6        13       0.0013
10       X          9        10       0.0007
14       X          6        12       0.0007
1       R           1         2       0.0005

Normalized residual

  4    2              0.1112
  4    3              0.0881
  1    7    8         0.0875
  3    8              0.0863
  4    6              0.0832
  4    1              0.0635
  4    4              0.0495
  2    5    6         0.0486
  0    1              0.0450
```

4	5		0.0448
3	4		0.0445
3	6		0.0421
2	6	5	0.0405
2	6	13	0.0338
3	5		0.0314
2	5	2	0.0313
1	3	4	0.0294
4	8		0.0288
2	4	2	0.0284
2	3	4	0.0283
2	7	8	0.0282
4	12		0.0277
4	13		0.0272
2	2	5	0.0243
1	6	13	0.0217
1	5	6	0.0214
1	6	5	0.0214
2	11	6	0.0212
1	4	7	0.0206
1	7	4	0.0206
1	2	3	0.0201
2	6	12	0.0200
2	1	2	0.0184
3	12		0.0181
1	6	11	0.0178
1	11	6	0.0168
4	11		0.0145
2	6	11	0.0139
4	9		0.0130
1	1	5	0.0125
1	6	12	0.0123
2	4	7	0.0120
1	9	4	0.0115
2	7	4	0.0113
1	5	2	0.0093
1	2	5	0.0092
2	9	7	0.0081
1	4	5	0.0079
2	1	5	0.0078
2	10	11	0.0078
3	13		0.0076
1	9	10	0.0075
1	2	1	0.0072
2	9	4	0.0072
2	2	1	0.0071
2	12	13	0.0070
2	9	10	0.0065
2	2	3	0.0064
1	9	14	0.0054
4	14		0.0053
3	10		0.0051
1	13	14	0.0047
1	4	2	0.0043
3	2		0.0035
2	7	9	0.0032
3	11		0.0032

```
 1   10   11          0.0030
 1    1    2          0.0029
 3    9               0.0021
 3    3               0.0017
 1   12   13          0.0016
 1    9    7          0.0015
 1    7    9          0.0015
 4   10               0.0013
 2    9   14          0.0011
 3    7               0.0011
 4    7               0.0010
 3   14               0.0008
 3    1               0.0006
 2    4    5          0.0005
 2   13   14          0.0001
```

This file contains the normalized Lagrange multipliers of the parameters and normalized residuals of the measurements.

Normalized Lagrange multiplier
1st columns: If the parameter is shunt capacitance, it is the connected bus number; if it is not, it is the branch number of that parameter.
2nd column: identifier for the parameter. R represents line resistance; X represents line reactance or transformer reactance; T represents transformer tap and S represents shunt capacitance.

For shunt capacitance:
3rd column: normalized Lagrange multiplier of that CB constraint.
For other parameters:
3rd to 4th columns: the start and end bus number of the branch that parameter belongs to.
5th column: normalized Lagrange multiplier of that CB constraint.

Normalized residual
1st column: identifier for the measurement. 1 represents real power flow measurement. 2 represents reactive power flow measurement. 3 represents real power injection measurement. 4 represents reactive power injection measurement. 0 represents voltage magnitude measurement.

For power flow measurement:
2nd to 3rd columns: the start and end bus number of that power flow measurement.
4th column: normalized residual of that measurement.

For power injection measurement or voltage magnitude measurement:
2nd column: connected bus number of that measurement.
3rd column: normalized residual of that measurement.

5.3 Input Data Files of Parameter Correction Program

Dataotp.dat

```
4       2
20      3
-99
```

This file contains the identified parameter errors by the parameter identification program.

1st column: If the parameter is shunt capacitance, it is the connected bus number; if it is not, it is the branch number of that parameter.
2nd column: identifier for the parameter. 1 represents line resistance; 2 represents line reactance or transformer reactance; 3 represents transformer tap and 4 represents shunt capacitance.

The other input data files are seinput.dat and measureinput.dat. They are the same as described earlier above.

5.4 Output Data Files of Parameter Correction Program

correctp.dat

```
The reactance of branch 4 is 0.17633
The tap of transformer 20 is 0.96000
```

There is only one output file.

The file provides the list of corrected parameter values for the identified parameter errors.

6. Conclusions and Future Work

This part of the report presents a method for identifying network parameter errors, even in the presence of bad analog measurements. The parameter error identification is accomplished by formulating the parameter errors as zero equality constraints and then testing the significance of the associated Lagrange multipliers. These are computed from the normalized measurement residuals obtained by the WLS state estimation. The method can deal with mixed-type multiple errors in measurements and network parameters. There is also no need to specify a set of suspect parameters before state estimation. Once the parameter error is identified, its correct value is estimated using the augmented state estimation method. Several examples are simulated to illustrate the effectiveness of the method. This report also shows the inherent limitations of error identification for certain special cases. The method can be readily implemented as a user-defined option by modifying an existing WLS state estimation code.

7. References

[1] A. de la Villa and A. Gómez-Expósito, “Implicitly constrained substation model for state estimation,” IEEE Trans. on Power Systems, vol. 17, no. 3, pp. 850-856, Aug. 2002.

[2] A. Abur and A. Gómez-Expósito, Power System State Estimation: Theory and Implementation. New York: Marcel Dekker, 2004.

Part II

Multi-Area State Estimation

Authors

Jun Zhu, Ph.D. Student
Ali Abur, Professor
Northeastern University

Table of Contents

List of Figures

List of Tables

1. Introduction

As power transmission systems merge to form large scale power systems containing several interconnected areas, operators are faced with the need to monitor these systems in real time in a computationally efficient manner. They use real time measurements which are processed by the state estimator, to accomplish this. Each control center has its own state estimator which processes the measurements received from its local substations. On the other hand, solution of the state estimation for the entire system will have to be obtained by a central state estimator. This requires access to wide area measurements and solution of a very large-scale state estimation problem. This is not only computationally difficult but may not always be practical. For instance, individual independent system operators (ISO) may not be willing to modify their existing hardware and software in order to meet the new specifications imposed by the central state estimator for the large-scale solution.

In this project, a new approach is used. This approach assumes that each individual ISO will keep its existing monitoring software and a central coordinator will consolidate their results to determine the state of the overall system. The project investigates the design and implementation of this scheme in detail.

It is noted that multi-area solution methods applied to power system state estimation problem have been proposed in the past by several researchers [1]-[6]. These proposals differ in the decomposition strategies for the network. It can be by nodes as done in [1], by tie-lines as in [2], [3], [6] or simply based on the structure of the gain matrix, as in [4]. Optimality of the solution when these methods are applied to the state estimation problem is always guaranteed. The main idea of these methods is that each area will estimate its own state using the available local area measurements. The boundary measurements may either be completely ignored or may be incorporated through some iterative scheme between the local and central computer. It should be noted that, bad boundary measurements will bias the overall system state if they are not identified and eliminated.

This project also takes into account the fact that, today it is possible to have synchronized phasor measurements in addition to the power flows, injections and voltage magnitude measurements at the substations. These measurements not only benefit substation control and protection functions but also facilitate state estimation, as shown in [7]-[10].

This report will first review the multi-area state estimation formulation, solution procedure and data requirements. Then, the method will be applied to the solution of some test systems containing several areas. Simulation results for different measurement configurations some of which contain bad data will be presented.

2. Formulation of the Problem

Multi-area estimation requires decomposition of network data and measurements into individual areas. In this project this decomposition is done in the following manner for an N-bus, n-area power system:

Area buses are classified into two types, internal buses (those having no connection to buses belonging to other areas) and boundary buses. Areas are separated by tie-lines whose terminal buses are assigned to both areas. Each area state estimator will cover and solve for bus voltages at all of its internal buses, boundary buses and boundary buses of all its neighboring areas. This is illustrated graphically in Figure 2.1 for a 3-area case.

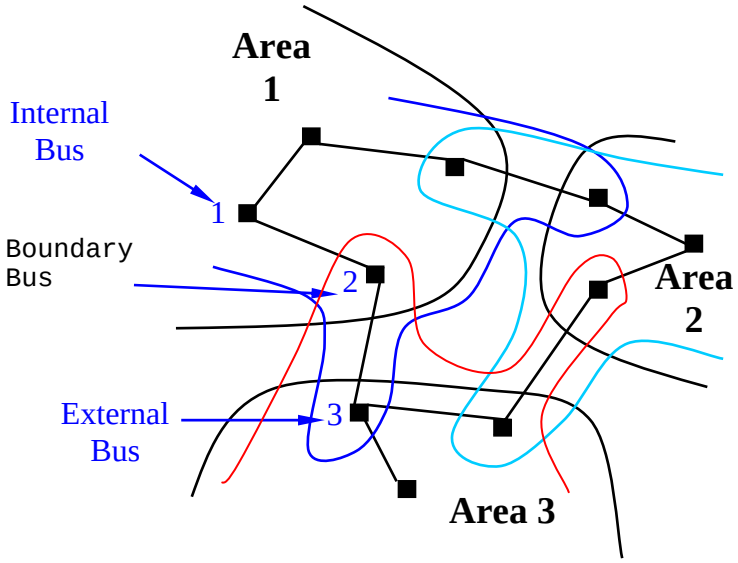

Figure 2.1 Overlapping Bus Assignments for Areas

Note that this particular decomposition scheme is proposed earlier in [2] and [3]. According to this decomposition, buses in each area "i" will be classified as follows:

- **Internal bus**, all of whose neighbors belong to the area i.
- **Boundary bus**, whose neighbors are area i internal buses and at least one boundary bus from another area.
- **External bus**, which is a boundary bus of another area with a connection to at least one boundary bus in area i.

Associated state variables will then be defined as:

- The vector x_i^b consisting of the voltage magnitudes and phase angles at the boundary buses of area i.

- The vector x_i^{int} consisting of the voltage magnitudes and phase angles at the internal buses of area i.
- The vector x_i^{ext} consisting of the voltage magnitudes and phase angles at the external buses of area i.

Individual Area State Estimation:
The phase angle of the chosen slack bus for the area will be excluded from the appropriate vector x_i^b, x_i^{int} or x_i^{ext}. Thus, the state vector for area i will be given by:

$$x_i \stackrel{\Delta}{=} \left[x_i^{bT}, x_i^{\text{int}\,T}, x_i^{ext\,T} \right]^T \tag{2.1}$$

whose dimension is n_i. As evident from the above definitions, each area state vector includes not only the states of that area but also part of the states belonging to its immediate neighbors. Hence, some of the states will be estimated simultaneously by two neighboring area estimators in the first stage where individual areas independently execute their state estimators based on their measurements.

Coordination of Area Estimates:
Once each area completes its own state estimation solution, a central coordinator will receive these solutions. These solutions as well as all boundary measurements will then be used by the central estimator in order to coordinate all area solutions and reach an integrated system solution. Note that, this estimator will also ensure that all bad data associated with the boundary measurements will be identified and corrected. The states, which are to be estimated in this stage are:

$$x_S \stackrel{\Delta}{=} \left[x^{bT}, u^T \right]^T \tag{2.2}$$

where:

$$x^b \stackrel{\Delta}{=} \left[x_1^{bT}, x_2^{bT}, \cdots, x_n^{bT} \right]^T$$

$$u \stackrel{\Delta}{=} [u_2, u_3 \cdots, u_n]$$

u_i is the phase angle of the slack bus of the *ith* area with respect to the slack bus of area 1. Area 1 is arbitrarily chosen to be the reference area with $u_1 = 0$.

So, a two level estimation scheme where in the first level each area estimator remains completely independent and their results are coordinated by a central processor in the second level, can now be implemented.

3. Implementation

3.1 Input Data and Measurements

Each area state estimator will receive and process locally acquired measurements that include:

- Voltage magnitude at internal and boundary buses.
- Power flows along internal lines and at the sending-end of tie-lines.
- Power injections at internal and boundary buses.
- If available, PMU measurements at internal or boundary buses.

Note that individual area state estimators can not use measurements that are functions of states belonging to other areas. Hence, injections, voltage magnitude and line flows measured at the remote end of tie-lines will be disregarded by individual area state estimators. State estimation solutions will be obtained for each area using the local measurements. Estimated states from each area and its own boundary measurements will then be sent to the coordination center where the second stage estimation will be executed. The second level state estimator will be responsible for the estimation of the coordination vector $x_S = \left[x^{b^T}, u^T \right]^T$ and also identifying and eliminating any bad data in the boundary measurements. It will also receive a limited set of synchronized phasor measurements, which are expected to significantly enhance the reliability and accuracy of the estimated states.

3.2 Individual Area State Estimation

In this project, the commonly used Weighted Least Squares (WLS) estimation method is adopted for all estimators. Hence, the individual area state estimation problem for each area is formulated as follows:

$$\textit{Minimize } J_i = r_i^T R_i^{-1} r_i \tag{3.1}$$

$$\textit{Subject to } z_i = h_i(x_i) + r_i \tag{3.2}$$

where:

z_i is the vector of available measurements in area *i* having m_i elements. They include not only all the internal measurements but also the injection and flow measurements incident at the boundary buses and the area tie-lines.

r_i is the residual of measurement z_i.

R_i is the measurement error covariance matrix for area i.

$h_i(x_i)$ is the measurement function for area i measurements.

It is assumed that it is the responsibility of individual areas to make sure that there is enough redundancy in the area measurement set to allow bad data identification and elimination for all internal area measurements. This means that at the completion of the individual area state estimations, the internal state estimate for area each area $\hat{x}^{\text{int}}$ can be assumed to be unbiased. If this is not the case, a proper meter placement program can be employed to upgrade the measurement system for the deficient area [11].

The individual area SE makes use of any available boundary injections and tie-line flows. Hence, the estimated state vector is augmented by the external states associated with the neighboring boundary buses. On the other hand, if there are not sufficient or no such measurements incident at the boundary buses, then the associated states will simply be unobservable and therefore will be ignored.

3.3 Calculation of System-wide State Estimation Solution

The central coordinator will process the SE solutions from all areas along with the GPS based phasor measurements and raw measurements from area boundary buses in order to reach an unbiased estimate for the entire system state. This requires the solution of the following optimization problem:

$$\begin{aligned} \textit{Minimize } J_S &= {r_S}^T {R_S}^{-1} r_S \\ &= [z_S - h_S(x_S)]^T {R_S}^{-1} [z_S - h_S(x_S)] \end{aligned} \tag{3.3}$$

$$\textit{Subject to } z_S = h_S(x_S) + r_S \tag{3.4}$$

where:

$z_S = \left[{z_u}^T, {z_{ps}}^T, \hat{x}^{bT}, \hat{x}^{extT} \right]^T$, which represents all the available data and measurements to the coordinator.

z_u: Boundary measurement vector, which includes the tie-line flows and injections incident at all boundary buses.

z_{ps}: GPS synchronized phasor measurements vector.

r_S: the residual vector of measurement z_S.

$\hat{x}^b = \left[{\hat{x}_1}^{bT}, {\hat{x}_2}^{bT}, \cdots, {\hat{x}_n}^{bT} \right]^T$: Boundary state variables estimated by individual area SEs.

These are treated as pseudo-measurements by the coordinator SE. The covariance of these pseudo-measurements is obtained from the covariance matrix of the states $R_{x,i}$ for individual areas. This matrix is equal to the inverse of the gain matrix associated with that area's WLS state estimator.

$\hat{x}^{ext} = \left[\hat{x}_1^{ext\,T}, \hat{x}_2^{ext\,T}, \cdots, \hat{x}_n^{ext\,T} \right]^T$, similar to $\hat{x}^b$, except defined for the external buses of each area.

The measurement model will then be given as:

$z_S = h_S(x_S) + e_S$

$x_S^T = \left[x^{bT}, u^T \right]$ is the coordination state vector whose dimension is n_S.

e_S is the error vector of measurements, having a Normal distribution with zero mean and $R_S = E(e_S e_S^T)$ covariance.

h_S is the non-linear function of x_i.

It is noted that, each area will communicate its SE results for its boundary states $\hat{x}^b, \hat{x}^{ext}$ and its state covariance matrix $R_{x,i}$ to the coordinator. Furthermore, in general a boundary bus may have two pseudo measurements associated with its state, one provided by the solution of its own SE and another provided by the neighbor's SE. These will have different variances provided by different area SEs. In addition, since processing of the boundary injections will require the topology information around those boundary nodes that should also be provided to the central coordinator. This is the only "raw" information that needs to be provided to the coordinator, in addition to the results of the individual area state estimation. This scheme is quite suitable since it meets the security requirements for each area without having them release details of their internal system topology.

As expected, the effectiveness of the coordinator estimation strongly depends on the measurement redundancy and quality for this estimator. Synchronized phasor measurements can provide this redundancy very effectively. In both the individual area and the coordinator state estimation, the Largest Normalized Residual Test [12] will be carried out to identify the bad data. Finally, it should be noted that due to the absence of iterations between the individual area and coordinator estimators, this two-part algorithm would in general not yield the same results as a single system-wide integrated estimator.

4. Simulation Results

4.1 Simulation Example of IEEE14 Bus System

This system is arbitrarily divided by two areas. Area 1 has 5 buses (1,2,3,4,5) and area 2 has 9 buses (6,7,8,9,10,11,12,13,14). Figure 4.1 shows the diagram and measurement placement of the integrated system. Figures 4.2 and 4.3 depict the segmented area 1 and area 2. Lastly, Figure 4.4 illustrates the buses that have to be estimated at the second level, and measurement placement for that.

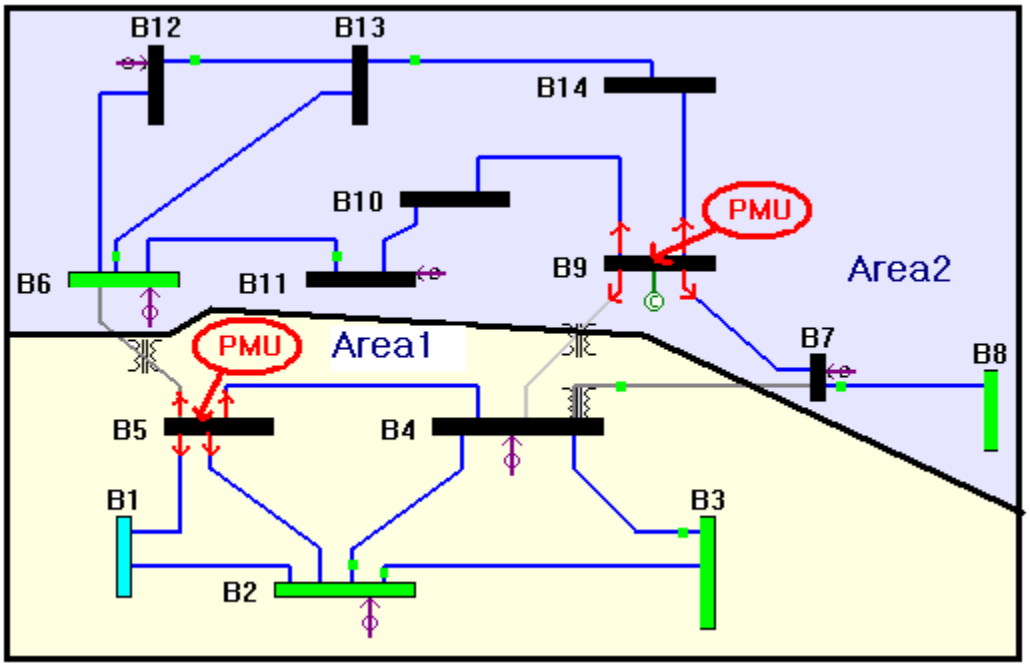

Figure 4.1 Diagram and Measurement Placement of Integrated System

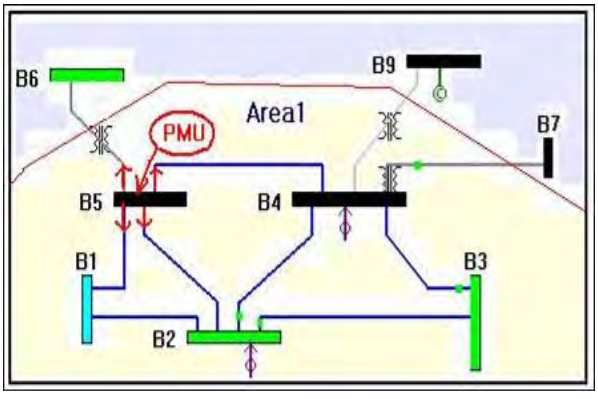

Figure 4.2 Diagram and Measurement Placement of Area 1

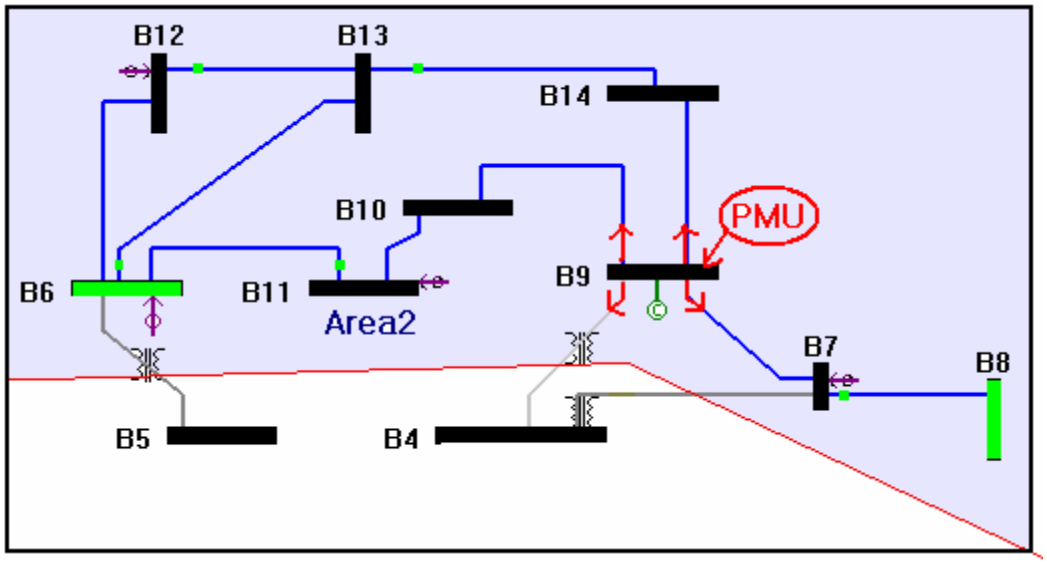

Figure 4.3 Diagram and Measurement Placement of Area 2

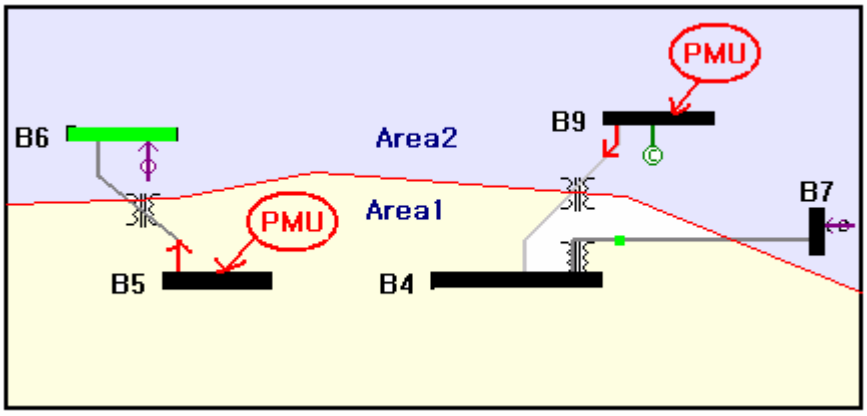

Figure 4.4 Second Level Estimation with Boundary Buses

Table 4.1 indicates the types and number of measurements and the error standard deviations for them. Gaussian errors are imposed to every measurement for the test from the exact values. Measurement data for the second level state estimation has boundary and external bus measurement variables, which are estimated from the first level estimator. The Gaussian standard deviations for the voltages and currents are small compared to the power injection and power flow measurement cases.

The results of the estimation for the different levels are summarized in Table 4.2. The objective functions of each cases are quite below the chi-squares limits, and the largest normalized residuals are also far below the criteria '3.0'. The result of this example indicates that the estimation is carried out successfully by two level estimation method with PMUs while including current measurements data.

Table 4.1 Type, Number, and Error S.D. for Different Estimation Levels

	Power inj.	Power flow	|V|	Voltage Angle	Real Current	Reactive Current	Boundary (|V|, d)	External (|V|, d)
Integrated	12	18	2	2	8	8		
First level (Area1)	4	8	1	1	4	4		
First level (Area2)	8	10	1	1	4	4		
Second level	6	2	2	2	8	8	10	10
Gaussian error S.D.	0.01	0.008	0.004	0.0001	0.001	0.001	*Diag-* $\left(G_i^{-1}(i,i)\right)$	*Diag-* $\left(G_i^{-1}(i,i)\right)$

Table 4.2 Estimation Results of IEEE14 Bus System

	Degree of Freedom	Chi-squares Limit	Objective Function J(x)	Largest r^N
Integrated	21	38.93	23.38	1.7791
Area1	6	16.81	2.52	1.3218
Area2	6	16.81	9.09	1.8095
Second-level	24	42.98	33.25	2.1457

Again, this method is tested for the bad data case, where there is a gross error in real power injection measurement at bus 6. The value of the Pinj(6), which was originally '-0.016', is replaced by '2' to simulate this gross error. Then, the WLS estimation solution is obtained using the proposed multi-area state estimation method. Figure 4.5 shows the measurement configuration and the location of simulated bad measurement.

Tables 4.3 to 4.4 are the chi-squares and the largest normalized residual test results of state estimation in area 2 at the first level estimation.

Table 4.3 State Estimation Results of Area 2 with Bad Data

Degree of Freedom	Chi-squares Limit	Objective Function J(x)
6	16.81	4.03

Table 4.4 Sorted Normalized Residuals of Area 2 Estimation

Measurement Type	Largest Normalized Residual (r^N)
Real part of current (9,10)	1.8095
Imaginary part of current (9,7)	1.8073
Real part of current (9,14)	1.6774

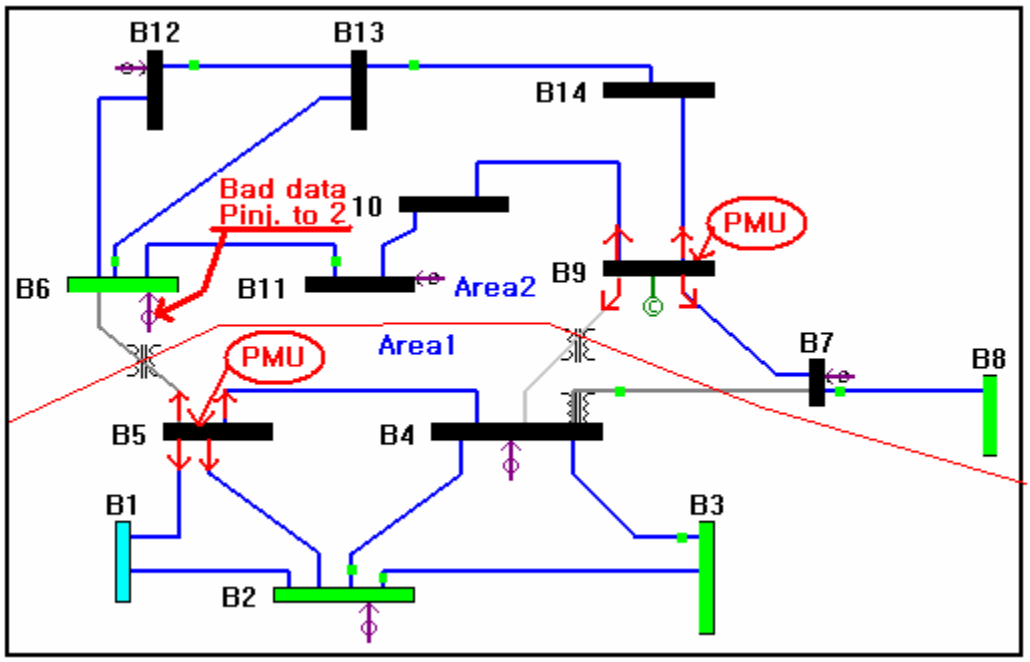

Figure 4.5 Diagram of IEEE14 Bus System with Bad Data

The objective function value '4.03' is far below the chi-squares limit '16.81', and the largest normalized residual is '1.8095' for the real current measurement (9,10). Therefore, the estimator does not suspect any bad measurement at the first (local) level estimation. The reason for this failure to detect bad data is that bad measurement belongs to a critical measurement in this example. However, at the coordination level, second level state estimator successfully detects and identifies the bad data as shown in Tables 4.5~4.6. The objective function value '27965' is larger than the chi-squares limit, and the largest normalized residual value is 146.43 (larger than the 3.0 cut-off) corresponding to the bad measurement Pinj(6).

Table 4.5 State Estimation Results for the Second Level SE with Bad Data

Degree of Freedom	Chi-squares Limit	Objective Function J(x)
24	42.98	27965

Table 4.6 Sorted Normalized Residuals for the Second Level SE

Measurement Type	Largest Normalized Residual (r^N)
Real power injection (6)	146.43
Real part of current (5,6)	117.54
Reactive power injection (6)	94.3880

The above simple example that uses IEEE14 bus test system illustrates that two-level state estimation can detect and identify bad data as long as the measurement is not

critical. The measurement may temporarily become critical during the individual state estimation phase in the first level estimation; however, it will be detected and identified during the second level estimation if it happens to carry bad data.

4.2 Simulation Example of IEEE118 Bus System

A much larger size power system is tested this time using the same method as applied to the IEEE14 bus case. This system is arbitrarily divided into nine areas with one PMU per area. Figure 4.6 shows the area designations and PMU locations.

Tables 4.7 and 4.8 illustrate the number of different bus types, number of measurements, and error standard deviations for the IEEE118 bus system.

Table 4.7 Number of Bus Types and PMUs for Different Estimation Levels

	Area1	Area2	Area3	Area4	Area5	Area6	Area7	Area8	Area9
Total Buses	13	13	12	14	13	13	13	14	13
Internal Buses	10	4	7	9	6	4	11	5	7
Boundary Buses	3	9	5	5	7	9	2	9	6
External Buses	4	10	6	7	6	13	4	8	6
Slack Bus Number	3	18	35	27	76	47	103	93	55
Voltage Meas. (PMU)	1	1	1	1	1	1	1	1	1
Current Meas. (PMU)	3	2	2	4	2	3	4	2	3

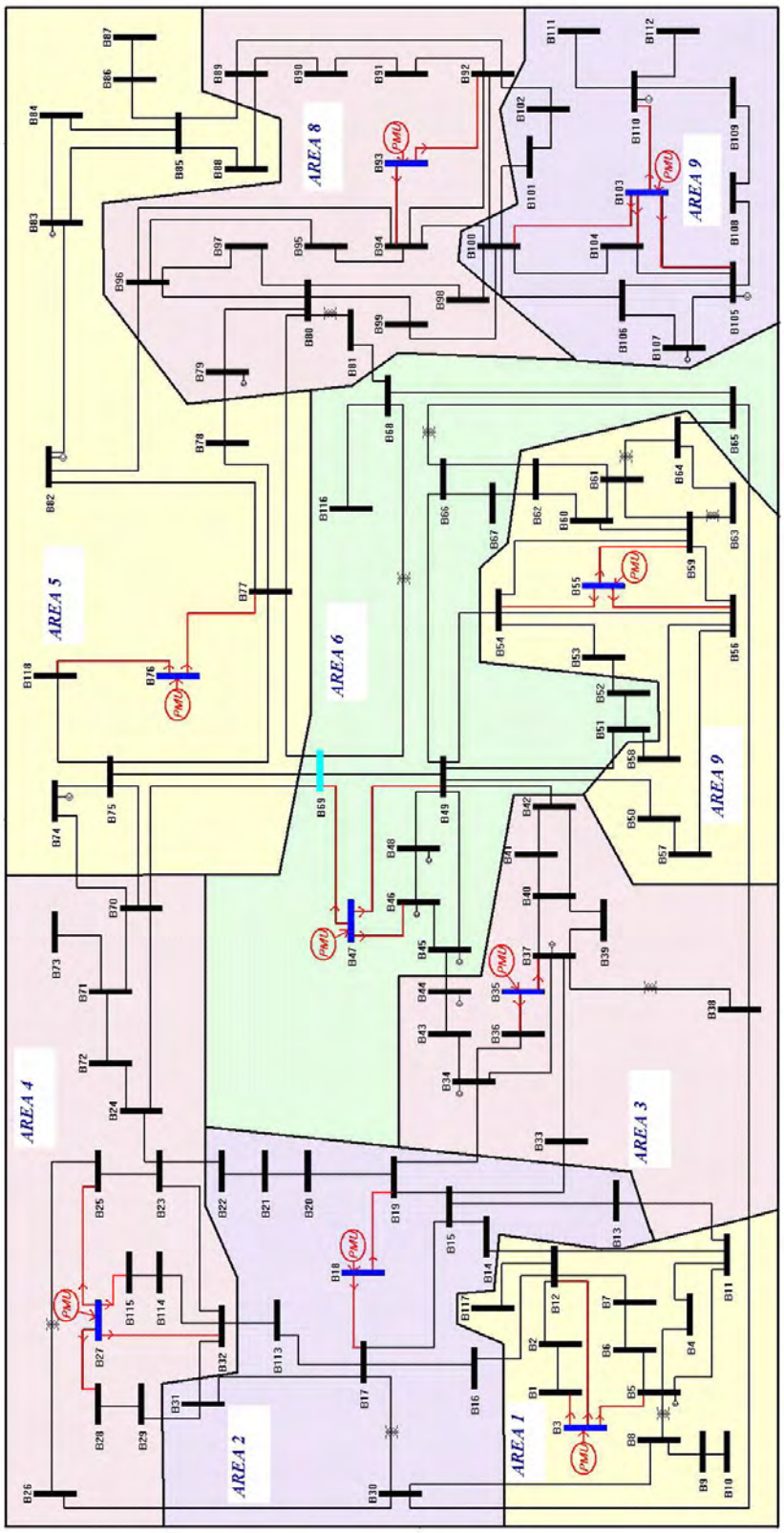

Figure 4.6 Diagram and PMU Placement of IEEE118 Bus System

Table 4.8 Type, Number, and Error Standard Deviation for Different Levels

	Power Inj.	Power Flow	|V|	Voltage Angle	Real Current	Reactive Current	Boundary (|V|,Angle)	External (|V|,Angle)
Integ-rated	110	274	9	.	.	.	.	.
Area1	6	8	1	.	.	.	.	.
Area2	18	30	1	.	.	.	.	.
Area3	10	26	1	.	.	.	.	.
Area4	10	32	1	.	.	.	.	.
Area5	14	28	1	.	.	.	.	.
Area6	18	42	1	.	.	.	.	.
Area7	4	30	1	.	.	.	.	.
Area8	18	30	1	.	.	.	.	.
Area9	12	28	1	.	.	.	.	.
Second-level	110	48	9	9	25	25	110	128
Gaussian (S.D)	0.01	0.008	0.004	0.00001	0.001	0.001	Diag-$\left(G_i^{-1}(m,m)\right)$	Diag-$\left(G_i^{-1}(m,m)\right)$

The results of the WLS state estimation for the integrated and two level multi-area state estimation solutions are summarized in Table 4.9. The table includes both the chi-squares and largest normalized residual test results. All the values of the objective function are below the chi-squares limit and the largest normalized residual values are also below the chosen threshold of '3.0'.

Table 4.9 State Estimation Results of IEEE118 Bus System

	Integ-rated	Area1	Area2	Area3	Area4	Area5	Area6	Area7	Area8	Area9	Second-level
Degree of Freedom	368	14	24	16	18	24	8	16	32	26	348
Chi-Squares Limit	404.04	29.14	42.98	32.00	34.81	42.98	20.09	32.00	53.49	45.64	412.30
Objective Function J(x)	113.69	6.62	6.66	4.94	9.77	6.18	12.59	3.73	11.09	10.98	324.68
Largest r^N	2.64	2.10	2.13	1.79	1.97	1.72	2.34	1.57	2.09	2.18	2.87

Then, one of the measurements is intentionally corrupted by bad data. The value of the real power injection Pinj(44) is changed from '-0.154' to '1' for this purpose as shown in Fig.4.7.

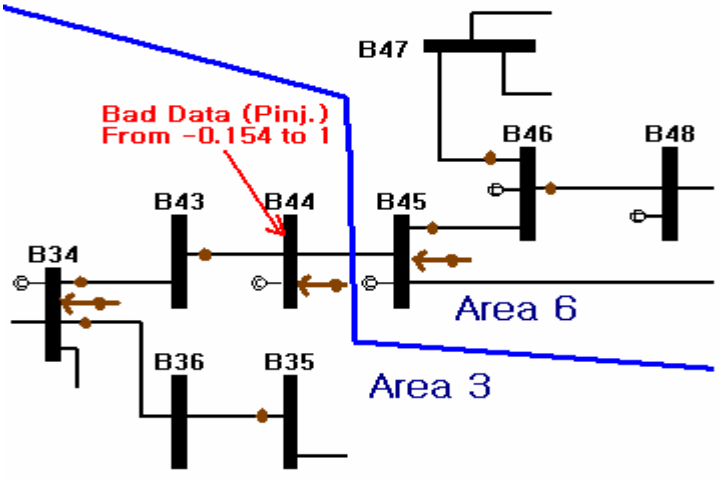

Figure 4.7 Diagram of Area 3 and Area 6 with Bad Data

Note that Pinj(44) will become a critical measurement for area 3 local estimator once the remote end measurements are ignored. Therefore, the first level estimation can not detect this bad data. Tables 4.10 and 4.11 show the results of this area 3 estimation. The two bad data tests find no evidence of bad data and declare the measurement set error free.

Table 4.10 State Estimation Results of Area 3 with Bad Data

Degree of Freedom	Chi-square limit	Objective function J(x)
16	32.00	4.94

Table 4.11 Sorted Normalized Residuals of Area 3 Estimation

Measurement Type	Largest normalized residual (r^N)
Reactive Power Flow (39,40)	1.79
Reactive Power Flow (37,40)	1.73
Reactive Power Flow (37,49)	1.67

However, the second level (coordinator) estimator detects and identifies the bad data as expected by this method. As shown in Table 4.12, the objective function value is larger than the chi-squares limit, and as evident from Table 4.13, largest normalized residual value correspond to the actual bad measurement Pinj(44) allowing its successful identification.

Table 4.12 State Estimation Results of the Second Level with Bad Data

Degree of Freedom	Chi-squares Limit	Objective Function J(x)
348	412.30	10586

Table 4.13 Sorted Normalized Residuals of the Second Level Estimation

Measurement Type	Largest normalized residual (r^N)
Pinj (44)	77.9204
External angle (45)	69.364
Boundary angle (45)	47.978

The above examples are two of many that have been tested in this project. The proposed method is observed to work reliably in detecting and identifying bad data even when they appear at the area boundaries.

References

[1] Clements K.A., Denison O.J. and Ringlee R.J., “A multi-area approach to state estimation in power system networks”, IEEE PES Summer Meeting, Paper C72 465-3, San Francisco, CA. 1973.

[2] Kobayashi H., Narita S. and Hamman M.S.A.A., “Model coordination method applied to power system control and estimation problems”, Proc. of the IFAC/IFIP 4th Int. Conf. on Digital Computer Applications to Process Control, 1974, pp. 114-128

[3] Van Cutsem Th., Horward J. L., and Ribbens-Pavella M. “A Two-level Static State Estimator for Electric Power Systems”, IEEE Transactions on PAS, Vol. PAS-100, Aug. 1981, pp.3722-3732.

[4] Wallach Y. and Handschin E., “An Efficient Parallel Processing Method for Power System State Estimation”, IEEE Trans. on PAS, Vol. PAS-100, Nov. 1981, pp.4402-4406.

[5] Th. Van Cutsem, and M. Ribbens- Pavella, “Critical survey of hierarchical methods for state estimation of electric power systems”, IEEE transaction on PAS, Vol. 102, No. 10, Oct. 1983.

[6] Abdel-Rahman, K.; Mill, L.; Phadke, A.; De La Ree, J.; Yilu Liu. “Internet Based Wide Area Information sharing and Its Roles in Power System State Estimation”. Power Engineering Society Winter Meeting, 2001.IEEE, Volume:2, 28 Jan.-1 Feb.2001 Pages:470 - 475 vol.2

[7] J. S. Thorp, A. G. Phadke, K.J. Karimi. “Real Time Voltage-Phasor Measurements for static state estimation”. IEEE Trans. on PAS, Vol. PAS-104, No.11, August, 1985.

[8] A. G. Phadke, J. S. Thorp, K. J. Karimi. “State Estimation with Phasor Measurements”. IEEE Trans. on Power Systems, February, 1986.

[9] Zivanovic, R., Cairns, C., “Implementation of PMU Technology in State Estimation: an Overview”. AFRICON, 1996, IEEE AFRICON 4th, Volume: 2, 1996 pp. 1006-1011.

[10] Liang Zhao, Ali Abur, “A Two-Level State Estimator for Multi-ISO Operation”, Proceedings of the Thirty-fifth Annual North American Power Symposium. 2003.

[11] Magnago, F.H. and Abur, A., "Unified Approach to Robust Meter Placement against Bad Data and Branch Outages", IEEE Trans. on Power Systems, Vol.15, No.3, August 2000, pp.945-949.

[12] Monticellli, A. and Garcia, A., “Reliable Bad Data Processing for Real-Time State Estimation”, IEEE Trans. on Power Apparatus and Systems, Vol. PAS-102, No.3, pp.1126-1139, 1983.

Part III

Sensor Location Strategies for the Enhancement of Power System State Estimators

Authors

Mark J. Rice
G. T. Heydt
Arizona State University

Table of Contents

List of Figures

List of Tables

Nomenclature

A	Incidence matrix; a generalized dense matrix
A/D	Analog to digital
AGC	Automatic generation control
c	Speed of light
CNP	Condition number placement
d	Singular distance
$E(\bullet)$	Expected value
E	Error
EIPP	Eastern interconnect phasor project
EMS	Energy management system
F	Scaling factor
f	Frequency
FACTS	Flexible alternating current transmission systems
G	Gain matrix
GPS	Global positioning system
H	Process matrix
h	Non-linear process functions
Δh	Augmented row to H
HVDC	High voltage direct current
IEEE	Institute of Electrical and Electronic Engineers
k	Number of buses with PMUs
K_G	Condition number of G using the 2^{nd} norm
K_p	Condition number using p^{th} norm
L_p	The p^{th} norm
LFC	Load frequency control
m	Number of measurements
MCT	Monte Carlo trials
N	Number of samples
n	Number of buses
N/S	Noise to signal ratio
N_b	Number of buses
NE	Normalized error
N_l	Number of lines
P	Active power
P_{AB}	Power flow from bus A to bus B
P_b	Power flow vector
PMU	Phasor measurement unit
PSS	Power system stabilizers
Q	Reactive power
r	Residual
R_P	Power error variance
R_V	Voltage error variance
randn	Random values with normal distribution
RTO	Regional transmission organization
S	Singular matrix
s	Number of states
SCADA	Supervisory control and data acquisition
SCDR	Symmetrical component distance relay
SOC	Second of century
t	Time
THD	Total harmonic distortion
TVE	Total vector error
V	Modal matrix; Voltage phasor
V_m	Voltage maximum
W	Weighting matrix
w	Weight
WACS	Wide area control system
WAMS	Wide area measurement system
x	State vector
X_{AB}	Reactance of line from A to B
x_{exact}	Exact solution of state variable x
$\hat{x}$	Estimated value of state variable x
z	Measurement vector
δ	Voltage phase angle
θ	Sampling angle
λ	Eigenvalues of a matrix
μ	Added measurements to H
σ	Singular value of a matrix
τ	Sample rate

1. State Estimators and Phasor Measurement Units

1.1 Background and Motivation

The electric power industry is undergoing multiple changes and restructuring towards deregulation. Some electric power utilities are increasing the loads on the transmission grid to generate more revenue. The increased power exchange has a concomitant requirement for *situational awareness*. This refers to the need for system operators to know the operating states of the system.

Most utilities have state estimators in the package of energy management systems. The main functions of state estimators are to represent steady state system voltage, currents, and power flows – utilizing mathematics to enhance the accuracy of measurements. State estimators may not accurately represent the system when *incorrect* measurements are used. There are several topics in state estimation being studied to improve the accuracy of the state estimation in power systems. In this report, the author examines how the new technology of phasor measurement units, a global positioning system (GPS) technology, can be used to enhance state estimation in electric power systems.

A growing number of power system protective digital relays are being introduced to the market with the ability to be used as phasor measurement units in addition to their protective relaying function. As phasor measurement unit technology becomes widely available; the electric utilities want to use this technology to the best of their ability. Present communication methods from the energy management system to the substations may not provide enough bandwidth for phasor measurement units to perform fully. Utilities want to know the cost benefit prior to investment in upgrading substation communications.

This report discusses state estimation enhancements attributed to phasor measurement units and how to determine the best location and number for these units.

1.2 State Estimation Literature Review

Schweppe was one of the first to formulate static state estimation for a power network based on the power flow model [1]. The idea is to estimate the electrical states of the power network, mainly voltage magnitudes and phase angles. These states might not be directly observable based on physical relationships between the measurements and the desired unknown states.

Another advancement in the field of state estimation was the introduction of a weight matrix to increase the accuracy of the results. Weighting is done to enhance the "input" of accurate measurements, and de-emphasize the less accurate measurements. It can be shown that the maximum likelihood estimate utilizes weights that are based on the covariance of the measurement devices [2]. The more accurate a measurement, the greater is the selected weight in the state estimator. Weighting is the practice of accounting for the confidence in a measurement. Over time, the confidence in a measurement may change. A solution to this problem is to auto tune of the weights of measurements. The suggested method of auto tuning the weights is to look at recent error variances of the measurements and use these to recalculate the weights of measurements from a short history [3]. References [2, 4-10] further relate to ideal weighting of measurements for power system state estimation.

Measurement errors are typically assumed to be statistically distributed with a zero mean [11]. Due to increase use in "sensorless" technologies such as A/D converters the zero mean as-

sumption is not always true [11]. A suggested method of overcoming this problem is to combine measurement calibration [12-15] with state estimation. Calibration of the measurements can be done in parallel with state estimation by noting the error of measurement over several scans of the measurement. The calibration error will be a constant compared to measurement error which is typically normally distributed [15].

The process of overcoming measurement noise is inherent in taking physical measurements, but there are situations in which the data is grossly erroneous. The data that are erroneous must be identified and eliminated. One method for the detection of bad data is the examination of the measurements and if the measurements deviate from expected values by some preset threshold the measurement can be assumed to be bad [16]. Another problem that causes state estimators inaccuracies is the power system model itself. Generally the simple linear model $Hx=z$ is used where the H is the measurement model (processing matrix), x is the state vector, and z is the measurements. If the process matrix is incorrect, the model does not represent what is physically happening in the system. The detection of both erroneous data or improper formation of the process matrix may be done by examining the residual of the equation $Hx=z$ [2]. A further modeling 'error' is a result of linearization. Since the process matrix is truly a function of operating state, $H=h(x)$. The linearization of the problem results in constant H.

References [4, 6, 10, 17] are textbooks relating to state estimation in power engineering; references [5, 8, 9, 18] are representative of solutions methods; and [16, 19] are case studies.

1.3 The Pseudoinverse and Least-Squares Estimation

The commonly used model for a linear static system is

$$Hx=z \tag{1.1}$$

with H as the process matrix (m by s matrix), x is the state vector (dimension s), and z is the measurement vector (dimension m) is overdetermined when m is larger than s. References [4, 6, 10, 17, 20] describe Equation (1.1). Equation (1.1) can be "solved" in the least-square sense by minimizing $||r||_2$,

$$r=Hx-z \tag{1.2}$$

where $\| \bullet \|_2$ refers to the 2-norm [17]. Properties of norms appear in [17] and Appendix A. It can be shown that $|| r ||_2$ is minimized when

$$x = \hat{x} = H^{+}z\,. \tag{1.3}$$

The notation $\hat{x}$ is the "estimate" of vector x, H^{+} pseudoinverse of H. References [4, 6, 10, 17, 20] describe the properties of the pseudoinverse. Equation (1.3) is known as an unbiased least squares estimator.

Other methods of determining the state variables are under study. One such method is weighted least absolute value. Unlike weighted least squares there is no explicit formula for the solution to linear weighted least absolute value. The weighted least absolute value is found by linear programming [21]. Another method suggested is to find the maximum agreement with

measurements. The state estimate agrees with the majority of the measurements taken in the system [7].

The least squares method of state estimation requires the system to be observable. Observability can be defined as: given a set of measurements and their locations (i.e., given *z* and *H*), then a unique estimate of the system state vector *x*, i.e. $\hat{x}$, can be found. A basis of observability analysis is graph theory. To determine which states are unobservable, set the measurement vector, *z*, to zero,

$$H\hat{x} = 0.$$

In the context of electric power systems, this yields a non-zero branch flow,

$$P_b = A\hat{x} \neq 0.$$

The *A* matrix, i.e. the branch-bus incidence matrix, is used to determine P_b, the vector of branch flows. Because the measurement set *z* is set to zero, there should be no power flowing through the branches. A non-zero branch flow indicates an *unobservable state* of $\hat{x}$ and those branches carrying nonzero power flows, will be referred to as *unobservable branches* [10]. The common technique in correcting the issue of unobservable areas is to provide an estimate of what the readings are in the unobservable areas to create an entire system model [22]. Other references discussing observability are [23-26].

Numerous other topics are discussed in the literature relating to state estimation in power systems including robustness [7, 27, 28], multiphase state estimation [29], and distributed computing [30].

1.4 Phasor Measurement Units Literature Review

Phasor measurement units (PMUs) are instruments that take measurements of voltages and currents and time-stamp these measurements with high precision. PMUs are equipped with Global Positioning Systems (GPS) receivers. The GPS receivers allow for the synchronization of the several readings taken at distant points [31]. To accomplish synchronization of measurements taken at distant points, several measurements are taken, and time stamped; then interpolation is used to obtain estimates of measurements at a given time within the time horizon of the measurements. PMUs were developed from the invention of the symmetrical component distance relay (SCDR). The SCDR development outcome was a recursive algorithm for calculating symmetrical components of voltage and current [32]. Synchronization is made possible with the advent of the GPS satellite system [33]. The GPS system is a system of 36 satellites (of which 24 are used at one time) to produce time signals at the earth's surface. GPS receivers can resolve these signals into (*x, y, z, t*) coordinates. The *t* coordinate is time. This is accomplished by solving the *distance=(rate)(time)* in three dimensions using satellite signals. The PMU records the sequence currents and voltages and time stamps the reading with time obtained by the GPS receiver. It is possible to achieve accuracy of synchronization of 1 microsecond or 0.021° for 60 hertz signal. This is well in the suitable range of measuring power frequency voltages and currents [32]. Based upon the research done at Virginia Tech, the Macrodyne Company was able to begin production of PMU devices, which lead to the IEEE Standard 1344 "Snychrophasor"

which defines the output data format of a PMU [32]. Figure 1.1 is a pictorial of PMU measurement system.

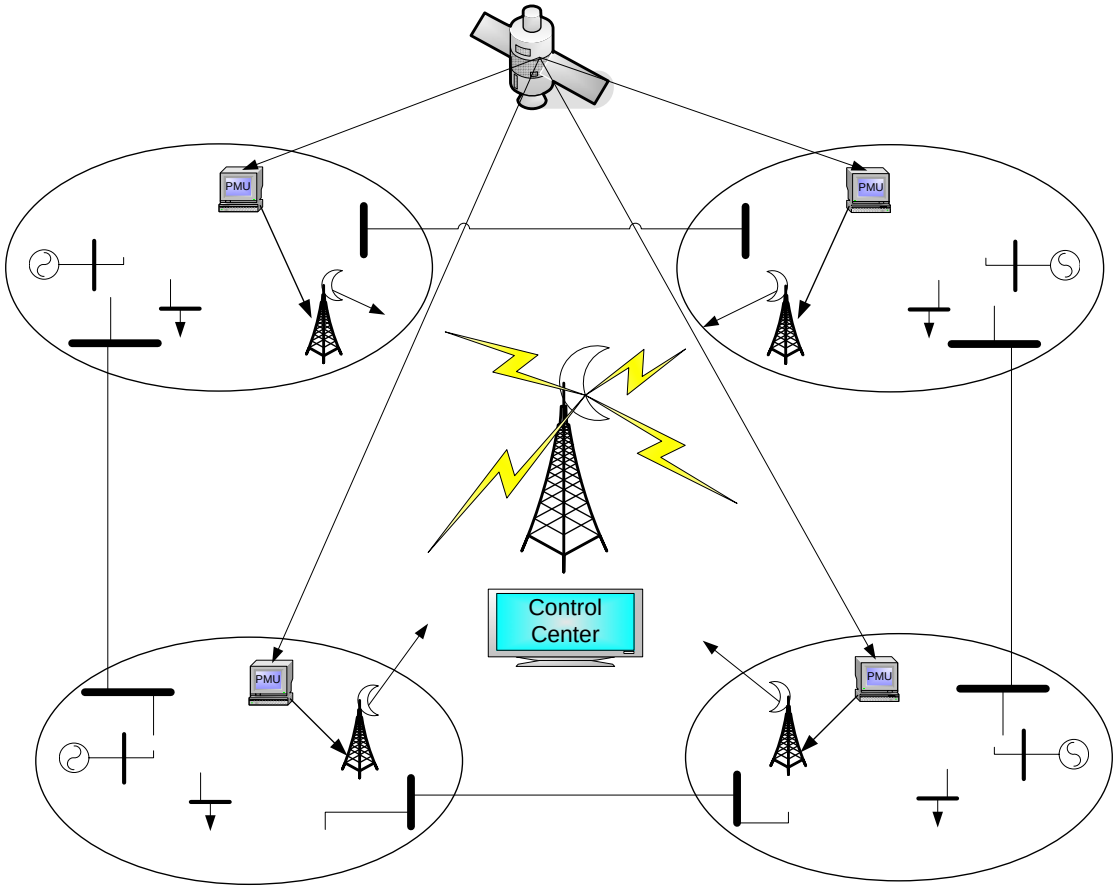

Figure 1.1 Conceptual diagram of a synchronized phasor measuring system
redrawn from [34]

The calculation of the phasor measurement can be done using discrete Fourier transforms. A sinusoidal quantity representing voltage

$$v(t) = V_m \cos(\omega t + \delta)$$

has a phasor representation

$$V = \frac{V_m}{\sqrt{2}} e^{j\delta}.$$

By sampling *v(t)* at sample rate of τ the sample of the length of $T=k\tau$

$$V = \frac{1}{\sqrt{2}} \frac{2}{N} \left(\left(\sum_{k=1}^{N} x_k \cos(k\theta) \right) - j \left(\sum_{k=1}^{N} x_k \sin(k\theta) \right) \right)$$

N is the number of samples in one period of the nominal power system frequency. The sampling angle θ corresponds to the sampling interval τ [35].

PMUs measure voltage and current with high accuracy at a rate of 2.88 kHz. It can calculate watts, vars, frequency, and phase angle 12 times a per 60 hertz cycle. The actually sampling rate used to achieve this output is 1.4 MHz [36]. Some examples of uses of PMUs are fault recording, disturbance recording, and transmission and generation modeling. Transmission and generation modeling includes state estimation [36].

PMUs are able to measure what was once immeasurable: phase difference at different substations. When completing a state estimation of a power system, one of the states to be estimated is the voltage phase angle at each bus. With PMUs the utilities are able to directly measure voltage angle as compared to the swing bus.

How PMUs could be integrated into state estimation has been discussed in the literature [15, 37-42]. There is a school of thought that the measurements from the PMU are far superior of SCADA data used in traditional state estimation and should be collected and used separate from this data [43]. Others admit there is difference in the information and it is viable to use PMU measurements in with SCADA data [44]. Hydro-Quebec believes that the PMUs are accurate enough to not need correlation between PMU measurements. Their algorithm is to place the PMUs based on the busses which minimize the correlation between measurements [45]. An dramatic improvement in the state estimate has been seen by using a 3-phase model and the use of GPS synchronized measurements [46].

With increased need for area multi-area of state estimation, there has been noted the possibility of the increased error in the state estimate as the size of the systems grows enormous [11]. PMUs are being investigated as a solution to this problem. The electric utilities in the regional transmission organization (RTO) would still do their state estimation. The RTO receives the results from the various state estimates of the areas under its control and PMU measurements from boundaries between electric utilities. The individual state estimators do not interact or exchange data with other state estimators allowing for each estimator to have its own unique algorithm with out affecting the performance of other area estimators [41].

The Eastern Interconnect Phasor Project (EIPP) the project is divided into two stages. The near term state goal is to use the expertise and equipment developed with sponsorship from the U.S. Department of Energy to deliver immediate value to project participants in the eastern interconnection. Most of the existing expertise involves off-line analysis and is supportive of planning activities. The long-term goal is to add value to the inter-regional information system and measurement system using PMUs [47].

Figure 1.2 is a pictorial that conceptualized the use of PMUs in state estimation measurements for increased observability.

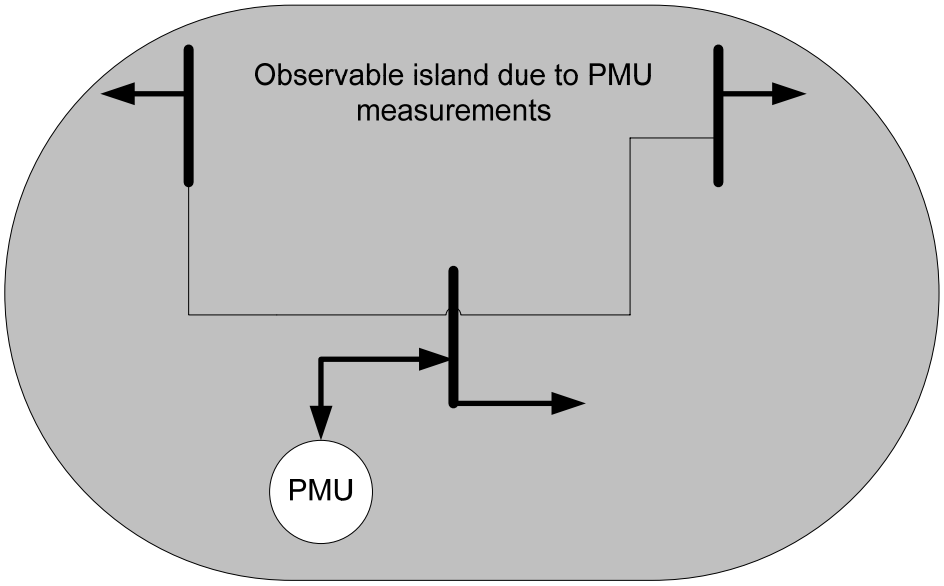

Figure 1.2 Pictorial expanded observability using PMU measurements

1.5 The IEEE Standard for Synchrophasors for Power Systems

The IEEE has recognized the need for standards for PMUs. The first standard for PMUs, IEEE 1344 [48], was written in 1995. The drafting of a standard for PMUs is, perhaps, documentation that PMUs are expected to occupy a significant role in power systems instrumentation. A working group was created in January 2001 to create a new standard for PMUs, IEEE C37.118, that has become a standard [49]. The updated standard provides clarification for phasor and synchronized phasor definitions. The standard defines synchronized phasor measurements in substations so that the measurement equipment can be readily interfaced with associated systems. Table 1.1 lists the major contents of the updated standard.

Table 1.1 Main contents of [49]

Body of Standard	Appendices

• Synchrophasor measurement
  o Definition of phasor and synchrophasor
  o Measurement timetag
  o System time synchronization
• Synchrophasor measurement requirements and compliance verification
  o Synchrophasor estimation
  o Accuracy limits
  o Compliance verification
• Message format
  o Message application
  o Message framework
  o Data frame
  o Configuration frame
  o Header frame
  o Command frame
	• Cyclic redundancy check codes
	• Time tagging and transient response
	• Message examples
	• Sources of synchronization
	• Time and synchronization communication
	• Benchmark tests
	• TVE evaluation and PMU testing
	• Synchrophasor message mapping into communications

To allow for integration of PMUs with other equipment, the standard provides common data format for exchanging information with PMUs. The data for time measurement shall consist of second-of-century (SOC) counts, fraction of second count, and a time status value. The SOC count is the number of seconds since the calendar time from midnight January 1, 1970. The accuracy of the time stamp required by this standard is 1 microsecond. The maximum phase time error allowable is 26 microseconds. Table 1.2 shows all the limitations imposed on the PMU.

Table 1.2 Influence quantities and allowable error limits for compliance levels 0-1 taken directly from [49]

Influence quantity	Reference condition	Range of influence quantity change with respect to reference and maximum allowable TVE in percent (%) for each compliance level			
		Level 0		Level 1	
		Range	TVE (%)	Range	TVE (%)
Signal frequency	$f_{nominal}$	± 0.5 Hz	1	± 5 Hz	1
Signal magnitude	100 % rated	80 – 120% rated	1	10 – 120% rated	1
Phase angle	0 radian	± π radians	1	± π radians	1
Harmonic distortion	< 0.2 % THD	1% any harmonic up to 50^{th}	1	10% any harmonic up to 50^{th}	1
Our band of interfering signal, at frequency f_i, where $\|f_i - f_0\| > f_s/2$, f_s= phasor reporting rate, $f_0 = f_{nominal}$	< 0.2 of input signal magnitude	1% of input signal magnitude	1	10% of input signal magnitude	1

1.6 The Migration from Wide Area Measurements to Wide Area Control

Wide area measurement systems (WAMS) are instrumentation infrastructures that span a wide geographic area, typically several control areas, and potentially several operating companies. Under WAMS, the time required to transmit the sensory information (latency) back to the central control center is significant compared to the dynamics of the measurement.

Because of the latency issue under WAMS, PMUs offer a technology time stamp measurements. PMUs allow several different state estimations to be integrated into a complete set of state estimates of the area [50]. In the deregulated market, the system operational conditions may change quickly and dynamic power flow patterns appear to the system operator [51]. Reference [52] discusses the ability to look at system dynamics using WAMS in the case of the North East blackout of August 14, 2003. A conclusion is that WAMS offer better characterization than digital fault recorders.

Figure 1.3 is intended to depict the roles of measurements versus control. With WAMS becoming increasingly used, researchers have begun examining the concept of wide area control systems (WACS). Some potential elements of WACS are depicted in Figure 1.3. Such studies include the use of WAMS to control power system stabilizers [53, 54]. Other system stability controls are being researched also as seen in [35, 51, 55].

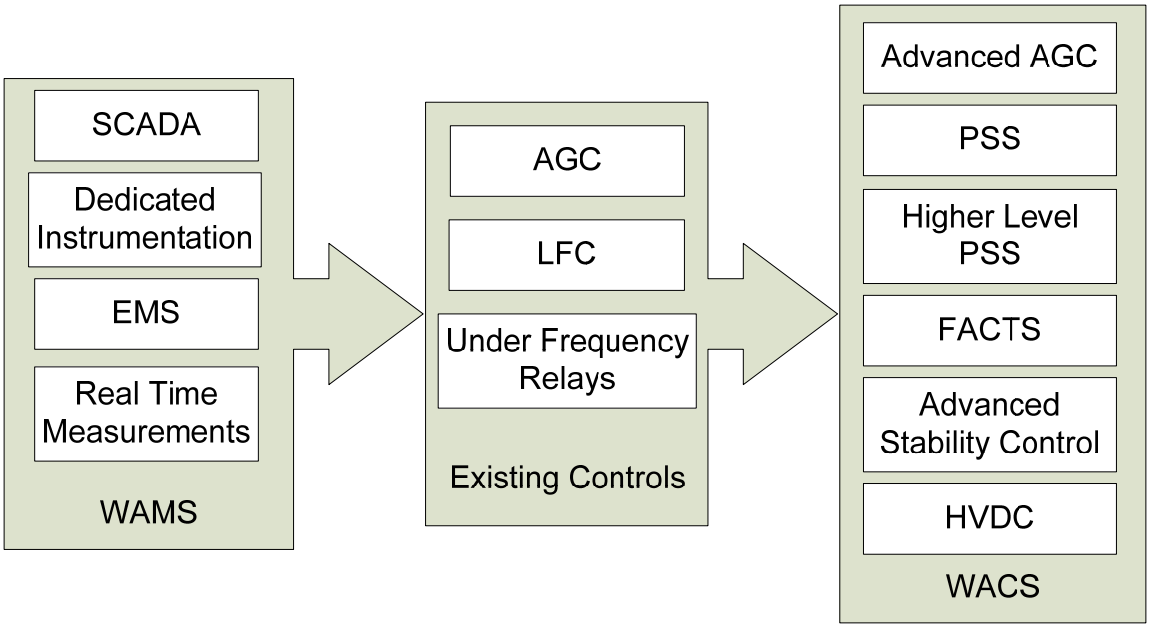

Figure 1.3 Pictorial of the transition of WAMS to WACS

1.7 Placement of Phasor Measurements

Power engineers have been looking at how to use PMUs to monitor and characterize the system. The PMUs have been implemented as a source of information to detect faults on transmission lines [33]. The implementation of PMUs to make the system more observable; starts with a spanning tree and looks for areas of the system which are unobservable. The next step is to impose certain criteria on the search of the proper placement for the PMUs. Three methods that have been examined are the modified simulated annealing method, direct combination, and the tabu search algorithm. All three were examined on tests on the IEEE 14, 30, and 57 bus systems and the results show that the proposed methods can find the optimal solution in an efficient manner [56]. Another method for determining the optimal placement of the PMU is to do a genetic algorithm search [57]. The authors of [58] suggest that a genetic search is the best because the two solution criteria may be in opposition to each other. In this case, criterion one is to maximize the redundancy and observable area of system. Criterion two is to minimize cost of the installation [58]. Integer programming can be used to find the optimal placement of PMUs for making the system observable [59]. Another paper argues there should be more criteria added to the optimal placement of PMUs. These criteria include the examination of the placement of the devices to best observe the system stability [43].

Another index and general philosophy being used to find the optimal location of PMUs relates to the use of the condition number of the measurement matrix [60]. An algorithm for finding a measurement matrix with a small condition number was suggested by [60]. The algorithm creates a measurement matrix of all possible measurements. Subsequently each measurement is removed individually and the condition number of the measurement matrix is computed. The measurement removed this iteration is the measurement associated with the smallest condition

number. This process is continued until the system is critically determined [60]. A later suggestion was to use the minimization of the condition number for harmonic state estimation [61].

Measurement placement problems are not unique to PMUs. Another technology for placement algorithms relates to remote terminal units. One search method used for placement of remote terminal units is the heuristic search. Step one of a heuristic search is to create a measurement configuration that minimizes the number of measurements needed for the system to be observable. Then the configuration is optimized by minimizing the number of remote terminal units used [62]. Another placement algorithm for remote terminal units suggests that the system should be observable when 1 or 2 measurements are lost including remote terminal measurements [63].

1.8 Format of This Report

Chapter 1 is an introduction to state estimation and phasor measurement including literature review of recent advances in these fields of study. Chapter 2 is theoretical basis of sensory placement for state estimation. Chapter 3 is case studies implementing theory presented in Chapter 2 about condition indicators, and Chapter 4 is contains a listing of four main areas of future work.

Appendices are used to supply supportive information:

Appendix A: Details of the examples used in this report
Appendix B: Properties of norms
Appendix C: Code used in the research of this report.

2. The Foundations of State Estimation Sensory Placement

2.1 Phasor Measurement Units for Power System State Estimation

The increasing availability of PMU devices has caused increased interest in using PMUs in state estimation. Not all PMUs installed can be used in state estimation because of system limitations, such as the bandwidth of the SCADA system measurements from remote substations and format and protocol inconsistencies. Further, company A may wish to place additional instrumentation in company B's system, and this issue may be problematic. When a power company is examining how to upgrade the system to allow for PMUs to be used for state estimation, one question that is asked is how incorporating this measurement into the state estimation affects the accuracy of the estimates. The answer relies on where the new PMU measurements are in the system. This report examines methods for determining the placement of PMUs for increasing the accuracy of the estimates.

2.2 The Method of Least Squares

Present state estimation techniques rely on the least squares approach to finding the best estimation of states. The method of least squares uses the linear equation,

$$z = Hx \tag{2.1}$$

H is the process matrix dimensioned (*m* x *s*), *x* is the state vector dimensioned (*s*), and *z* is the measurement vector dimensioned (*m*). Equation 2.1 is the linearized form. In state estimation it assumed that the system is over determined, meaning there are more measurements than states. However, rarely are the measurements perfect, and therefore z is actually a perfect measurement plus 'noise.' The problem becomes how to find the best fit between measurements *z* and states *x*. In the least squares approach idea is minimize the difference L_2 norm of the residual,

$$r = z - H\hat{x} \tag{2.2}$$

$$|r|_2^2 = (Hx - z)^t (Hx - z). \tag{2.3}$$

To minimize Equation 2.3, take the derivative, which results in Equation 2.4. Then simple algebra is used to separate the best estimate of *x*, namely $\hat{x}$,

$$\left.\frac{\partial |r|_2^2}{\partial x}\right|_{x=\hat{x}} = 0 = H^t H\hat{x} - H^t z \tag{2.4}$$

$$H^t H\hat{x} = H^t z$$

$$\hat{x} = (H^t H)^{-1} H^t z. \tag{2.5}$$

The formulation in (2.5) is valid only when H^tH is nonsingular. The singular case is rarely encountered but can be handled by an alternative formatting. There are two notable terms in Equation (2.5): the $(H^tH)^{-1}H^t$ term also known as the pseudoinverse and the gain matrix (*G*),

$$G = H^t H \tag{2.6}$$

$$H^+ = \left(H^t H\right)^{-1} H^t . \tag{2.7}$$

The notation H^+ refers to the pseudoinverse [4, 6, 10, 17].

A drawback of the least squares approximation is that the all the measurements are treated with the same weight. This procedure is unbiased. This implies that all the measuring tools are measuring with the same accuracy and precision. In power engineering, this is rarely the case. A term is added to the least squares to provide emphasis for accurate measurements. This is accomplished by weighting the residual r using a weighting matrix W. The matrix W is m by m, and the weighted residual is $\sqrt{W}\left(Hx - Z\right)$. It can be shown that if the measurement noise is gaussian with zero mean, the W matrix is the inverse of the covariance matrix of the measurements in order to obtain the maximum likelihood solution [6],

$$W = \begin{bmatrix} \sigma_1^{-2} & & & & \\ & \sigma_2^{-2} & & & \\ & & \ddots & & \\ & & & \ddots & \\ & & & & \sigma_m^{-2} \end{bmatrix} \tag{2.8}$$

$$r = \sqrt{W}\left(Hx - z\right) \tag{2.9}$$

$$|| r ||_2^2 = \left[\sqrt{W}\left(Hx - z\right)\right]^t \left[\sqrt{W}\left(Hx - z\right)\right]. \tag{2.10}$$

Equation (2.9) is the weighted residual equation. Moving the $\sqrt{W}$ inside the parenthesis, a formulation similar to the unbiased case is found. To find $\hat{x}$ that minimizes $\|r\|_2^2$ take the derivative,

$$|| r ||_2^2 = \left(\sqrt{W}Hx - \sqrt{W}z\right)^t \left(\sqrt{W}Hx - \sqrt{W}z\right)$$

$$H' = \sqrt{W}H$$

$$z' = \sqrt{W}z$$

$$|| r ||_2^2 = \left(H'x - z'\right)^t \left(H'x - z'\right) \tag{2.11}$$

$$\left.\frac{\partial \| r \|_2^2}{\partial x}\right|_{x=\hat{x}} = 0 = H'^t H'\hat{x} - H'^t z'$$

$$\hat{x} = \left(H'^t H'\right)^{-1} H'z' . \tag{2.12}$$

There is a caution in the use of the symbolism $\sqrt{W}$. Because there are several different matrices *B* that satisfy

$$B^t B = W$$

(i.e., there are several 'square roots' of the matrix *W*), the notation $\sqrt{W}$ is ambiguous. Let the term "symmetric positive definite matrix" refer to a symmetric matrix with all positive real eigenvalues. For a symmetric positive definite *W* and since *W* is a covariance matrix, it is the form $E\left(zz^t\right)$, and all covariance matrices are positive definite [64], there are exists a unique symmetric positive definite *B* such that $B^t B = W$ [20]. Hence the notation $\sqrt{W}$ will refer to that unique symmetric positive definite *B* such that $B^t B = W$.

2.3 State Estimation Accuracy

The weighted least squares method of state estimation is only as accurate as the measurements and models used. The model in this case is the set of equations that describe the system.. If there is no error in the measurements, then the measurements lie within a surface created by the equations of the model. When there is error in the measurement then the weighted least squares solution minimizes the distance from the point of measurement to the surface as seen in Figure 2.1. In essence, the depiction in Figure 2.1 illustrates that the method of least squares estimation minimizes the impact of error in measurements.

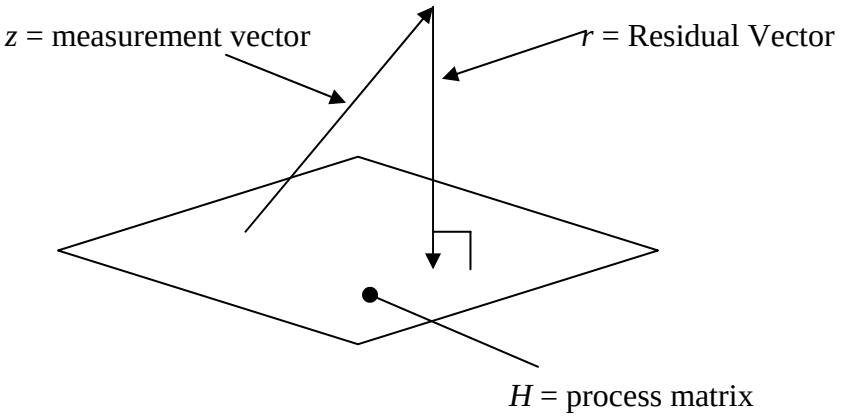

Figure 2.1 Projection of *z* onto *H*

The constraint given by [65] of the L_p norm of the residual is

$$\|r\|_p \le K_p(H)\|e\|_p \qquad (2.13)$$

where are $\|r\|_p$ is the L_p norm of the residual and *e* is the vector of error in the measurements and $K_p(H)$ is the L_p condition number of the process matrix, *H*. The condition number of a square nonsingular matrix *A* is (2.14) and Table 2.1 is list of properties of matrix norms,

$$K_p(A) = \|A\|_p \left\|A^{-1}\right\|_p . \tag{2.14}$$

Table 2.1 Matrix norm properties [65]

Eigenvalues of Matrix A	$\frac{1}{\left\|A^{-1}\right\|} \le \lvert\lambda\rvert \le \|A\|$	
Lp Norm of Matrix A	$\|A\| = Max \frac{\|Ax\|_p}{\|x\|_p}$	The task of computing a matrix norm is difficult if *p>1*. Since, it is a nonlinear optimization problem with constraints.
Maximum Absolute Column Sum	$\|A\|_1 = \max_j \sum_{i=1}^{N} \lvert a_{i,j}\rvert$	
Spectral Norm	$\|A\|_2 = \sqrt{\max\left(\lambda\left(A^H A\right)\right)}$	
Maximum Absolute Row Sum	$\|A\|_\infty = \max_i \sum_{j=1}^{N} \lvert a_{i,j}\rvert$	
Note	$\|A\|_2^2 \le \|A\|_1 \|A\|_\infty$	

The matrix H^tH is also called the gain matrix G and it is of dimension s by s and G is symmetric. The calculation shown in (2.5) is closely related to the condition number of matrix G (the condition number K_G of G, using the 2-norm, is defined as the scalar $||G||_2||G^{-1}||_2$ where $||.||_2$ denotes the 2-norm [20]). As shown in [66], the sensitivity of the estimate of x to noise is improved (i.e., lessened) when K_G is small, and the sensitivity is worsened (increased) when K_G is large. Typical threshold values of K_G in state estimation applications, beyond which designers of the state estimator become concerned, are about 10^5.

The eigenvalues of G are also equal to the singular values of G in this application when the G matrix is nonsingular; and the ratio of the largest to smallest eigenvalue of G is the condition number of G,

$$\mathrm{K_G} = \frac{\lambda_s}{\lambda_1} = \frac{\sigma_s}{\sigma_1} \tag{2.15}$$

where λ, σ denote the eigenvalues and singular values of G respectively, and subscript s refers to the largest eigenvalue and singular value, and subscript 1 refers to the smallest values. Throughout this paper, the condition number based on the 2-norm shall be used because of its convenience and connection with the power engineering state estimation problem solved by minimum least squares; however, it is possible to use other norms (e.g., 1-norm and infinite norm).

2.4 The Singular Distance and Scaling Factor

The foregoing remarks focus on conventional thoughts in contemporary state estimation technology. As an example, the state estimation performance connection with the condition number K_G has been discussed in the literature [20, 40, 66, 67]. At this juncture, the use of indicators such as K_G is expanded in the form of several innovative measures of the 'condition' of the matrix G. The objective is to utilize all the information from the eigenspectrum of G to obtain an assessment of the sensitivity of the solution of the state estimation to errors in measurements.

It is clear that the gain matrix G has a substantial impact on the state estimator response to measurements and measurement noise and error. Inspection of (2.5) indicates that $G = H^tH$ should be as 'far from' singular as possible. With this as motivation, define the 'distance' from G to the nearest singular matrix S as d,

$$d = \min_S ||H^tH - S||_2$$

where the minimum is taken over all possible singular matrices S. Then d is the 'distance' from the gain matrix G to the nearest singular matrix, and this is termed here as the *singular distance.* It can be shown that the singular distance d is equal to the smallest singular value σ_1. Therefore

$$d = \frac{\sigma_s}{K_G} = \frac{\lambda_s}{K_G} = \sigma_1 \qquad (2.16)$$

Again, recall that the eigenvalues and singular values are all positive and real, and ordered as $\lambda_1 \le \lambda_2 \le ... \le \lambda_s$, $\sigma_1 \le \sigma_2 \le ... \le \sigma_s$. At the other end of the singular spectrum or eigenspectrum are the values σ_s, λ_s. These quantities may be interpreted as scaling factors which need to be reduced in order to decrease the generalized concept of gain from z to $\hat{x}$. For this reason, σ_s, λ_s are termed the scaling factor F,

$$F = \sigma_s = \lambda_s.$$

Then,

$$F = dK_G.$$

It is desired to make the singular distance as large as possible to improve the state estimator response. Similarly, it is desired to make the scaling factor as small as possible.

The condition indicators F, K_G, and d are proposed as tools to assess the number and placement of PMUs in a power system state estimation.

2.5 Augmenting State Estimation Software with PMU Hardware

In this section, a review is given relating to the synchrophasor device or PMU as it relates to use in state estimation. A PMU is a "sensorless" device meaning it uses an A/D converter to create the measurement of time, active power, vars, frequency, current, and voltage. The PMU works by taking several samples and then approximating the best curve to fit the sample set. PMU take as many as 12 measurements per 60 Hz cycle. The PMU reads in data at the rate of 1.4 MHz [36]. Synchronous time signal received from GPS is accurate with in 1 microsecond or 0.0012° per 60 Hz cycle [32]. The accuracy obtained of the measurements of PMU devices is at least 2 orders of magnitude greater than the accuracy of measurements obtained from SCADA devices.

The process of finding the phase angle using a PMU is a set of state estimations. The determination of time using GPS is computed from the synchronized time signals being sent from the satellites. To determine time. there must be at least four satellite signals being received because three other states (x,y,z) are also being identified simultaneously. The GPS unit receives time signals from the satellites and using distance equations shown in Figure 2.2 it does an iterative process to determine (x,y,z,t).

For PMUs, measurements of voltages and currents that are time stamped result in 2,880 measurements per second, 48 measurements per cycle, meaning measurements are estimated using only data samples from only part of the cycle as seen in Figure 2.3. The distance between samples is exaggerated for purpose of clarity.

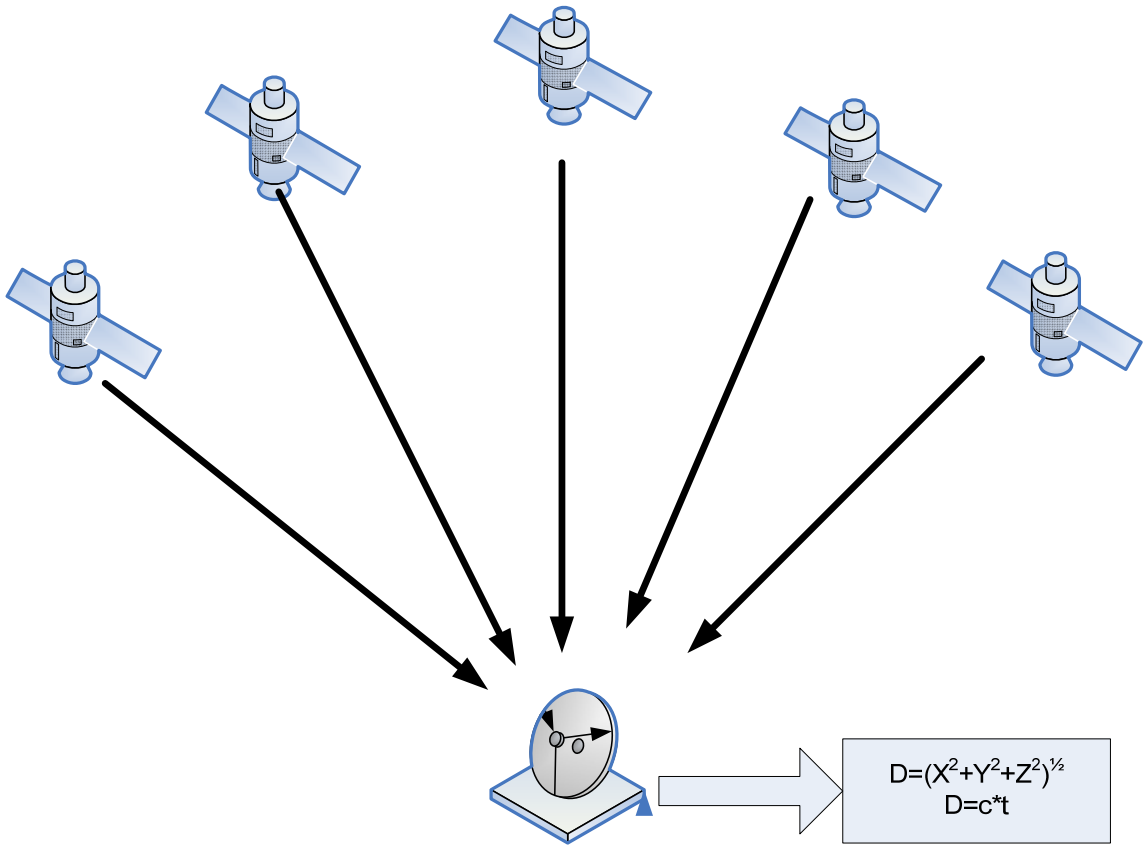

Figure 2.2 A representation of GPS system of a PMU

The measurements of voltage phase angles by PMUs are considered to be much more accurate than those made by other measurements in the system. Presently there are no other methods of directly measuring phase angle. Another advantage of PMU measurements over SCADA measurements is that PMU measurements have a time stamp of when the measurement was taken. This allows for synchronizing of PMU measurements that may be reported to EMS at different times.

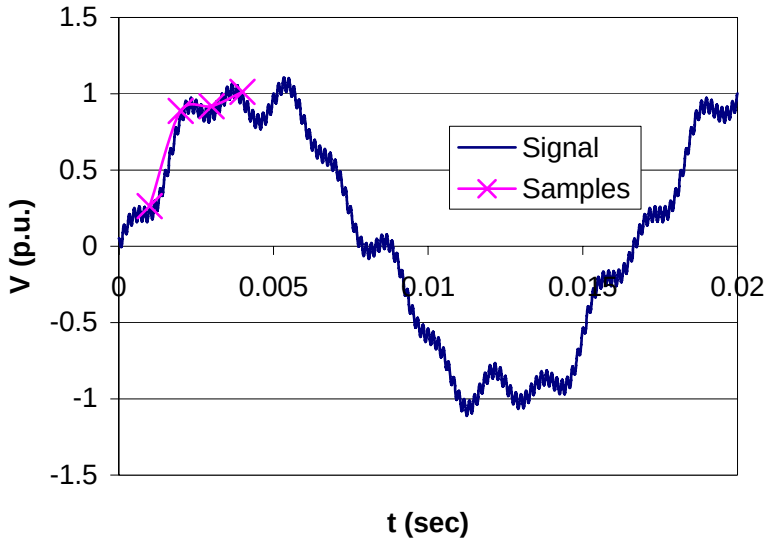

Figure 2.3 Illustrative noisy voltage signal and PMU samples

2.6 Location of PMUs

PMU placement can be done using several different criteria including security concerns, observabiity, and improvement in state estimation. In this report the criterion used to determine the location of PMUs will be improvements in the state estimation. The improvement in state estimation can be further broken down into two parts: increase in accuracy; and robustness of the state estimator.

The residual vector is typically used to determine the fit of the measurements to the model in power system state estimation. The residual is used because when state estimation is being conducted for an actual system, the 'true' values of the states are not known. The residual vector as discussed earlier is $r = z - H\hat{x}$. It is convenient to use the 2-norm of the r as an index of the agreement of the measurement equations,

$$\|r\|_2 = \sqrt[2]{r^t r} \ .$$

At the solution,

$$r = z - H\hat{x} \ .$$

In this study, it is possible to examine the deviation of $\hat{x}$ from the "exact" value of x. Normally this comparison is not possible but because of the use of a test bed with a *known solution*, it is possible to use normalized error, *NE*, to assess the accuracy of $\hat{x}$,

$$NE = \frac{\|x_{exact} - \hat{x}\|_2}{\|x_{exact}\|_2} \ . \qquad (2.17)$$

The normalized error has benefits for comparing direct substitution to weighted least squares. The normalization permits comparison of residual norms for residual vectors of different dimensions. Table 2.2 shows the various measurements of error.

Table 2.2 List of various measurements of error in the state vector

Normalized Error	$NE = \dfrac{\left\|x_{exact} - \hat{x}\right\|_2}{\left\|x_{exact}\right\|_2}$
Norm of the Residual	$\left\|r\right\|_2 = \left\|z - H\hat{x}\right\|_2$
Weighted Residual Norm	$\left\|r_w\right\|_2 = \left\|\sqrt{W}z - \sqrt{W}H\hat{x}\right\|_2$
RMS of Residual	$R_{rms} = \dfrac{1}{\sqrt{m}}\left\|z - H\hat{x}\right\|_2$

As discussed in Section 2.3 the minimization of the condition number of the *G* matrix can provide a location for PMU placement. Having an *G* with a smaller condition number will result in state estimator that will provide more accurate results when noise is present in the measurement vector. Examination of a radial system indicates simple expressions for the gain matrix *G* and also for various condition indicators of *G*. The work done in [68] resulted a determination of the condition number for a radial system with only power flow measurements and between all the busses are the same. The condition number can then be computed as

$$K_1(H) = 2n(n+1). \tag{2.18}$$

where *n* is the number of buses in the system, thus as the number of buses in the system increases so does the condition number. The reference [68] also presents a method for finding the condition number of radial system with only power injection measurements.

Another paper examined what would happen to condition number as power measurements are replaced by PMU measurements in the radial case. The results of [66] were that with proper weighting of the measurements the condition number could be determined as function of number of PMUs and number of buses. Let μ be the number of PMU buses and *n* be the number system of buses. If

$$\frac{4}{R_p} < \frac{1}{R_v}$$

and

$$R_v < \frac{R_p(n-\mu)(n-\mu+1)}{2},$$

then the condition number is

$$K_1(H) = \frac{R_p(n-\mu)(n-\mu+1)}{2R_v}. \qquad (2.19)$$

Note that the foregoing focused on the radial configuration. Figure 2.4 is a graphic that depicts the "spectrum" of the degree of networking of a system. The fully networked case (i.e., all the buses connected to all other buses) is shown to the right of Figure 2.4 and fully radial systems are to the far left of Figure 2.4. "Real" networks lie in between these extremes.

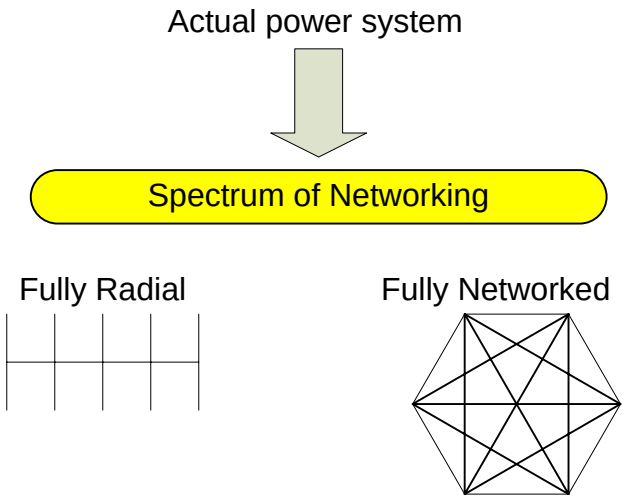

Figure 2.4 "Spectrum" of the networking extremes of electric power systems

It can be shown that a similar equation to (2.18) is valid for the fully networked system. Equation 2.20 is the condition number of the fully networked system as it relates to the number of buses in the system,

$$K_1(H) = 2n - 3. \qquad (2.20)$$

Note that (2.20) is linear compared to the quadratic form in (2.18) and that the fully networked system condition number is always smaller than the radial system of the same size. The condition number of a "real" system will be in between values found using (2.18) and (2.20).

2.7 The Sensitivity of Condition Indicators to Added State Measurements

Added measurements to an existing system which already contains m measurements causes the process matrix H to augment with added rows. State estimator design is often considered for an existing system with a previously designed set of measurements. Consider the case of μ added measurements to a system with m measurements already in place. Further, let the added measurements be of states (i.e., entries of the state vector x). The addition of added state measurements is pertinent due to the interest in the utilization of phasor measurement units (PMUs) or synchrophasor measurements [35, 69]. Then H becomes a $m + \mu$ by s matrix, but the dimension

of G remains s by s. Consider further the case that the added measurements are direct measurements of μ states. Then the added rows of H consist of all zero entries except in μ columns which may be collectively called columns k where the nonzero entries are $\Delta h_{k1}, \Delta h_{k2}, ..., \Delta h_{k\mu}$. The gain matrix G experiences the addition of $+(\Delta h_{k1})^2, +(\Delta h_{k2})^2, ..., (\Delta h_{k\mu})^2$ in the $\{k_1,k_1\}$, $\{k_2,k_2\}$, … , $\{k_\mu,k_\mu\}$ diagonal positions. Thus the condition indicators of G will change due to the added measurements. The change in eigenstructure of a matrix due to the change of elements of that matrix is well known. For example, the sensitivity of the eigenvalue λ_j of G to a single diagonal entry $G_{i,\,i}$ is given by [67],

$$\frac{\partial \lambda_j}{\partial G_{i,i}} = (V_{i,j})^2 \tag{2.21}$$

where V is the s by s matrix of eigenvectors of G arranged column-by-column, and the eigenvectors are selected as unit length. The matrix V is called the modal matrix of G. The sensitivity of λ_j to several changes of entries on the diagonal of G, namely $+(\Delta h_{k1})^2, +(\Delta h_{k2})^2, ...$ in the positions $\{k_1,k_1\}$, $\{k_2,k_2\}$, … is found using (2.17) and superimposing (adding) the several sensitivities corresponding to $i = k_1, k_2, \ldots$. Because the condition indicators are intimately related to the eigenvalues of G, it is possible to 'design' (i.e., locate, and assign measurement weights) the added state measurement entries with a view of improving the several condition indicators.

For purposes of discussion, the condition analysis of added state measurements is now confined to the addition of one measurement at state k, *i.e.*, μ=1. The generalization to the case of many added state measurements is discussed below. If the added measurement of state k results in Δh_k in the H matrix, and $(\Delta h_k)^2$ is sufficiently small, (2.21) may be used to estimate the condition indicators using

$$\Delta \lambda_j \approx \frac{\partial \lambda_j}{\partial G_{i,i}} \Delta G_{i,i} .$$

The results are

$$\Delta d = V_{k1}^2 (\Delta h_k)^2 \tag{2.22}$$

$$\Delta K_G = \frac{V_{ks}^2 - k_G V_{k1}^2}{\lambda_1 + V_{k1}^2 (\Delta h_k)^2} (\Delta h_k)^2 \tag{2.23}$$

$$\Delta f = V_{ks}^2 (\Delta h_k)^2 . \tag{2.24}$$

Note that in (2.22 – 2.24), the difference condition indicator terms are given by, for example, $\Delta d = d_{new} - d_{old}$. For the case that $(\Delta h_k)^2$ is small, the following approximation may be used in place of (2.23),

$$\Delta K_G = \frac{V_{ks}^2 - K_G V_{k1}^2}{\lambda_1} (\Delta h_k)^2 . \qquad (2.25)$$

2.8 Summary of Proposed Innovative Concepts

The in depth study and review of condition analysis for state estimation revealed a correlation between decreasing the condition number of the gain matrix and increasing the accuracy of state estimates. Some other innovative concepts presented in Chapter 2 include:

- *Singular distance* – calculating the distance between matrix *A* and the closest singular matrix.
- *Scaling factor* – viewing the largest singular value of matrix *A* as a condition indicator.
- *Measurement placement using eigenvectors* – the use of eigenvector of smallest eigenvalue to find placement of measurements.

3. Illustrative Applications of Condtion Indices Based Approaches to State Estimatior Design

3.1 The Spectrum of Condition Indicators in State Estimator Applications

As a quick illustration of the usual order of magnitude of some singular distances, scaling factors and condition numbers in this power engineering application, see Table 3.1. For convenience, the collective reference to K_G, d, and f shall be as to *condition indicators*. The study of the condition indicators will be termed *condition analysis*.

Table 3.1 Condition indicators of some illustrative power systems*

		Radial system of N buses	Fully networked system of N busses (all buses connected to all other buses)
Impedances of lines		All unity	All unity
Number of buses		N	N
Number of lines		N-1	$\frac{N}{2}(N-1)$
Number of line P measurements		N-1	$\frac{N}{2}(N-1)$
Number of line Q measurements		N-1	$\frac{N}{2}(N-1)$
Number of bus $\|V\|$ measurements		N	N
Number of injection measurements		0	0
Number of measurements, m		$3N$-2	N^2
Number of states, s		$2N$-1	$2N$-1
Condition indicators	K_G	$2N^2$	$N+1$
	d	$2.5/N^2$	1
	F	5	$N+1$

3.2 Two Test Beds for Condition Analysis

The two previous examples are of the extremes of the "spectrum" of networking, engineering intuition indicates that the IEEE 57 test bed [56] lies somewhere in between. Figure 3.1

* 2-norms are used for the condition indicators. Representative results are shown for the cases indicated. All bus voltages measured, all line P,Q measured; unbiased estimates, at the first iteration. Values shown are for large N.

is an oneline diagram of the IEEE 57 test bed system. The IEEE 57 bus test bed (System 1) has 30 buses in which there are 2 lines connected to the bus (i.e. similar to a radial system) and 1 bus that has one line connected to the bus. System 1 has 26 buses in which there are 3 or more lines connected and there are 80 lines total in the system. Table 3.2 shows these bus connection data comprising the two systems being studied. Note that in Table 3.2 the notation $\delta(a)$ is the discrete dirac delta function which is zero everywhere except when $a=1$ where $\delta(a)=1$.

Table 3.2 Topology characteristics of Systems 1 and 2

System	N_b	N_l	Number of Buses at which only 1 line incident	Number of Buses at which 2 lines incident	Number of buses at which ≥ 3 lines incident
Radial	*N*	*N-1*	*2*	*N-2*	*0*
IEEE 57 (System 1)	57	80	1	30	26
Representative power system in the southwest US (System 2)	180	254	12	103	65
Fully Networked	*N*	*N(N-1)/2*	*2δ(N-2)*	*3δ(N-3)*	*N*

The *H* matrix for the IEEE 57 bus test bed has varying admittance values this will influence the condition number of the *H* matrix. The measurement set for the *H* matrix is all the real and reactive power flows and real and reactive power injections at busses 1, 2, 3, 6, 7, 9, 12, 25, 53, 18 for Example 1. The reactance of the lines in the system range from 0.0152 p.u. to 1.355 p.u. or two orders magnitude between the smallest line parameters to the largest line parameters.

The other system to be studied in this report is representative of the power system in the southwest US (System 2). System 2 contains 180 busses, and 254 lines. The system has impedances from $1x10^{-5}$ to 0.4787. The measurement set is 239 power flow measurements, 236 reactive power flow measurements, 99 power injection measurements, 99 reactive power injection measurements, and 75 bus voltage measurements. Table 3.3 is list of *condition indicators* for both System 1 and 2.

Table 3.3 Condition indicators of System 1 and System 2

		IEEE 57 bus system [40]	Representative power system in the southwest US
Impedances of lines		Actual line impedances used	Actual line impedances used
Number of buses		*57*	*180*
Number of lines		*80*	254
Number of line *P* measurements		*80*	239
Number of line *Q* measurements		*80*	236
Number of bus |*V*| measurements		*0*	75
Number of injection measurements		*24*	*198*
Number of measurements, *m*		*184*	748
Number of states, *s*		*113*	*359*
Condition indicators	K_G	24,593	$6.9x10^{10}$
	D	0.4633	1.1648
	F	11,368	$8.0019x10^{10}$

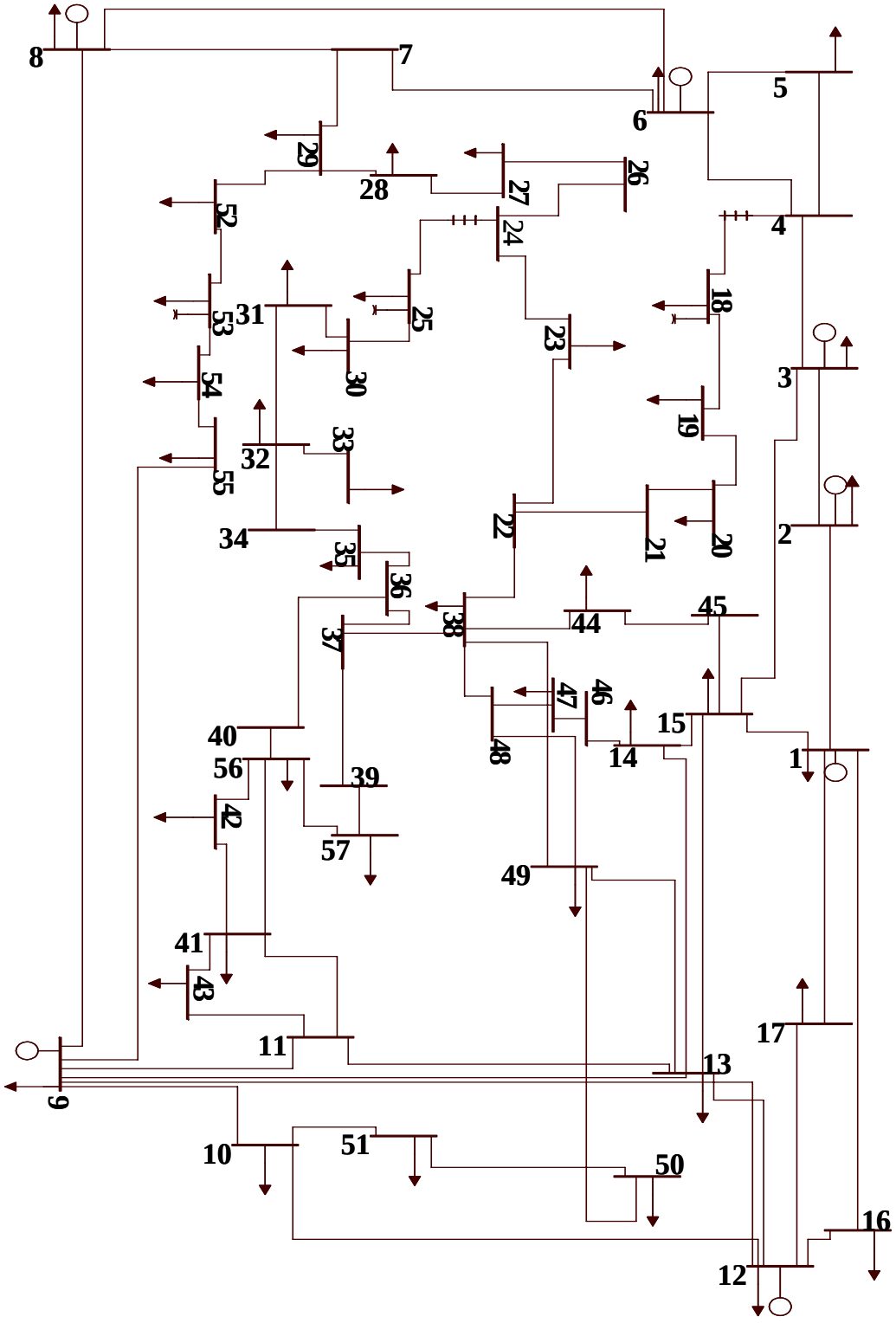

Figure 3.1 Oneline diagram of the IEEE 57 test bed case study (System 1) taken directly from [56]

3.3 Linearized Approximations of Condition Indicators Using the Power-Phase Quadrant of the H matrix

At this point, several examples are presented to illustrate the use of condition indicators for state estimation design. All examples appear in detail in Appendix A.

Example 1 is performed on System 1 but is only power-phase quadrant of the *H* matrix. Example 1 is constructed to verify (2.22), the approximation of *d*, distance to the nearest singular matrix. Distance to the nearest singular matrix is also the smallest eigenvalue. In Example 1, an extra row is augmented to the *H* matrix in which a single +1 is inserted in the column corresponding to the bus location at which a phasor angle measurement is added.

Figure 3.2 shows that the linear approximation, noted as "Predicted," is a good indicator for which +1 change in the *H* will have the greatest impact on *d*. Both the linearized and actual change in *d* show the greatest improvement for a phasor measurement placed at bus 32. Figure 3.2 also shows that the predicted change in *d* can be significantly larger than what is actually observed.

Example 2 is performed on System 1 using only the power-phase quadrant of H. Example 2 will examine how the size of Δh affects the accuracy of the prediction of *d* from (2.22). In Example 1 it was seen the best improvement in *d* could be found by placing a phasor measurement at bus 32. For Example 2, the phasor measurement will be placed at bus 32. The size of Δh will be varied from 0 to 2.

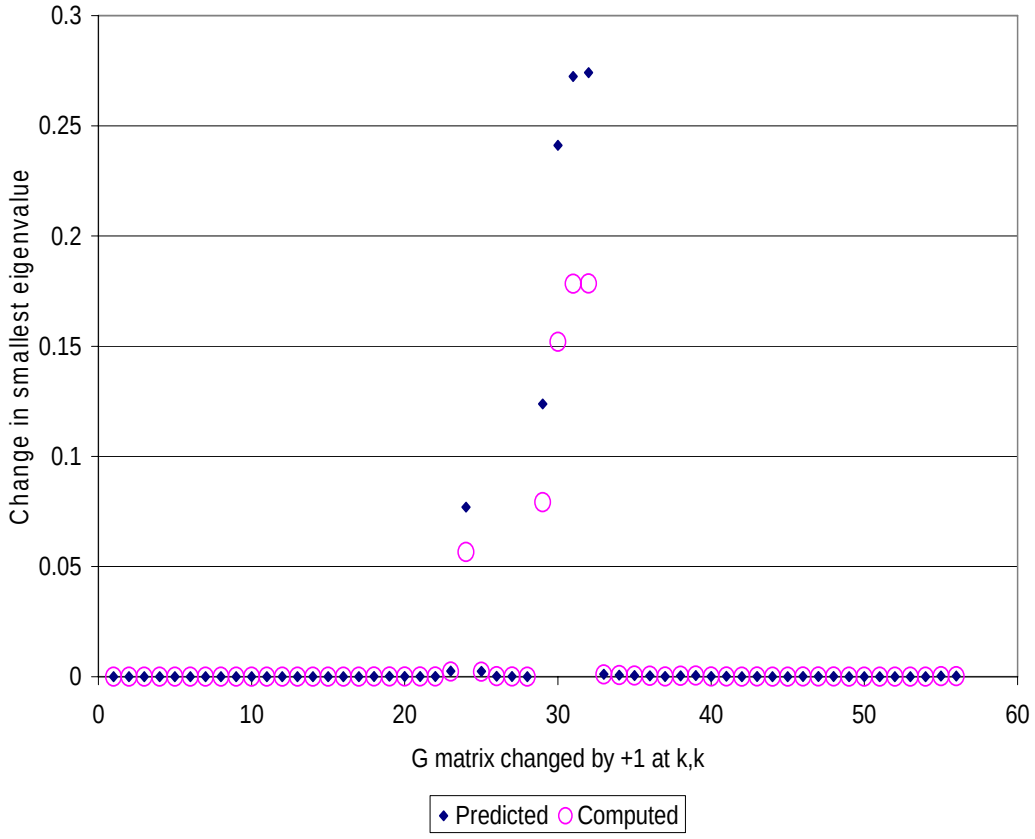

Figure 3.2 Impact on *d* of placement of a phasor measurement at one bus (Example 1)

Figure 3.3 depicts the predicted change in d using (2.22) and the actual change in d. It can be noted that in (2.22) there is a quadratic relationship between Δh and change in d. In Figure 3.3, the actual change in d "levels off" as Δh continues to increase. This can be contributed to the smallest eigenvalue of G is no longer the same eigenvalue. That is, as elements of H change, the eigenvalues of G migrate. The eigenvalues of G "move" smoothly as $h_{i,j}$ changes and it is possible that the locus of the smallest eigenvalues will cross the locus of another eigenvalue. In this sense, the previously identified smallest eigenvalues may not longer be the smallest.

To confirm that the leveling off in Example 2 is attributed to smallest eigenvalue being different after the addition of phasor measurement, Example 3 was constructed. In Example 3 the power-phase quadrant of H of System 1 was used. A phasor measurement at bus 32 was augmented to the H matrix with a +1 in the 32nd column. Figure 3.4 shows the spectrum of the eigenvalues of G. Note there is very little change in the eigenvalues of G by the addition of phasor measurement at bus 32. Also note that the eigenvalues predicted using (2.22) agree with the actual values found after the augmentation of H.

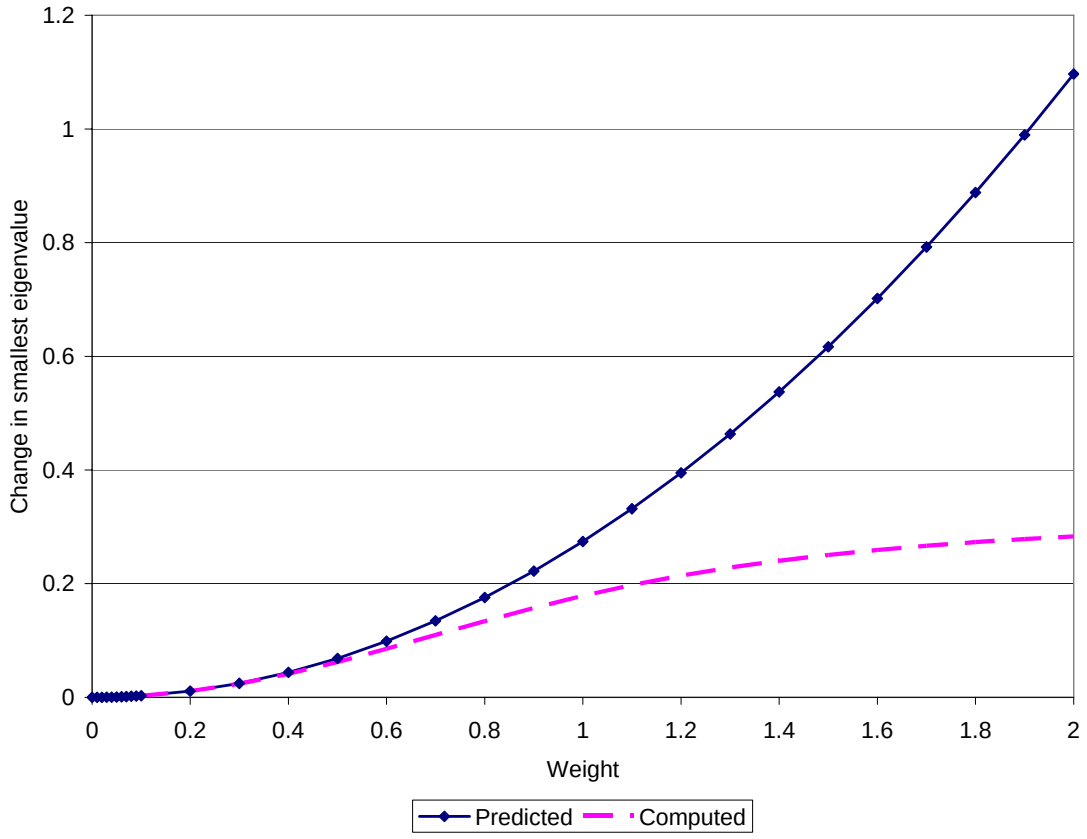

Figure 3.3 Magnitude variations in Δh versus change in d (Example 2)

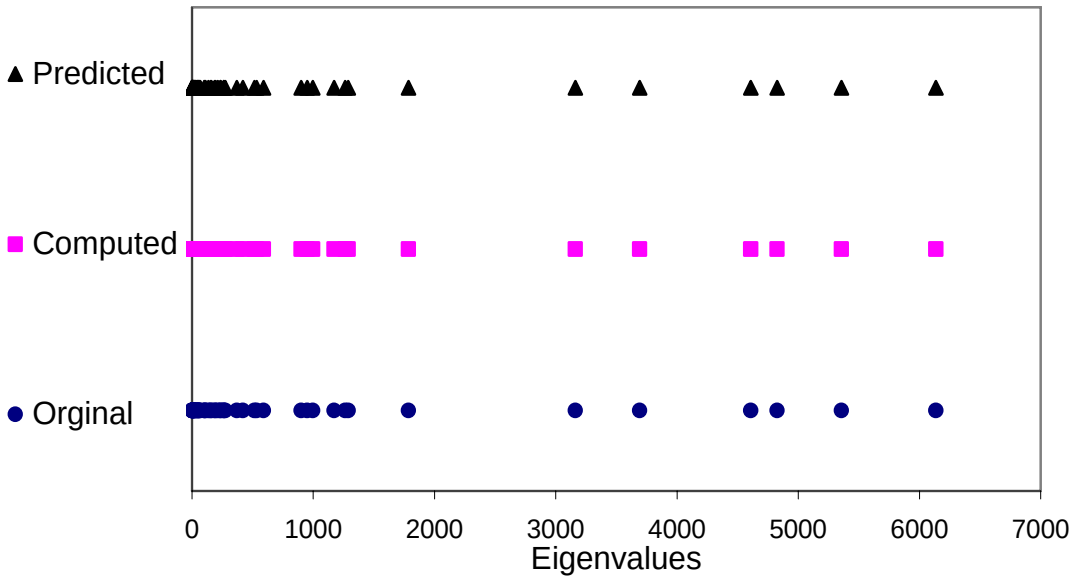

Figure 3.4 Spectrum of eigenvalues of Example 3

3.4 Linearized Approximations of Condition Indicators Using the Full H Matrix

The next series of examples examines the impact of linearizations when two measurements are added, one being the phasor measurement, and two being the voltage measurement. Equation 2.22 can be used with changes in multiple columns of H provided the columns of H are linearly independent. The change in d will be addition of the changes in the columns of H mapped onto the changes in the smallest eigenvalue by (2.22).

Example 4 is performed on System 1 using entire H matrix. Example 4 is to verify (2.22), the approximation of d, distance to the nearest singular matrix. In Example 4, two rows are augmented to the H in which +1 is inserted in the columns corresponding to the phase angle locations at which phasor angle measurements were added.

Figure 3.5 shows linear approximation, noted as "Predicted," is a good indicator for which change in the H will have the greatest impact on d. Both the linearized and actual change in d show the greatest improvement for a phasor measurement placed at bus 32. Figure 3.5 also shows that predicted change in d can be significantly larger than what is actually change in d.

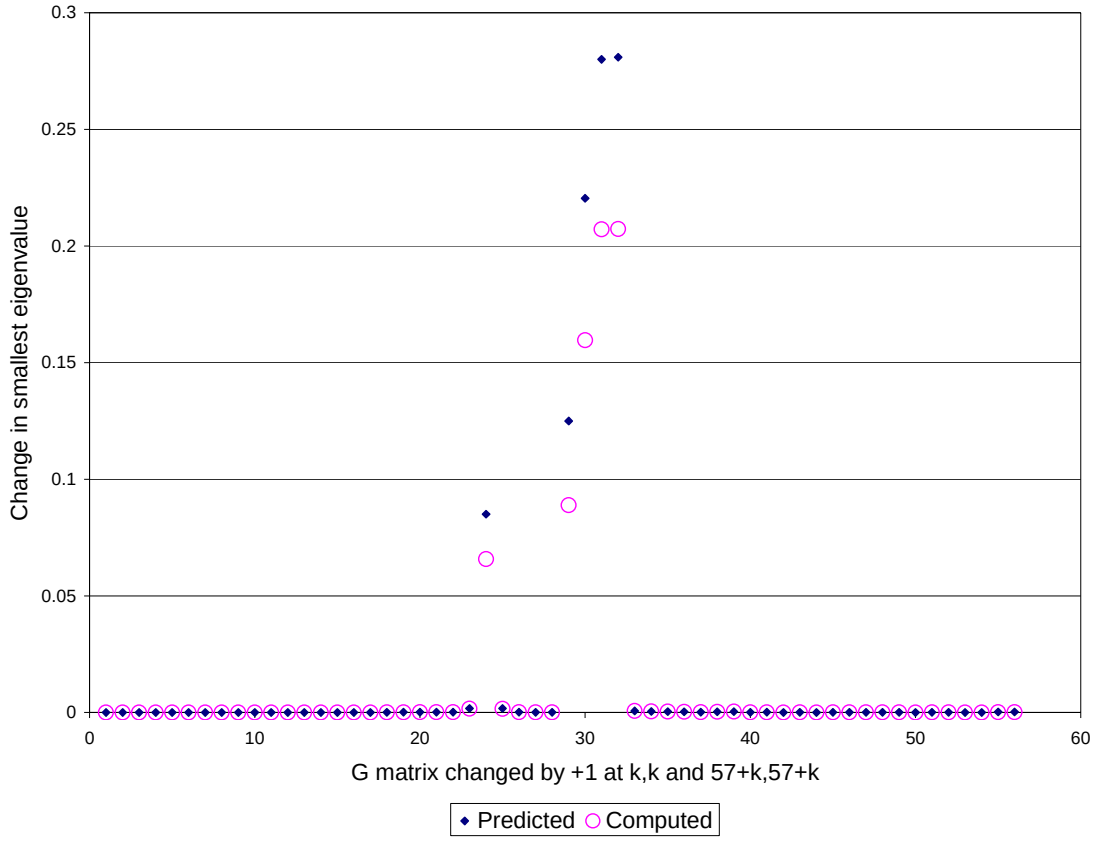

Figure 3.5 Impact on *d* of placement of a phasor measurement and voltage magnitude at one bus (Example 4)

Equation 2.25 is a linearized model for the change in condition number of *G* based on the change in Δh. Figure 3.6 is displays the change in condition number of *H* as a voltage magnitude and phase angle measurement are added to the *H* matrix. Note that Bus 32 is the bus with greatest change in both the using (2.25) and actual change in condition number. Also note that the predicted change is much greater than the actual change.

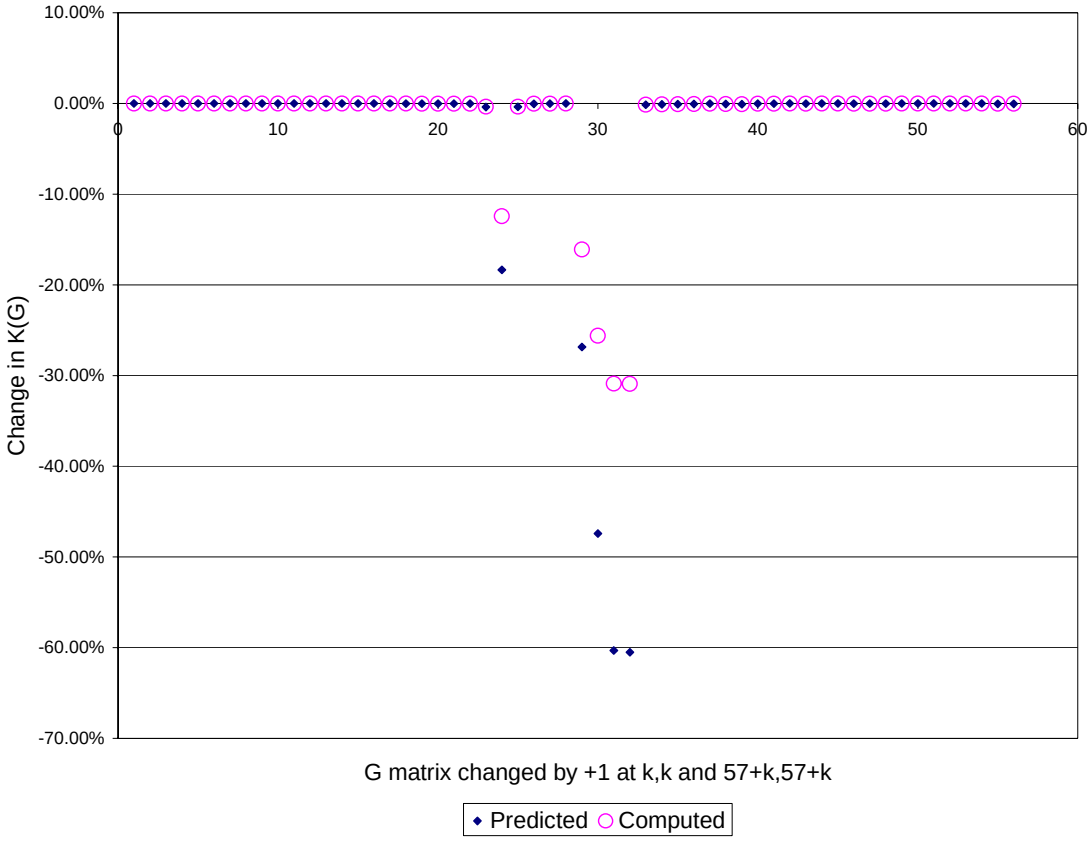

Figure 3.6 Impact on condition number of *G* of placement of a phasor measurement and voltage magnitude at one bus (Example 4)

Figure 3.7 shows Example 1 and Example 4 on the same chart. Note that the improvement seen *d* is greater for the full *H* (Example 4) than just the power-phase quadrant of *H* (Example 1).

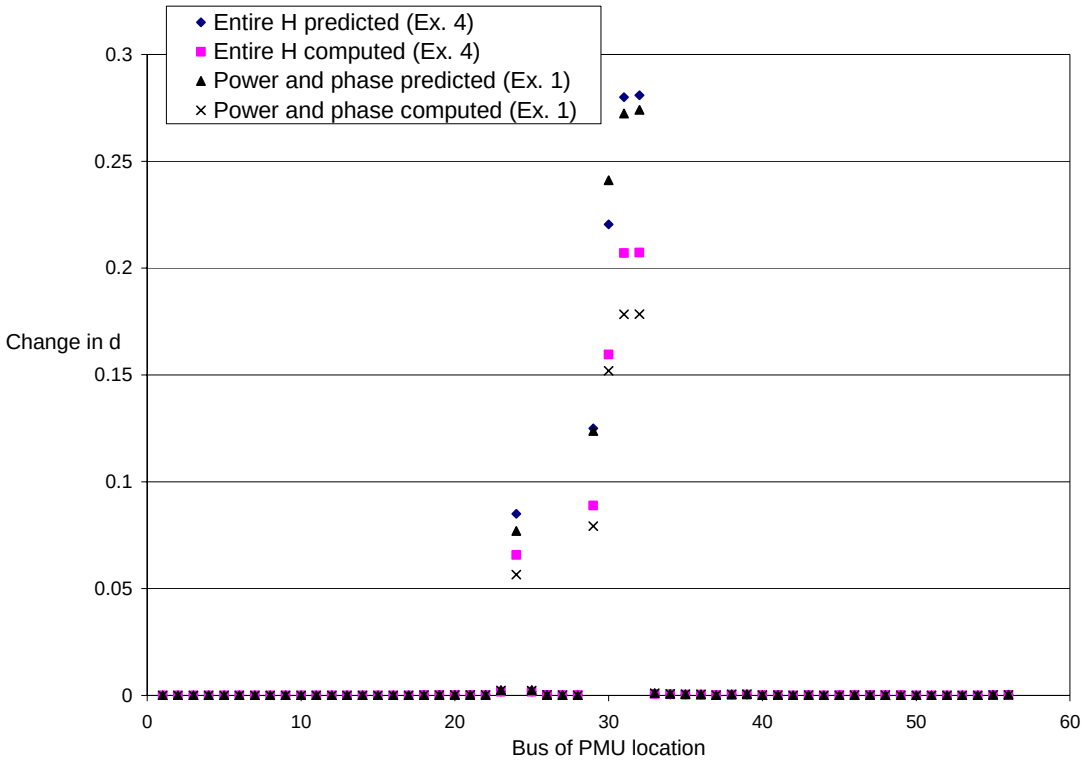

Figure 3.7 Example 1 and Example 4 changes in *d*

Example 5 is performed on System 1 using the entire *H* matrix. Example 5 will examine how the size of Δh affects the accuracy of the prediction of *d* from (2.22). In Example 4, it was seen that the best improvement in *d* could be found by placing a phasor and voltage magnitude measurement at bus 32. For Example 5, the phasor measurement and voltage magnitude measurement will be placed at bus 32. The size of Δh will be varied from 0 to 2.

Figure 3.8 show the predicted change in *d* using (2.22). This is compared to the actual change in *d*. It can be noted that in (2.22) there is a quadratic relationship between Δh and change in *d*. In Figure 3.8 the actual change in *d* levels off as ΔH continues to increase. This flattening can be attributed to the fact that the smallest eigenvalue of *H* is no longer the "same" eigenvalue.

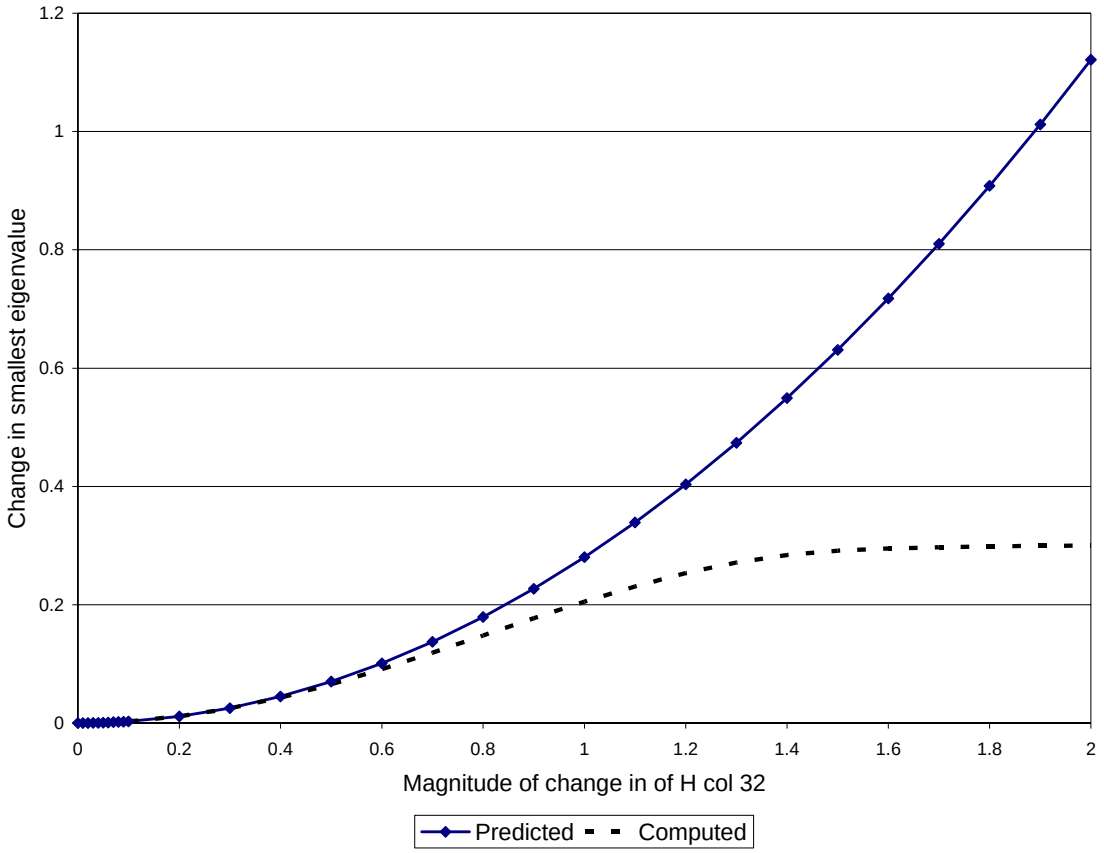

Figure 3.8 Magnitude variations in Δh versus change in d (Example 5)

Example 6 was constructed to confirm that the leveling off in Example 5 is attributed to smallest eigenvalue being different after the addition measurements. In Example 6, the entire H of System 1 was used. A phasor measurement at bus 32 was augmented to the H matrix with +1 in 32nd column. A voltage magnitude measurement at bus 32 was augmented to the H matrix with +1 in 89th column. Figure 3.9 shows the spectrum of the eigenvalues of G for the three cases discussed. Note there is very little change in the eigenvalues of G by the addition of a phasor measurement at bus 32. Also note that the eigenvalues predicted using (2.22) agree with the actual values found.

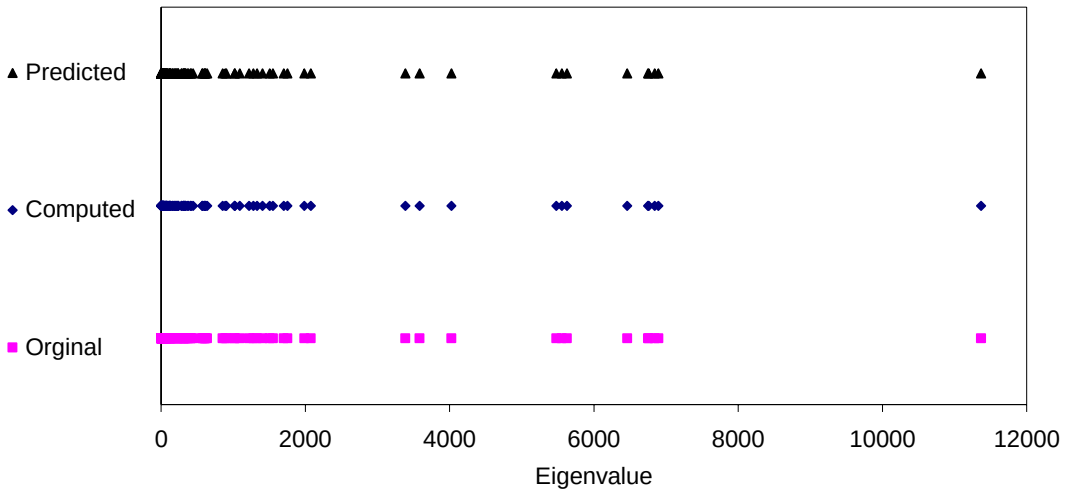

Figure 3.9 Spectrum of eigenvalues of Example 6

3.5 Summary of Examples

Table 3.4 summarizes Examples 1-6. The main observations are:

- Small change is seen between the prediction of the change in the smallest eigenvalue using the power-phase quadrant of H (Example 1) and using the entire H (Example 4).
- Equation 2.22 predicted the correct location of the largest improvement of the smallest eigenvalue, d, but yielded a significantly larger estimate of improvement than the actual computed value.
- Equation 2.22 can predict all eigenvalues using limited information from the eigenvector matrix.
- Decreasing the weight applied to the added measurement will improve the accuracy of (2.22).
- The augmentation of one PMU to System 1 in Example 4 decreased the condition number by 30.91%.

Table 3.4 Summary of Examples 1 - 6

Example	Intent of Example	Conditions	Outcome
1	To find greatest improvement in smallest eigenvalue of the power-phase quadrant of *H* using (2.22)	Augment power-phase quadrant of *H* with a +1 at (*m*+1, *k*)	Equation 2.22 predicted the correct location of the largest change
2	To see the effects of weighting the augmented measurement	Augment power-phase quadrant of *H* with 0<*w*<2 at (*m*+1, 32)	Decrease weight on the augmented measurement produced more accurate prediction *d* using (2.22)
3	Verify (2.22)	Augment power-phase quadrant of *H* with a +1 at (*m*+1, 32)	Equation 2.22 can predict the change in all eigenvalues accurately using a single row in the eigenvector matrix
4	To find greatest improvement in smallest eigenvalue of *H* using (2.22)	Augment of *H* with a +1 at (*m*+1, *k*) and (*m*+2, *k+57*)	Equation 2.22 predicted the correct location of the largest change
5	To see the effects of weighting the augmented measurement	Augment *H* with a +1 at (*m*+1,32) and (*m+2,* 89)	Decrease weight on the augmented measurement produced more accurate prediction *d* using (2.22)
6	Verify (2.22)	Augment power-phase quadrant of *H* with 0<*w*<2 at (*m*+1, 32) and (m+2, 89)	Equation 2.22 can predict the change in all eigenvalues accurately using two rows in the eigenvector matrix

4. Algorithm For the Placement of Phasor Measurements

4.1 Introduction

In this chapter, future work is presented for the application of condition indicators for state estimator design. The designs utilize PMU measurements. Also, an innovative analogy to capacity outage tables [70] is proposed to study "measurement outages" (i.e., measurement failure). The concept is to tabulate all possible sensory failure scenarios and evaluate the expected state estimation error over all scenarios.

The main topics discussed in this chapter are:

- The focus of discussion in this report has been on the *G* and *H* matrices of the linearized state estimator problem. That is, the first iteration *G* and *H* were studied. It is proposed as future work to examine the effect of the progress of the iterations on a full nonlinear state estimator on the *G* and *H*, and the concomitant response of the condition indicators.
- A procedure for state estimation design using PMU measurements. The concept of condition indicators is to be used.
- The measurement outage table approach to calculation of expected state estimation error
- The utilization of a large test bed to demonstrate the design procedure
- A comparison of the proposed method with other methods.

4.2 State Estimation Design via Condition Indicators

The process of designing the state estimator with phasor measurement units is represented in Figure 4.1. In Figure 4.1, it is suggested to utilize the condition indicators to assess the effectiveness of added sensory measurements. The steps shown in Figure 4.1 are preliminary and future research will be to refine these steps. The focus is to locate measurements and to calculate the corresponding gain matrix.

As an example of the research approach, it is proposed to compute the condition indicators for all possible sensor locations. In this procedure it is determined if the state estimator is observable using the condition indicators, (i.e., if d=0 then the gain matrix is singular, and the system is not observable). If the system is not observable, place PMUs at locations such that the system becomes observable. If the system is observable, place PMUs at proper locations to improve the condition number indicators (i.e., place a PMU in locations such that the singular distance, *d*, would increase). Subsequently the best performance is identified from the condition indicators.

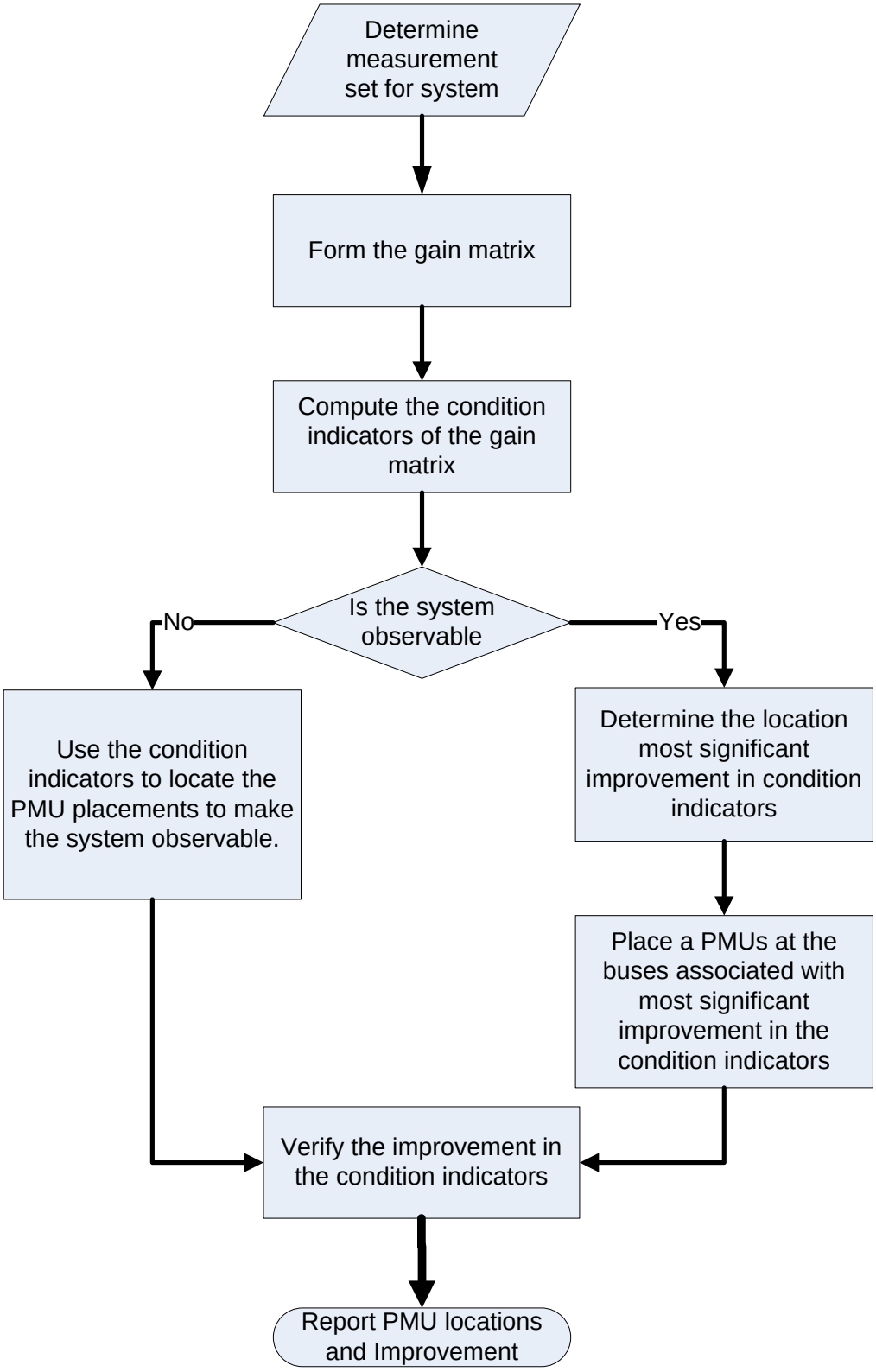

Figure 4.1 Coarse flow chart for state estimator design via condition indicators.

4.3 The Measurement Outage Table

The concept of a "measurement outage table" is proposed. This table is a tabulation of possible failure status scenarios versus their probability of occurrence. The measurement outage table will be based on the capacity outage tables described in [70]. The measurement outage table will use the probability of a measurement failure analogous to the probability of loss of generation in a generation capacity outage table [70]. Table 4.1 is a sample capacity outage table from [70]. Table 4.1 also does not the outcome of the loss of generation (i.e., if the system is power system is still capable of operating). Table 4.2 is a proposed measurement outage table. Note in Table 4.2 along with the amount of loss of measurement the table includes which measurement has failed, and the outcome of the measurement failure.

Table 4.1 Sample capacity outage table taken directly from [70]

Unit 1 (5 MW)	*Unit 2 (3 MW)*	*Unit 3 (3 MW)*	*Capacity out of service (MW)*	*Individual probability*	*Cumulative probability*
1	1	1	0	0.941192	1.000000
1	1	0	3	0.019208	0.058808
1	0	1	3	0.019208	0.039600
0	1	1	5	0.019208	0.020392
1	0	0	6	0.000392	0.001184
0	1	0	8	0.000392	0.000792
0	0	1	8	0.000392	0.000400
0	0	0	11	0.000008	0.000008

Status 1 = in service
Status 0 = out of service

The measurement outage table is offered as a potential tool to analyze state estimation sensory impacts. For example, using the right most columns of Table 4.2, it is possible to statistically evaluate the condition indicators. It is conjectured that it is possible to identify where a phasor measurement can be placed to increase the robustness of the state estimator design, (i.e., the entire system is still observable after a measurement failure). The performance indicators used in the table should not only detect if a measurement outage produces a unobservable island, but should also detect how "well conditioned" the process matrix, *H*, is, and the impact of measurement failure on state estimator expected error.

Table 4.2 Representation of a possible measurement outage table

	Sensor Outage State							Individual Prob.	Cumulative Prob.	State Estimator Performance			
	1	2	3	4	…	*m*-1	*m*			K_G	λ_1	*E(error)*	*f*
For one sensor failure	1	1	1	1	…	1	0			The state estimation performance indicators might include: expected error value, condition number, smallest eigenvalue, largest eigenvalue, singular distance, and scaling factor.			
	1	1	1	1		0	1						
	…					…							
	1	0	1	1	…	1	1						
	0	1	1	1		1	1						
For two sensors failure	1	1	1	1	…	0	0						
	…					…							
	0	0	1	1	…	1	1						
for "N-3," "N-4," … cases													

4.4 Test Bed of Demonstration

The experiments performed in this report have been performed on the IEEE 57 bus test bed (System 1). System 1 has 57 buses, 80 transmission lines, 184 measurements, and 113 states. This system is moderate in size. A larger test bed developed to be used in future research. It is proposed to use System 2, a system representative of the US southwest in summer 2005. Table 4.3 contains pertinent data of System 2. This system is approximately 3 times the size of System 2.

Table 4.3 Summary of System 2 parameters

Number of Buses	180
Number of Transmission Lines	254
Number of States	359
Number of Measurements	748

4.5 Comparison of Alternative Phasor Measurement Placement Methods

The design of state estimator described in 4.3 will be compared to several methods of finding the "best" placement of PMUs:

- *Genetic Search / Random Search* – the search method using a small sample set to determine the global optimum of search criteria,
- *Graph Theory* – the PMUs are placed until the entire power system is observable,
- *Residual Sensitivity Matrix Analysis* – placement of PMUs is done based on identification of critical measurements.

The comparison between the above mentioned state estimator design criteria will be both quantitative and qualitative. Most of the results from the comparisons will be qualitative due to the diverse optimal placement algorithms having alternative definitions of optimal placement. Quantitative comparisons can be made if the state estimator designs are performed on the same system with similar design objectives.

References

[1] J. W. F. Shweppe, D. Rom, "Power system static state estimation: part I, II, and III," in *Power Industry Computer Conference*, 1969.

[2] P. Zarco and A. G. Exposito, "Power system parameter estimation: a survey," *IEEE Transactions on Power Systems*, vol. 15, pp. 216-222, 2000.

[3] S. Zhong and A. Abur, "Auto tuning of measurement weights in WLS state estimation," *IEEE Transactions on Power Systems*, vol. 19, pp. 2006-2013, 2004.

[4] A. Monticelli, *State estimation in electric power systems : a generalized approach*. Boston: Kluwer Academic Publishers, 1999.

[5] A. Monticelli, "Electric power system state estimation," *Proceedings of the IEEE*, vol. 88, pp. 262-282, 2000.

[6] A. J. Wood and B. F. Wollenberg, *Power generation, operation, and control*, 2nd ed. New York: J. Wiley & Sons, 1996.

[7] S. Gastoni, G. Granelli, and M. Montagna, "Robust state-estimation procedure based on the maximum agreement between measurements," *IEEE Transactions on Power Systems*, vol. 19, pp. 2038-2043, 2004.

[8] J. B. Carvalho and F. M. Barbosa, "A modern state estimation in power system energy," *International Conference on Electric Power Engineering, PowerTech Budapest*, 1999, p. 270.

[9] O. Alsac, N. Vempati, B. Stott, and A. Monticelli, "Generalized state estimation," *IEEE Transactions on Power Systems*, vol. 13, pp. 1069-1075, 1998.

[10] A. Abur and A. Gómez Expósito, *Power system state estimation : theory and implementation*. New York, NY: Marcel Dekker, 2004.

[11] A. P. S. Meliopoulos and G. K. Stefopoulos, "Characterization of state estimation biases," *International Conference on Probabilistic Methods Applied to Power Systems*, 2004, pp. 600-607.

[12] M. M. Adibi, K. A. Clements, R. J. Kafka, and J. P. Stovall, "Remote measurement calibration," *IEEE Computer Applications in Power*, vol. 3, pp. 37-42, 1990.

[13] M. M. Adibi, K. A. Clements, R. J. Kafka, and J. P. Stovall, "Integration of remote measurement calibration with state estimation-a feasibility study," *IEEE Transactions on Power Systems*, vol. 7, pp. 1164-1172, 1992.

[14] J. G. Moreno, J. L. M. Vigil-Escalera, and R. S. Alvarez, "Statistical measurement calibration based on state estimator results," in *IEEE Transmission and Distribution Conference*, 1999, pp. 184-189 vol.1.

[15] S. Zhong and A. Abur, "Combined state estimation and measurement calibration," *IEEE Transactions on Power Systems*, vol. 20, pp. 458-465, 2005.

[16] M. E. El-Hawary, "Bad data detection of unequal magnitudes in state estimation of power systems," *Power Engineering Review, IEEE*, vol. 22, pp. 57-60, 2002.

[17] F. C. Schweppe, *Uncertain dynamic systems*. Englewood Cliffs, N.J.,: Prentice-Hall, 1973.

[18] I. O. Habiballah, "Modified two-level state estimation approach [for power systems]," *Generation, IEE Proceedings- Transmission and Distribution*, vol. 143, pp. 193-199, 1996.

[19] M. V. F. Pereira and N. J. Balu, "Composite generation/transmission reliability evaluation," *Proceedings of the IEEE*, vol. 80, pp. 470-491, 1992.
[20] G. H. Golub and C. F. Van Loan, *Matrix computations*. Baltimore: Johns Hopkins University Press, 1983.
[21] R. A. Jabr and B. C. Pal, "Iteratively reweighted least-squares implementation of the WLAV state-estimation method," *IEE Proceedings- Generation, Transmission and Distribution*, vol. 151, pp. 103-108, 2004.
[22] B. Gou and A. Abur, "An improved measurement placement algorithm for network observability," *IEEE Transactions on Power Systems*, vol. 16, pp. 819-824, 2001.
[23] E. Castillo, A. J. Conejo, R. E. Pruneda, and C. Solares, "State Estimation Observability Based on the Null Space of the Measurement Jacobian Matrix," *IEEE Transactions on Power Systems*, vol. 20, pp. 1656-1658, 2005.
[24] R. F. Nuqui and A. G. Phadke, "Phasor measurement unit placement techniques for complete and incomplete observability," *IEEE Transactions on Power Delivery*, vol. 20, pp. 2381-2388, 2005.
[25] E. Castillo, A. J. Conejo, R. E. Pruneda, and C. Solares, "Observability analysis in state estimation: a unified numerical approach," *IEEE Transactions on Power Systems*, vol. 21, pp. 877-886, 2006.
[26] B. Gou, "Jacobian matrix-based observability analysis for state estimation," *IEEE Transactions on Power Systems*, vol. 21, pp. 348-356, 2006.
[27] S. Pajic and K. A. Clements, "Power system state estimation via globally convergent methods," *IEEE Transactions on Power Systems*, vol. 20, pp. 1683-1689, 2005.
[28] P. Ristanovic, "State estimation based real-time markets - challenges and practical solutions," 2005, pp. 2849-2850 Vol. 3.
[29] A. V. Jaen, P. C. Romero, and A. G. Exposito, "Substation data validation by a local three-phase generalized state estimator," *IEEE Transactions on Power Systems*, vol. 20, pp. 264-271, 2005.
[30] S. S. Lin and C. Huay, "An efficient algorithm for solving distributed state estimator and laboratory implementation," 2005, pp. 689-694 Vol. 1.
[31] K.-S. Cho, J.-R. Shin, and S. H. Hyun, "Optimal placement of phasor measurement units with GPS receiver," *IEEE Power Engineering Society Winter Meeting*, 2001, pp. 258-262 vol.1.
[32] A. G. Phadke, "Synchronized phasor measurements-a historical overview," *IEEE/PES Transmission and Distribution Conference and Exhibition: Asia Pacific*, 2002, pp. 476-479 vol.1.
[33] W. Lewandowski, J. Azoubib, and W. J. Klepczynski, "GPS: primary tool for time transfer," *Proceedings of the IEEE*, vol. 87, pp. 163-172, 1999.
[34] X. Dongjie, H. Renmu, W. Peng, and X. Tao, "Comparison of several PMU placement algorithms for state estimation," *Eighth IEE International Conference on Developments in Power System Protection*,2004, pp. 32-35 Vol.1.
[35] A. G. Phadke, B. Pickett, M. Adamiak, M. Begovic, G. Benmouyal, R. O. Burnett, Jr., T. W. Cease, J. Goossens, D. J. Hansen, M. Kezunovic, L. L. Mankoff, P. G. McLaren, G. Michel, R. J. Murphy, J. Nordstrom, M. S. Sachdev, H. S. Smith, J. S. Thorp, M. Trotignon, T. C. Wang, and M. A. Xavier, "Synchronized sampling and phasor measure-

ments for relaying and control," *IEEE Transactions on Power Delivery,* vol. 9, pp. 442-452, 1994.
[36] R. O. Burnett, Jr., M. M. Butts, and P. S. Sterlina, "Power system applications for phasor measurement units," *IEEE Computer Applications in Power,* vol. 7, pp. 8-13, 1994.
[37] H. Bai, S. Zhou, and Z. Guo, "Innovation Network Graph State Estimation Based PMUs," *IEEE/PES Transmission and Distribution Conference and Exhibition: Asia and Pacific,* 2005, pp. 1-6.
[38] J. Chen and A. Abur, "Improved bad data processing via strategic placement of PMUs," *IEEE Power Engineering Society General Meeting,* 2005, pp. 509-513 Vol. 1.
[39] D. Junce and C. Zexiang, "Mixed Measurements State Estimation Based on Wide-Area Measurement System and Analysis," *IEEE/PES Transmission and Distribution Conference and Exhibition: Asia and Pacific,* 2005, pp. 1-5.
[40] C. Rakpenthai, S. Premrudeepreechacharn, S. Uatrongjit, and N. R. Watson, "An Improved PMUs Placement Method for Power System State Estimation," *The 7th International Power Engineering Conference, IPEC,* 2005, pp. 1-4.
[41] L. Zhao and A. Abur, "Multi area state estimation using synchronized phasor measurements," *IEEE Transactions on Power Systems,* vol. 20, pp. 611-617, 2005.
[42] E. Price, "Practical considerations for implementing wide area monitoring, protection and control," *59th Annual Conference for Protective Relay Engineers,* 2006.
[43] G. B. Denegri, M. Invernizzi, and F. Milano, "A security oriented approach to PMU positioning for advanced monitoring of a transmission grid," *Proceedings of International Conference on Power System Technology, PowerCon,* 2002, pp. 798-803 vol.2.
[44] R. Zivanovic and C. Cairns, "Implementation of PMU technology in state estimation: an overview," *IEEE AFRICON 4th,* 1996, pp. 1006-1011 vol.2.
[45] I. Kamwa and R. Grondin, "PMU configuration for system dynamic performance measurement in large, multiarea power systems," *IEEE Transactions on Power Systems,* vol. 17, pp. 385-394, 2002.
[46] S. B. M. Ingram, S. Matthews, A. P. Meliopoulos, G Cokkinides, "Use of phasor measurements, SCADA and IED data to improve the state estimation," *7th Fault and Disturbance Analysis Conference,* April 26-27, 2004.
[47] M. Donnelly, "Eastern Interconnect Phasor Project."
[48] IEEE, "IEEE Standard for Synchrophasor for Power Systems. IEEE std. 1344-1995,"
[49] "IEEE Standard for Synchrophasors for Power Systems," *IEEE Std C37.118-2005 (Revision of IEEE Std 1344-1995),* pp. 1-57, 2006.
[50] J. Bertsch, M. Zima, A. Suranyi, C. Carnal, and C. Rehtanz, "Experiences with and perspectives of the system for wide area monitoring of power systems," *CIGRE/IEEE PES International Symposium: Quality and Security of Electric Power Delivery Systems,* 2003, pp. 5-9.
[51] D. Karlsson, M. Hemmingsson, and S. Lindahl, "Wide area system monitoring and control - terminology, phenomena, and solution implementation strategies," *IEEE Power and Energy Magazine,* vol. 2, pp. 68-76, 2004.
[52] J. F. Hauer, N. B. Bhatt, K. Shah, and S. Kolluri, "Performance of "WAMS East" in providing dynamic information for the North East blackout of August 14, 2003," in *IEEE Power Engineering Society General Meeting,* 2004, pp. 1685-1690 Vol.2.

[53] K. E. Holbert, G. I. Heydt, and H. Ni, "Use of satellite technologies for power system measurements, command, and control," *Proceedings of the IEEE,* vol. 93, pp. 947-955, 2005.
[54] I. Kamwa, R. Grondin, and Y. Hebert, "Wide-area measurement based stabilizing control of large power systems-a decentralized/hierarchical approach," *IEEE Transactions on Power Systems,* vol. 16, pp. 136-153, 2001.
[55] K. Tomsovic, D. E. Bakken, V. Venkatasubramanian, and A. Bose, "Designing the next generation of real-time control, communication, and computations for large power systems," *Proceedings of the IEEE,* vol. 93, pp. 965-979, 2005.
[56] R. Christie, "Power System Test Archive." http://www.ee.washington.edu/research/pstca/
[57] M. Mitchell, *An Introduction to Genetic Algorithms*. Cambridge, MA: MIT Press, 1998.
[58] B. Milosevic and M. Begovic, "Nondominated sorting genetic algorithm for optimal phasor measurement placement," *IEEE Transactions on Power Systems,* vol. 18, pp. 69-75, 2003.
[59] B. Xu and A. Abur, "Observability analysis and measurement placement for systems with PMUs," *IEEE PES Power Systems Conference and Exposition*, 2004, pp. 943-946 vol.2.
[60] C. Madtharad, S. Premrudeepreechacharn, N. R. Watson, and D. Saenrak, "Measurement placement method for power system state estimation: part I," *IEEE Power Engineering Society General Meeting, 2003, IEEE*, 2003, p. 1632 Vol. 3.
[61] C. Madtharad, S. Premrudeepreechacharn, N. R. Watson, and R. Saeng-Udom, "An Optimal Measurement Placement Method for Power System Harmonic State Estimation," *IEEE Transactions on Power Delivery*, vol. 20, pp. 1514-1521, 2005.
[62] G. M. Huang, J. Lei, and A. Abur, "A heuristic approach for power system measurement placement design," *Proceedings of the 2003 International Symposium on Circuits and Systems, ISCAS*, 2003, pp. III-407-III-410 vol.3.
[63] J. B. A. London, G. L. R. Brito, and N. G. Bretas, "Method for meter and RTU placement for state estimation purposes," *IEEE Bologna Power Tech Conference Proceedings,* 2003, p. 6 pp. Vol.1.
[64] R. L. Dykstra, "Establishing the Positive Definiteness of the Sample Covariance Matrix," *The Annals of Mathematical Statistics*, vol. 41, pp. 2153 - 2154, Dec., 1970.
[65] R. C. Penney, *Linear algebra: ideas and applications*. New York: John Wiley and Sons, 1998.
[66] R. Ebrahimian and R. Baldick, "State estimator condition number analysis," *IEEE Transactions on Power Systems*, vol. 16, pp. 273-279, 2001.
[67] D. K. a. V. N. F. Faddeev, *Computational methods of linear algebra*. San Francisco,: W. H. Freeman, 1963.
[68] K. A. C. J. W. Gu, G. R. Krumpholz, P. W. Davis, "The Solution of Ill-Conditioned Power System State Estimation Problems Via the Method of Peters and Wilkison," *IEEE Transactions on Power Apparatus and Systems*, vol. PAS-102, pp. 3473 - 3480, October 1983.
[69] A. G. Phadke, "Synchronized phasor measurements in power systems," *IEEE Computer Applications in Power*, vol. 6, pp. 10-15, 1993.

[70] R. Billinton, *Reliability evaluation of power systems / Roy Billinton and Ronald N. Allan,* 2nd ed. ed. New York, Plenum Press, 1996.

Appendix A: Summary of Examples

Table A.1 Summary of Examples 1 - 6

Example	Intent of Example	System	Conditions	Outcome
1	To find greatest improvement in smallest eigenvalue of the power-phase quadrant of H using (2.22)	System 1 (IEEE 57 bus test bed)	Augment power-phase quadrant of H with a +1 at (m+1, k)	Equation 2.22 predicted the correct location of the largest change
2	To see the effects of weighting the augmented measurement	System 1 (IEEE 57 bus test bed)	Augment power-phase quadrant of H with $0<w<2$ at (m+1, 32)	Decrease weight on the augmented measurement produced more accurate prediction d using (2.22)
3	Verify (2.22)	System 1 (IEEE 57 bus test bed)	Augment power-phase quadrant of H with a +1 at (m+1, 32)	Equation 2.22 can predict the change in all eigenvalues accurately using a single row in the eigenvector matrix
4	To find greatest improvement in smallest eigenvalue of H using (2.22)	System 1 (IEEE 57 bus test bed)	Augment of H with a +1 at (m+1, k) and (m+2, k+57)	Equation 2.22 predicted the correct location of the largest change
5	To see the effects of weighting the augmented measurement	System 1 (IEEE 57 bus test bed)	Augment H with a +1 at (m+1,32) and (m+2, 89)	Decrease weight on the augmented measurement produced more accurate prediction d using (2.22)
6	Verify (2.22)	System 1 (IEEE 57 bus test bed)	Augment power-phase quadrant of H with $0<w<2$ at (m+1, 32) and (m+2, 89)	Equation 2.22 can predict the change in all eigenvalues accurately using two rows in the eigenvector matrix

Appendix B: Norms

The state estimation technique presented relies on the L_2 being a satisfactory in representing the error between the measurements and the states. The L_p norm is,

$$|| r ||_p = \sqrt[p]{\sum_{i=0}^{m} \left(| x_i | \right)^p} \, . \tag{B.1}$$

There are several L norms however three most commonly discussed are the L_1, L_2, and the L_∞ norm. The L_1 norm is the sum of the absolute of the number as seen in Equation B.1. The L_2 norm is the square root of the sum of the squares, and the L_∞ norm is the largest single value in the vector,

L_1-Norm
$$|| r ||_1 = \sum_{i=1}^{m} | x_i | \tag{B.2}$$

L_2-Norm
$$|| r ||_2 = \sqrt{\sum_{i=1}^{m} \left(x_i \right)^2} \tag{B.3}$$

L_∞-Norm
$$|| r ||_\infty = \sqrt[\infty]{\sum_{i=1}^{m} \left(| x_i | \right)^\infty} = \max | x_i | \, . \tag{B.4}$$

A plot can be created of the different norms of a vector of dimension two,

$$x = (x_1, x_2)^t \tag{B.5}$$

$$|| x ||_p^p = k^p \, . \tag{B.6}$$

Figure B.1 shows loci of $||x||_p = k$. L norms are a way of collapsing data stored in a vector into a single value.

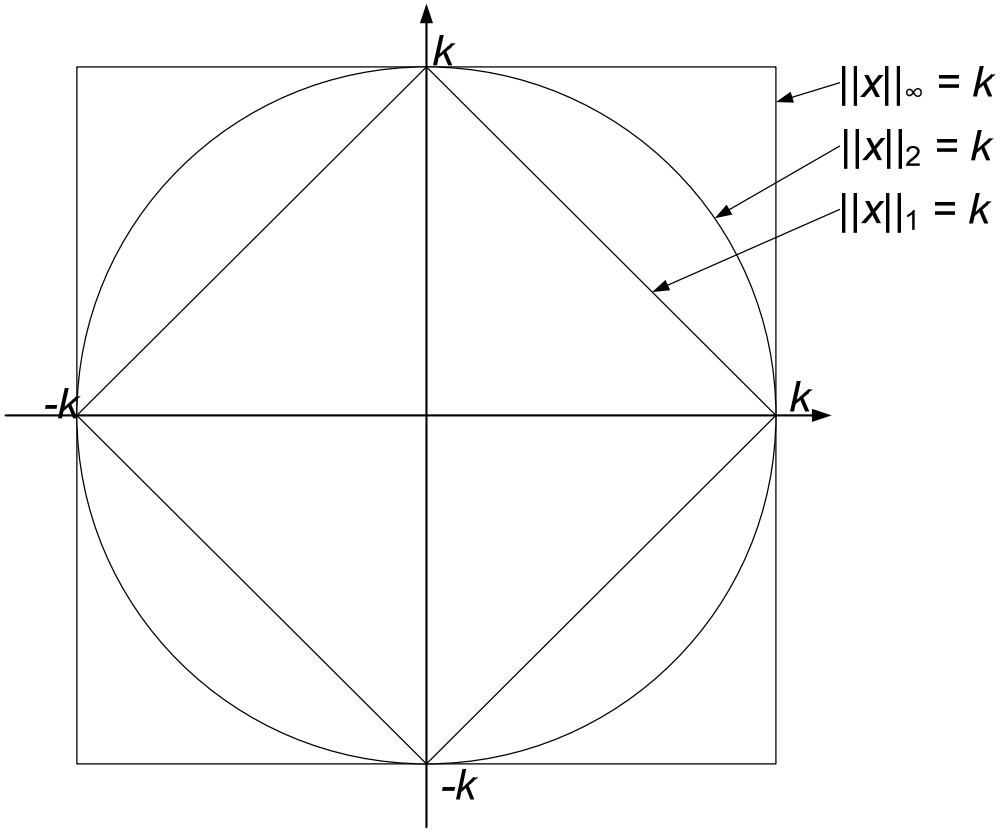

Figure B.1 Graphical representations of L-norms

Appendix C: Example of Matlab Scripts

```
clear
system='ieee57cdf.dat'
[Y]=IEEEtoYbus(system);
G=real(Y);
B=imag(Y);

%intial guess Flat start
[Vo,Phaseo]=IEEEintialguess(system);
V=Vo;
Phase=Phaseo;

%Mesurement Set Uses PSAT power flow solution
MeasureSet='57BaseCaseMeasure.txt';
[BusP, Pinj, BusQ, Qinj, sendQ, reciveQ, Qflow, Pflow, sendP, re-
civeP,LineIDp,LineIDq]=Measurementreader(MeasureSet);

%Branch Information for Power Flow Measurements
[send,recive,Circuit,g,b,Charging] = IEEEBranchInfo(system);
Z=[Pinj;Qinj;Pflow;Qflow];
[r,c]=find(Y~=0);
HpV=zeros(size(BusP,1),size(Y,1));
HpPhase=zeros(size(BusP,1),size(Y,1));
hPinj=zeros(size(BusP,1),1);
hQinj=zeros(size(BusQ,1),1);
for k=1:size(BusP,1)
   m=BusP(k);
   Hcolumn=0;
   Hcolumn=find(r==m);
   for l=1:size(Hcolumn)
      n=c(Hcolumn(l));
      if n~=m
         HpPhase(k,n)=V(n)*V(m)*(G(m,n)*sin(Phase(m)-Phase(n))-B(m,n)*cos(Phase(m)-Phase(n)));
         HpPhase(k,m)=-HpPhase(k,n)+HpPhase(k,m);
         HpV(k,n)=V(m)*(G(m,n)*cos(Phase(m)-Phase(n))+B(m,n)*sin(Phase(m)-Phase(n)));
         HpV(k,m)=V(n)*(G(m,n)*cos(Phase(m)-Phase(n))+B(m,n)*sin(Phase(m)-Phase(n)))+HpV(k,m);
         hPinj(k,1)=V(m)*V(n)*(G(m,n)*cos(Phase(m)-Phase(n))+B(m,n)*sin(Phase(m)-Phase(n)))+hPinj(k,1);
      else
         HpV(k,m)=V(m)*(G(m,m)*cos(Phase(m)-Phase(m))+B(m,m)*sin(Phase(m)-
Phase(m)))+HpV(k,m)+V(m)*G(m,m);
         HpPhase(k,m)=-V(n)*V(m)*(G(m,n)*sin(Phase(m)-Phase(n))-B(m,n)*cos(Phase(m)-
Phase(n)))+HpPhase(k,m)-V(m)*V(m)*B(m,m);
      end
   end
end
HqV=zeros(size(BusQ,1),size(Y,1));
HqPhase=zeros(size(BusQ,1),size(Y,1));
for k=1:size(BusQ,1)
   m=BusQ(k);
   Hcolumn=0;
   Hcolumn=find(r==m);
   for l=1:size(Hcolumn)
      n=c(Hcolumn(l));
```

```
      if n~=m
         HqPhase(k,n)=V(n)*V(m)*(-G(m,n)*cos(Phase(m)-Phase(n))-B(m,n)*sin(Phase(m)-Phase(n)));
         HqPhase(k,m)=-HqPhase(k,n)+HqPhase(k,m);
         HqV(k,n)=V(m)*(G(m,n)*sin(Phase(m)-Phase(n))-B(m,n)*cos(Phase(m)-Phase(n)));
         HqV(k,m)=V(n)*(G(m,n)*sin(Phase(m)-Phase(n))-B(m,n)*cos(Phase(m)-Phase(n)))+HqV(k,m);
         hQinj(k,1)=V(m)*V(n)*(G(m,n)*cos(Phase(m)-Phase(n))-B(m,n)*sin(Phase(m)-Phase(n)))+hQinj(k,1);
      else
         HqV(k,m)=V(n)*(G(m,n)*sin(Phase(m)-Phase(n))-B(m,n)*cos(Phase(m)-Phase(n)))+HqV(k,m)-
V(m)*B(m,m);
         HqPhase(k,m)=-V(n)*V(m)*(-G(m,n)*cos(Phase(m)-Phase(n))-B(m,n)*sin(Phase(m)-
Phase(n)))+HqPhase(k,m)-V(m)*V(m)*G(m,m);
      end
   end
end

for k=1:size(sendQ,1)
   BusS=sendQ(k);
   BusR=reciveQ(k);
   branch=0;
   S=[];
   S=find(send==BusS);
   for m=1:size(S,2)
      if recive(S(m))==BusR
         if Circuit(S(m))==LineIDq(k)
            branch=S(m);
         end
      end
   end
   if branch==0
      S=find(recive==BusS);
      for m=1:size(S,2)
        if send(S(m))==BusR
           if Circuit(S(m))==LineIDq(k)
              branch=S(m);
           end
        end
      end
   end
   HqfPhase(k,BusS)=-V(BusS)*V(BusR)*(g(branch)*cos(Phase(BusS)-Phase(BusR))-
b(branch)*sin(Phase(BusS)-Phase(BusR)));
   HqfPhase(k,BusR)=-HqfPhase(k,BusS);
   HqfV(k,BusS)=-V(BusR)*(g(branch)*sin(Phase(BusS)-Phase(BusR))-b(branch)*cos(Phase(BusS)-
Phase(BusR)))-2*(b(branch)+imag(Charging(branch)))*V(BusS);
   HqfV(k,BusR)=-V(BusS)*(g(branch)*sin(Phase(BusS)-Phase(BusR))-b(branch)*cos(Phase(BusS)-
Phase(BusR)));
   hQflow(k,1)=-V(BusS)*V(BusS)*(b(branch)+imag(Charging(branch)))-
V(BusR)*V(BusS)*(g(branch)*cos(Phase(BusS)-Phase(BusR))+b(branch)*sin(Phase(BusS)-Phase(BusR)));
end

for k=1:size(sendP,1)
   BusS=sendP(k);
   BusR=reciveP(k);
   branch=0;
   S=[];
   S=find(send==BusS);
```

```
   for m=1:size(S,2)
      if recive(S(m))==BusR
         if Circuit(S(m))==LineIDp(k)
            branch=S(m);
         end
      end
   end
   if branch==0
      S=find(recive==BusS);
      for m=1:size(S,2)
       if send(S(m))==BusR
          if Circuit(S(m))==LineIDp(k)
             branch=S(m);
          end
       end
      end
   end
   HpfPhase(k,BusS)=V(BusS)*V(BusR)*(g(branch)*sin(Phase(BusS)-Phase(BusR))-
b(branch)*cos(Phase(BusS)-Phase(BusR)));
   HpfPhase(k,BusR)=-HpfPhase(k,BusS);
   HpfV(k,BusS)=-V(BusR)*(g(branch)*cos(Phase(BusS)-Phase(BusR))-b(branch)*sin(Phase(BusS)-
Phase(BusR)))+2*(g(branch)+real(Charging(branch)))*V(BusS);
   HpfV(k,BusR)=-V(BusS)*(g(branch)*cos(Phase(BusS)-Phase(BusR))-b(branch)*sin(Phase(BusS)-
Phase(BusR)));
   hPflow(k,1)=V(BusS)*V(BusS)*(g(branch)+real(Charging(branch)))-
V(BusR)*V(BusS)*(g(branch)*cos(Phase(BusS)-Phase(BusR))+b(branch)*sin(Phase(BusS)-Phase(BusR)));
end

% Formation of the intial H matrix
H=[HpfPhase, HpfV; HpPhase,HpV;HqfPhase,HqfV;HqPhase,HqV];
H(:,1)=[];
Hphase=[HpfPhase;HpPhase];
Hphase(:,1)=[];
[Hprows,Hpcolomns]=size(Hphase)
Gphase=Hphase'*Hphase;
RankHphase=rank(Hphase)
[Vphase,Eigphase]=eig(Gphase);

% Testing the Equations

% Insertion of the First PMU  Effects on Just Power Phase matrix
deltG=1
for k=1:size(Vphase,1)
   PredictedEig(k,1)=Vphase(k,1)^2*deltG;
end
for k=1:Hpcolomns
   Hphasep=[Hphase;zeros(1,Hpcolomns)];
   Hphasep(Hprows+1,k)=1;
   EV=eig(Hphasep'*Hphasep);
   ExpEig(k,1)=EV(1);
   DeltaEigExp=ExpEig-Eigphase(1,1);
end
S=1:56;
plot(S,PredictedEig,'r+', S,DeltaEigExp,'go')
xlabel('G matrix changed by +1 at k,k')
```

```
ylabel('Change in smallest Eigenvalue')
legend('Predicted','Actual')
title('H of Power and Phase')
w=[0:0.01:.1,.2:.1:2];
for k=1:size(w,2)
   WPredictedEig(k,1)=Vphase(32,1)^2*w(k)^2;
   Hphasep=[Hphase;zeros(1,Hpcolomns)];
   Hphasep(Hprows+1,32)=w(k);
   EV=eig(Hphasep'*Hphasep);
   WExpEig(k,1)=EV(1);
   WDeltaEigExp(k,1)=WExpEig(k,1)-Eigphase(1,1);
end
figure
plot(w,WPredictedEig,'g--',w,WDeltaEigExp,'r:')
xlabel('Size in Change of H matrix col 32')
ylabel('Change in smallest Eigenvalue')
legend('Predicted','Actual')
title('H of Power and Phase')
for k=1:Hpcolomns
   PredictedEigDelta(k,1)=Vphase(32,k)^2*deltG;
   PreEig(k,1)=Eigphase(k,k)+PredictedEigDelta(k);

end
Hphasep=[Hphase;zeros(1,Hpcolomns)];
Hphasep(Hprows+1,32)=1;
EV=eig(Hphasep'*Hphasep);
Orginal=ones(56,1);
Predicted=2*Orginal;
Exp=3*Orginal;
K0=cond(Gphase);
KPredicted=max(PreEig)/min(PreEig);
Kactual=cond(Hphasep'*Hphasep);
figure
plot(diag(Eigphase),Orginal,'r+',PreEig,Predicted,'go',EV,Exp,'b^')
axis([0,6500,0,4])
xlabel('EigenValues')
legend('Original','Predicted','Actual')
title('H of Power and Phase')

%  PMU measures both phase and angle What would the including volt measure
%  do
[Hrows,Hcolomns]=size(H);
G=H'*H;
RankH=rank(H);
[VG,EigG]=eig(G);

deltG=1;
kG=cond(G)
for k=1:size(Vphase,1)
   PredEigPV(k,1)=VG(k,1)^2*deltG+VG(k+57,1)^2*deltG;
   LargestEig(k,1)=VG(k,113)^2*deltG+VG(k+57,113)^2*deltG;
   deltaK(k,1)=(VG(k,113)^2-kG*VG(k,1)^2)/(EigG(1,1));
end
for k=1:56
   Hp=[H;zeros(2,Hcolomns)];
```

```
   Hp(Hrows+1,k)=1;
   Hp(Hrows+2,k+57)=1;
   EV=eig(Hp'*Hp);
   ExpEigPV(k,1)=EV(1);
   K2(k,1)=cond(Hp'*Hp);
end
DEigExpPV=ExpEigPV-EigG(1,1);
dK2=K2-kG;
figure
plot(S,PredEigPV,'r+', S,DEigExpPV,'go')
xlabel('G matrix changed by +1 at k,k and 57+k,57+k')
ylabel('Change in smallest Eigenvalue')
legend('Predicted','Actual')
title('Entire H')
figure
plot(S,deltaK,'r+', S,dK2,'go')
xlabel('G matrix changed by +1 at k,k and 57+k,57+k')
ylabel('Change in Condition Number')
legend('Predicted','Actual')
title('Entire H')
w=[0:0.01:.1,.2:.1:2];
for k=1:size(w,2)
   WPredEigG(k,1)=VG(32,1)^2*w(k)^2+VG(32+57,1)^2*w(k);
   Hp=[H;zeros(2,Hcolomns)];
   Hp(Hrows+1,32)=w(k);
   Hp(Hrows+2,32+57)=w(k);
   EV=eig(Hp'*Hp);
   WExpEigG(k,1)=EV(1);
   WDeltaEigExpG(k,1)=WExpEigG(k,1)-EigG(1,1);
end
figure
plot(w,WPredEigG,'g--',w,WDeltaEigExpG,'r:')
xlabel('Magnitude of Change of H matrix col 32')
ylabel('Change in smallest Eigenvalue')
legend('Predicted','Actual')
title('Entire H')
for k=1:Hcolomns
   PredEigDeltaG(k,1)=VG(32,k)^2*deltG+VG(32+57,k)^2*deltG;
   PreEigG(k,1)=EigG(k,k)+PredEigDeltaG(k);
end
Hp=[H;zeros(2,Hcolomns)];
Hp(Hrows+1,32)=1;
Hp(Hrows+2,32+57)=1;
EVG=eig(Hp'*Hp);
Orginal=ones(113,1);
Predicted=2*Orginal;
Exp=3*Orginal;
figure
plot(diag(EigG),Orginal,'r+',PreEigG,Predicted,'go',EVG,Exp,'b^')
%plot(diag(EigG),Orginal,'r+',PreEigG,Orginal,'go',EVG,Orginal,'b^')
axis([0,6500,0,4])
xlabel('EigenValues')
legend('Original','Predicted','Actual')
title('Entire H')
K0g=cond(G)
KPredictedg=max(PreEigG)/min(PreEigG);
```

```
Kactualg=cond(Hp'*Hp);

figure
plot(S,PredEigPV,'r+', S,DEigExpPV,'go',S,PredictedEig,'rx', S,DeltaEigExp,'g+');
```

Part IV

Hybrid State Estimation

Author

Sakis Meliopoulos
Georgia Institute of Technology

Table of Contents

List of Figures

List of Tables

1. Introduction

State estimation was introduced by Gauss and Legendre around 1800. The basic idea was to "fine-tune" state variables by minimizing the sum of the residual squares. This is the well-known least squares (LS) method, which has become the cornerstone of classical statistics. The reasons for its popularity are easy to understand: At the time of its invention there were no computers, and the fact that the LS estimator could be computed explicitly from the data (by means of some matrix algebra) made it the only feasible approach. Even now, most statistical packages still use the same technique because of tradition and computational speed. Also, for one-dimensional problems, the LS criterion yields the arithmetic mean of the observations, which at that time seemed to be the most reasonable estimator. Afterwards, Gauss introduced the normal (or Gaussian) distribution as the error distribution for which LS is optimal. Since then, the combination of Gaussian assumptions and LS has become a standard mechanism for the generation of statistical techniques.

Control and operation of electric power systems is based on the ability to determine the system state in real time. In a real time environment, state estimation was applied to power systems by Schweppe and Wildes in the late 1960's [1]. Over the past thirty five years, the basic structure of power system state estimation has remained practically the same: (a) Single phase model, (b) P, Q, V measurement set, (c) Non-simultaneousness of measurements, and (d) Single frequency model. This basic structure of the power system state estimation implies the following assumptions (which in turn result in a biased state estimator): (1) all current and voltage waveforms are pure sinusoids with constant frequency and magnitude, (2) the system operates under balanced three phase conditions, and (3) the power system is a symmetric three phase system which is fully described by its positive sequence network. These assumptions introduce deviations between the physical system and the mathematical model (bias) and have resulted in practical difficulties manifested by poor numerical reliability of the iterative state estimation algorithm. Substantial efforts to fine tune the mathematical models in actual field implementations are required. In practice, even for a well tuned SE, these reasons manifest themselves by the fact that the state estimation algorithm occasionally diverges. This “unreliability” of the state estimator has been reported in the order of 1% to 5%.

The trends in the electric power industry towards larger systems and especially the recent government announcement for mega RTOs, raises the question: what will be the performance of the state estimation in these systems. In this work these problems are discussed and some thoughts are offered for methods to investigate this problem. We discuss the biases of the traditional state estimation problem and project the effect of these biases as the system size increases. Specifically, the following issues are discussed: (1) Sources of Bias in Traditional SE, (2) Effects of System Size on Bias Error, (3) Effects of Bias Error on Bad Data Detection, (4) Effects of Time Skewness on SE Accuracy, and (5) Effects of System Size on Computational Effort. Subsequently, we propose an approach that may mitigate these problems. Yet, extensive numerical experiments are required to determine whether the proposed SE will meet the challenge of providing a practical SE for mega systems.

2. Sources of Bias in Traditional State Estimation

The LS state estimation procedure is an unbiased estimator if and only if the model is accurate (exact) and the measurement errors are statistically distributed. Both of these conditions may not exist in a practical system. In this section we concentrate on the bias resulting from model inaccuracies and we discuss the effect of measurement errors. In particular model inaccuracies result from: (a) unbalanced operating conditions and (b) asymmetries of power system models.

2.1 Balanced operation

An actual power transmission system operates near balanced conditions. The imbalance may be small or large depending on the design of the system. As an example, Fig. 1 illustrates the three phase voltages and currents on an actual system. Note for example a 10% difference in the currents of Phases A and B of transmission line to GILBOA. The voltage in this case has only a 0.2% difference between two phases.

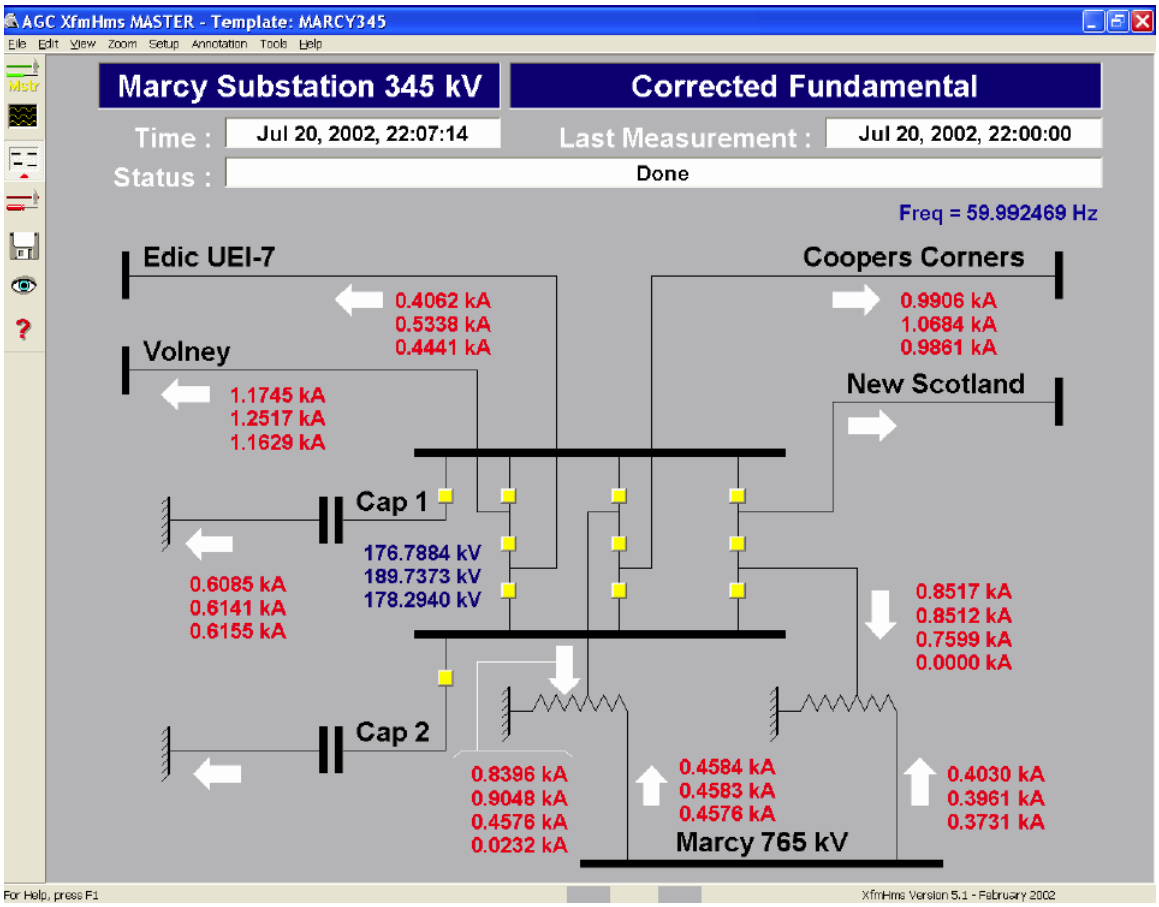

Figure 1 Actual three phase voltages and currents in MARCY substation

Because of imbalance, the measurements may have an error. We represent this as follows:

$$z = z_t + \Delta z\,, \tag{1}$$

where z_t is the true measurement (assuming a balance system), Δz is the measurement error due to imbalance, and z is the actual measurement Application of the LS state estimation procedure, assuming no other error sources, yields:

$$x = x_t + (H^T W H)^{-1} H^T W \Delta z\,, \tag{2}$$

where x_t is the true state of the system or the unbiased state estimate, and the second term is the bias resulting from the imbalance measurement error. Note that the bias from unbalanced operation depends on the level of imbalance as well as the system parameters (matrix H).

2.2 System symmetry

An actual power transmission system is never symmetric. While some power system elements are designed to be near symmetric, transmission lines are never symmetric [2-5]. The impedance of any phase is different than the impedance of any other phase. In many cases, this imbalance can be corrected with transposition. Because of cost many lines are not transposed.

The asymmetry may be small or large depending on the design of the system. One power system component that contributes to the asymmetry is the three phase untransposed line. As an example, Fig. 2 illustrates an actual three phase line.

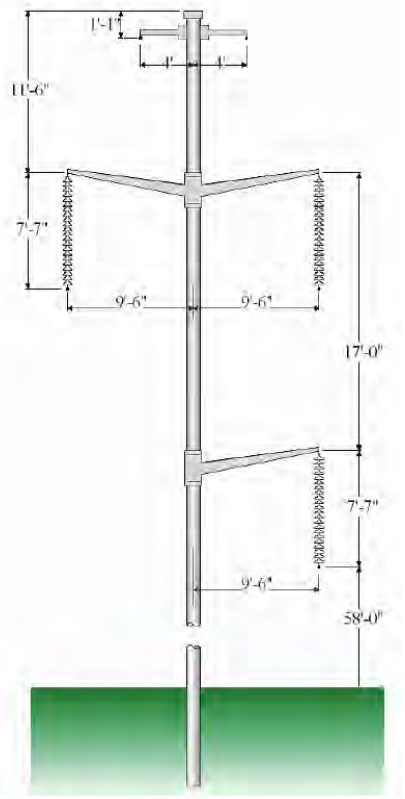

Figure 2 Typical transmission line construction.

For the purpose of quantifying the asymmetry of this line, two asymmetry metrics are defined:

$$S_1 = \frac{1}{2}\frac{|z_{\max} - z_{\min}|}{|z_1|} \tag{3}$$

$$S_2 = \frac{1}{2}\frac{|y_{\max} - y_{\min}|}{|y_1|} \tag{4}$$

where z_1 is the positive sequence series impedance of the line, z_{max} and z_{min} are the max and min series impedances of the individual phases, y_1 is the positive sequence shunt admittance of the line, y_{max} and y_{min} are the max and min shunt admittances of the individual phases.

The above indices provide, in a quantitative manner, the level of asymmetry among phases of a transmission line. As a numerical example, these metrics have been computed for the line of Fig. 2 and are presented in Fig. 3. Note that the asymmetry is in the order of 5 to 6%.

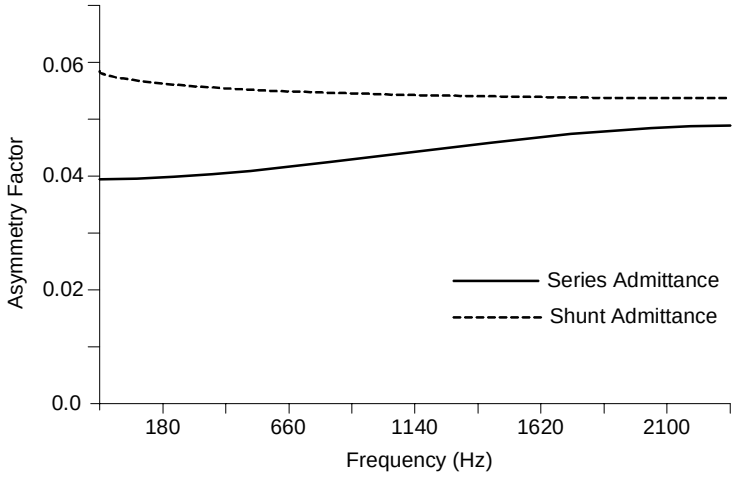

Figure 3 Line Asymmetry Indices (Line of Fig. 2).

Because of the presence of non-symmetric components, the state estimate using single phase measurement set is biased. An estimate of the bias can be computed as follows. First observe that because of power system component asymmetry, the relationship of a measurement to the system model will have an error. Specifically:

$$z = h(x) + \Delta h(x), \tag{5}$$

where h(x) is the function relating the measurement to the state vector assuming symmetric power system components, Δh(x) is the difference between the symmetric model and the asymmetric model. Now the Jacobian matrix of the measurements becomes:

$$H = H_s + \Delta H\ , \tag{6}$$

where H_s is the Jacobian matrix assuming symmetric power system elements. Application of the LS state estimation procedure, assuming no other error sources, yields:

$$x = (x_t + (H^T WH)^{-1} H^T W\Delta z)(\Delta H^T WH)^{-1}(I + 2(\Delta H^T WH)(H^T WH)^{-1})^{-1}(\Delta H^T WH), \qquad (7)$$

where x_t is the state of the system assuming a symmetric model, and the other terms represent the bias resulting from the system asymmetry.

2.3 Measurement errors

State estimators are based on the assumption that measurement errors are statistically distributed with zero mean. The traditional implementation of state estimation uses sensors of V (magnitude), P and Q. When the sensors are properly calibrated, the measurement error is very close to meeting the requirements of state estimation. However, recent trends resulted in the use of sensorless technology for power system measurements. Sensorless technology refers to the use of A/D converter technology to sample the voltage and current waveforms. Once the sampled waveforms are available, the required measurements can be retrieved with numerical computations.

Independently of the technology used for measurements, it is important to examine whether there is bias in the measurements. This can be best achieved by examining the entire measurement channel of a typical power system instrumentation [6]. The major sources of error (see Fig. 4) are (a) the instrument transformers, (b) the cables connecting the instrument transformers to the sensors or A/D converters and (c) the sensors or A/D converters. Fig. 5 illustrates the transfer functions of a typical instrument transformer. It can be observed that the characteristics of instrument transformers near the power frequency are flat. One can conclude that for power frequency measurements, there is no appreciable measurement bias from instrument transformers. However for measurements at harmonic frequencies, a substantial measurement bias can occur. Another source of measurement bias may result from A/D converters. Fig. 6 illustrates the transfer function of a specific A/D converter (Crystal Semiconductor, 16 bit). Note the magnitude and phase bias even at power frequency. It is important to note that the measurement bias is dependent upon the design of the A/D converter. The measurement bias resulting from control cables is variable depending on the total length of the cables. Figure 7 illustrates biases introduced by instrumentation cables.

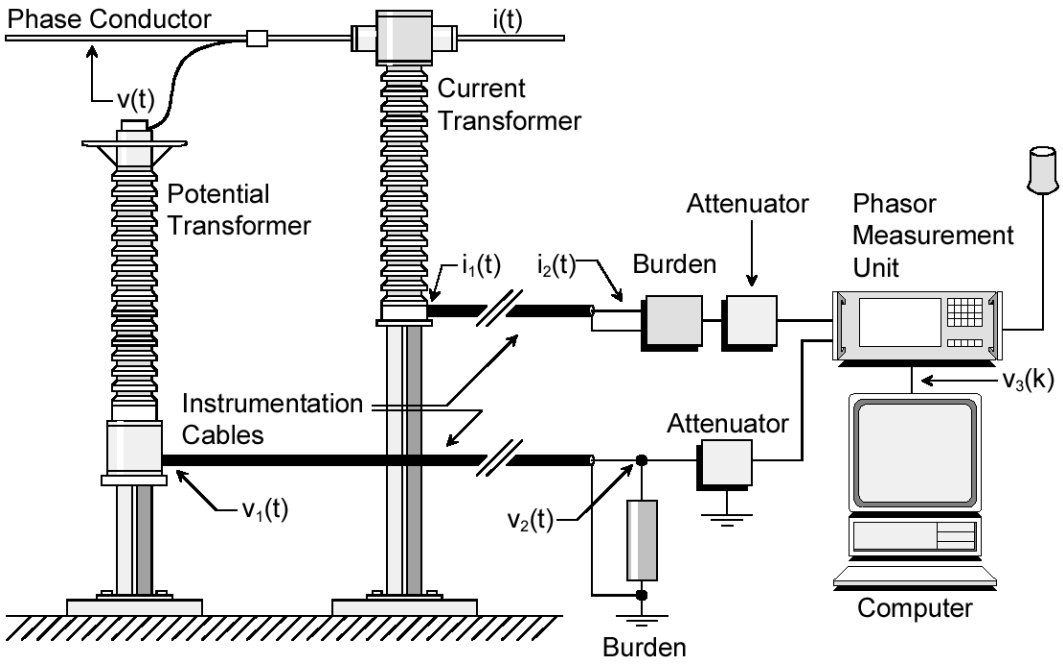

Figure 4 Components of typical voltage and current instrumentation channel.

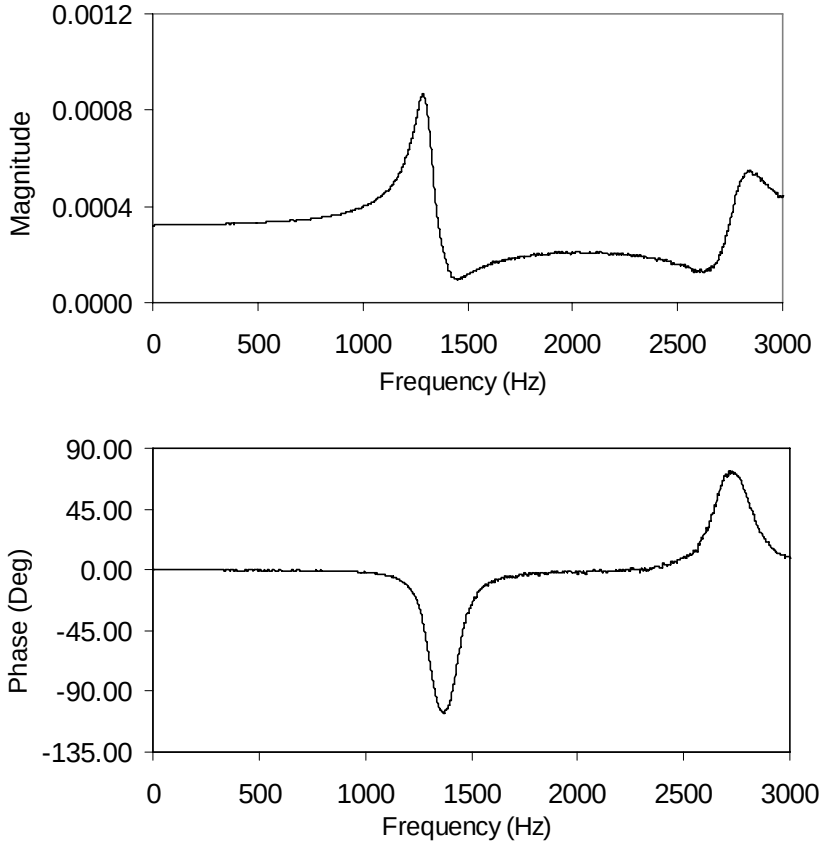

Figure 5 Magnitude and phase of frequency response of a 200 kV/115 potential transformer

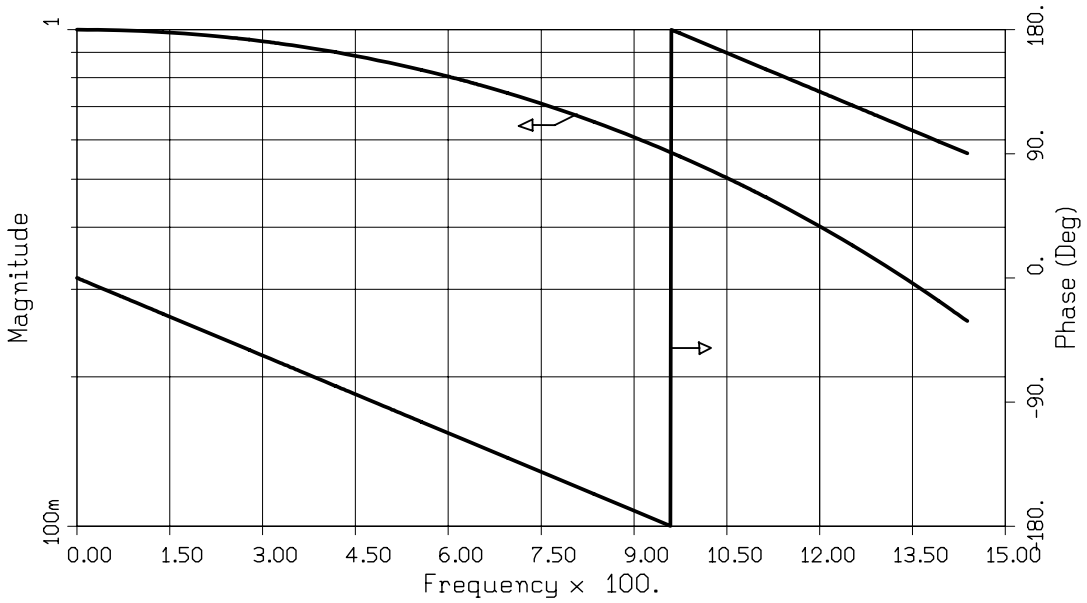

Figure 6 Magnitude and phase of frequency response of the PMY-1620 unit.

Instrumentation Errors

Instrumentation Cable Phase Error

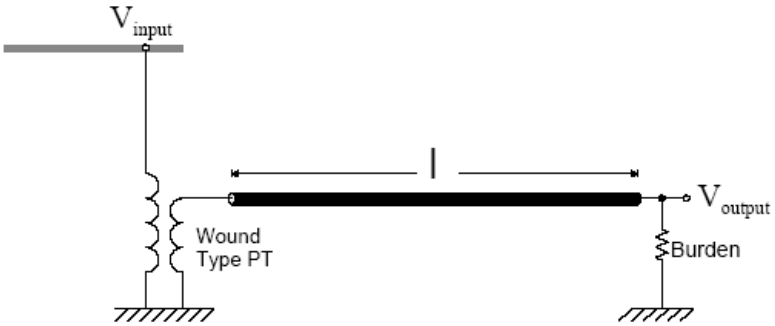

Cable Length (l)	Phase (V_{out} / V_{in})
75 m	0.04^0
150 m	0.07^0
225 m	0.11^0
300 m	0.14^0

PMU Phase Accuracy is 0.01 degrees

Figure 7 Phase error in instrumentation cables.

The measurement bias can be corrected with software. Such methods have been developed [7,8], but their use in state estimation is very limited. It is important to note that the above sources of error cannot be corrected with better (more accurate) instrumentation. To avoid these sources of error, three phase measurements and a three phase system model is required. Such a system has been developed and it is described next.

3. Effects of System Size on Bias Error

The effect of bias error in SE has been studied only in a limited basis. The size of this error as the size of the system increases is an unknown. There are scientists that they believe that this error will remain constant as the system size grows. Others believe that this may not be true. It is important to design numerical experiments that will allow the study of the bias error size as a function of system size. The purpose of this preliminary work is to suggest some numerical experiments that can be used to study this issue and to provide some initial numerical results for the behavior of the state estimation errors in relation with the power system size.

3.1 Design of numerical experiments

The procedure is based on data provided by simulated system conditions. These data are used instead of actual measurements and are the input of the state estimation algorithm. However, the system model used for the simulations differs from the equivalent circuit based model that is used in the state estimation algorithm. The elements of the power system are represented by physically based models, that take into account the actual structure of each element and the possible asymmetries and imbalances that may appear. That is, for example, a transmission line, which is one of the most asymmetric power system elements is not represented by it sequence equivalent circuits, but by a physical model that take into account the geometry of the line. The same holds for all the other elements. In addition the system is simulated using full three-phase analysis. So, the asymmetries of the components and the imbalances are in fact taken into consideration and appear in the simulation results. We may, therefore, assume that the models represent in great detail the actual power system. Furthermore, the simulation results represent in great accuracy the actual quantities that would be measured in an actual power system. Finally the use of such data ensures that no other sources of error, like measurement noise or bad data, except for the model inaccuracies are present. Therefore, a basic assumption of the experiments is that the data that are used as measurements are assumed to be free of errors, so the only source of bias is the inaccuracies of the mathematical model used by the state estimation algorithm.
Using the bus voltage magnitudes and the line flows obtained by the simulation as measurements, the classical state estimator algorithm is executed. Measurements of voltage magnitude and active and reactive power flow are considered. Power injection measurements are not used. The state estimator uses the typical single phase equivalent circuit representation of the system. The state vector, x, consists of the phase angles of the voltage at each bus, except for the slack bus, and the voltage magnitude at every bus. The measurement equations that relate the measured data to the state vector are of the form

$$Z = h(x) + v, \tag{8}$$

where Z is the measurement vector consisting of voltage, active and reactive power flow measurements, $h(x)$ is the vector function that relates the measurements and to the state vector and v is the noise vector. The mathematical form of these equations depends on the system model.

The transmission lines are modeled using the positive sequence pi-equivalent circuit, as presented in Fig. 7. The active power flow through the line can be computed, as a function of the state vector x by

$$P_{ij}(x) = V_i^2\left(g_{ij} + g_{sij}\right) - V_i V_j a_{ij}\,, \tag{9}$$

and the reactive flow as

$$Q_{ij}(x) = -V_i^2\left(b_{ij} + b_{sij}\right) - V_i V_j \beta_{ij}\,, \tag{10}$$

where:

$$a_{ij} = g_{ij}\cos(\delta_i - \delta_j) + b_{ij}\sin(\delta_i - \delta_j) \tag{11}$$

and

$$\beta_{ij} = g_{ij}\cos(\delta_i - \delta_j) - b_{ij}\sin(\delta_i - \delta_j) \tag{12}$$

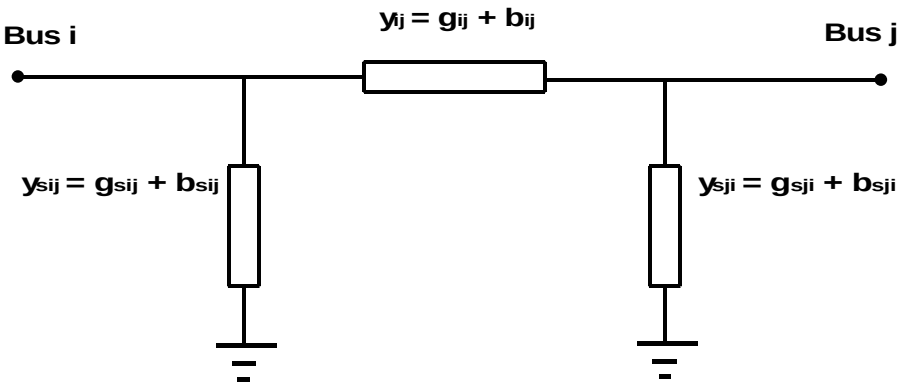

Figure 8 Pi-equivalent transmission line model.

The transformers are modeled similarly, but using only a series admittance, as presented in Fig. 9.

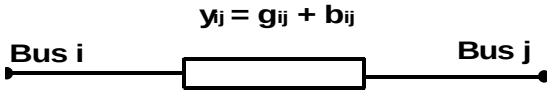

Figure 9 Transformer model.

The active power flow through the transformer can be computed, as a function of the state vector x by

$$P_{ij}(x) = V_i^2 g_{ij} - V_i V_j a_{ij}\,, \tag{13}$$

and the reactive flow as

$$Q_{ij}(x) = -V_i^2 b_{ij} - V_i V_j \beta_{ij}\,, \tag{14}$$

where a_{ij} and β_{ij} are defined as in (11) and (12). These are the equations that connect the flow measurements with the unknown state vector. The equations for the voltage magnitude measurements are simply:

$$V_i(x) = V_i, \tag{15}$$

where V_i is the corresponding voltage magnitude measurement at bus i.

Assuming that voltage magnitude is measured at every one of the n system buses, and power flows are measured at every one of the m circuit branches, at both ends of each branch, the measurement set consists of:

- n voltage measurements,
- $2m$ active power flow measurements,
- $2m$ reactive power flow measurements.

The total number of measurements is $M = n + 4m$, while the size of the state vector is $N = 2n - 1$. After the estimation algorithm has converged and an estimation of the system voltages and angles is available and estimation of the measurements can also be obtained through the measurement equations. Comparison of the measurement estimation and the actual measurements provides the estimation error for each measurements, $\hat{e}_j = z_j - \hat{z}_j$. The weighted sum of the squares of these errors, where the weights are considered to be the inverse of the variance of each measurement, is $J(\hat{x}) = \sum_{j=1}^{M} \frac{\hat{e}_j^{\,2}}{\sigma_j^2}$. If the noise of each measurement is normally distributed, then $J(\hat{x})$ follows the x^2-distribution with $M - N$ degrees of freedom. Through the value of $J(\hat{x})$ the confidence level of the estimation can be evaluated. By considering various test cases with increasing system sizes, it is possible to study the behavior of the state estimation bias due to model inaccuracies as the size of the system increases.

The test cases used for the study of the state estimation errors are based on a rather simple system configuration. The basic system module used consists of two main load buses. A constant power and constant impedance load are connected on each bus, and each bus is also connected to a generator through a step up transformer. The two load-buses are connected through an overhead transmission line. The system contains all the basic elements that are typical to a power system. The diagram of the basic two-bus module is presented in Fig. 10.

Based on this configuration the size of the system is increased by repeating this module in a radial way, and therefore increasing the number of buses that exist on the system. As an example the four-bus system is show in Fig. 11. Using the simulation results as measurement the state estimation results are obtained for each system and the errors are calculated. This way the state estimation performance relatively to the system size can be evaluated. The behavior of the errors as the system size increases is also an indication of the performance of the state estimation algorithm as the system size increases.

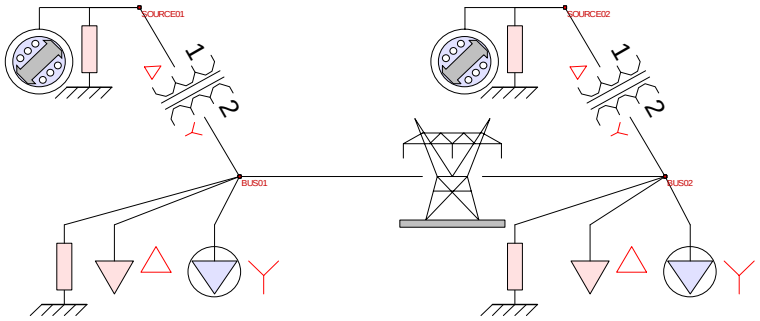

Figure 10 Two-bus test-system.

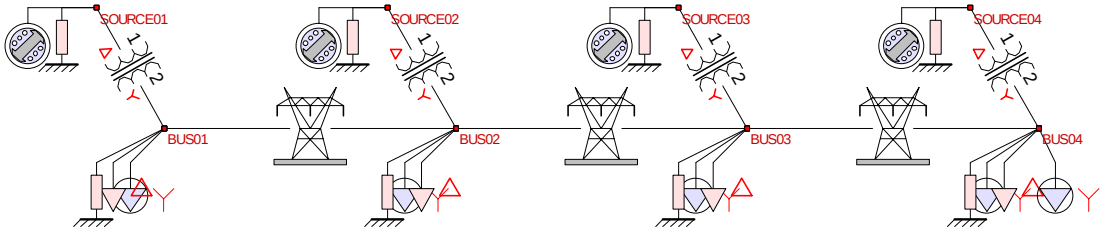

Figure 11 Four-bus test-system.

The quantities that are considered system measurement are the voltage magnitudes at each bus and the active and reactive power flows at each network branch. The flows are measured at both ends of each branch. Three measurement scenarios are considered:

Scenario 1: The typical single phase measurement approach, that is commonly used and assumes symmetry and balanced loading, is assumed. The voltage magnitude of phase A is considered and only the power flows of phase A are measured and the total line flow is calculated by multiplying this measurement by three.

Scenario 2: The second measurement scenario is the same as the first one with the exception that the data from phase B are used as measurements instead of phase A.

Scenario 3: The third scenario assumes again voltage measurements of a single phase, phase A, but three-phase measurements of active and reactive power flow. So the power measurements provided to the state estimation algorithms are the sum of the measurements for all three phases.
The purpose of these three cases is to capture the effects of the asymmetries in the system to the performance of the state estimation algorithm. In fact the system operates under balanced loading conditions, but the main source of asymmetry is the transmission line structure. The type and of transmission line pole used is presented in Fig. 12. There is significant asymmetry at the structure and phase A is expected to be differently loaded than phases B or C.

The simplest system consists of two buses and the rest of them consist of 4, 8 and 16 buses. It should be mentioned that the numbers refer to high voltage load buses, which are connected through transmission lines, and the generation buses are not taken into account. However, this implies that the actual number of buses is double, in each one of the cases, that is each case contains 4, 8, 16 and 32 buses respectively. Based on the radial structure of the test networks, if n is the number of buses, then the number of braches is $n-1$, and therefore the total number of measurements is $5n-4$. Since the number of states is $2n-1$, the measurement redundancy is $3n-3$, and this is also the number of degrees of freedom in each case, and the redundancy index is $r=\frac{5n-4}{2n-1}$. As the system size increases, that is, as $n\to\infty$, $r\to\frac{5}{2}=2.5$.

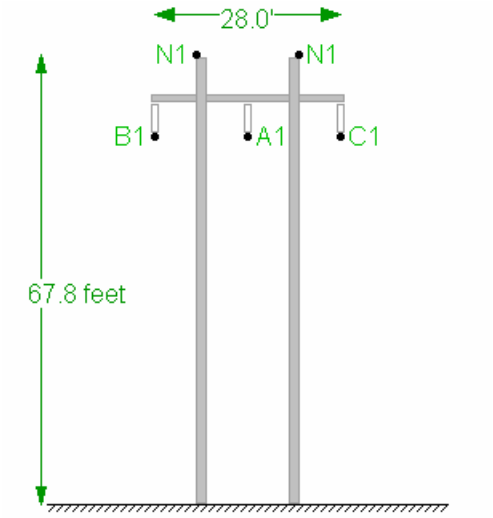

Figure 12 Transmission line pole structure.

3.2 Numerical test results

The results of the state estimation algorithm reveal the fact that the estimation errors due to the model inaccuracies tend to increase as the system size increases. Fig. 13 through 15 present the maximum absolute errors for voltage magnitude, active power flow and reactive power flow respectively.

It should be again stated that since simulation data are used there are no other sources of error except for model inaccuracies in each case. So, the increase in the estimation errors is solely due to the increasing model inaccuracies because of the system asymmetries as the system size increases. It is therefore projected that if the system size becomes extremely large the results of the classical state estimator will eventually become unreliable and the errors very large. Numerical experiments for much larger systems are to be carried out to verify these conclusions. The increase in the error is much greater in the voltage magnitude, rather than in the power measurements, where it seems that the error tends to stabilize. In an actual situation, where other sources of bias are also present this will make the state estimation results impractical.

Although the errors seem to grow in the case of using single phase power measurements, this does not seem to be the case in scenario 3, where the sum of the flows of all three phases is used

as measurement. In this case the estimation error is much lower and in addition it remains almost constant as the system size grows.

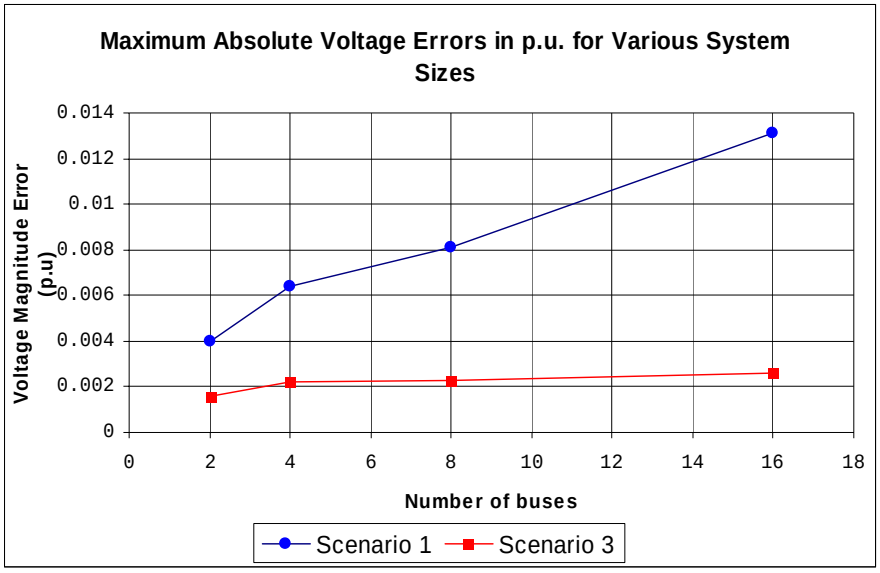

Figure 13 Maximum absolute voltage error vs. system size.

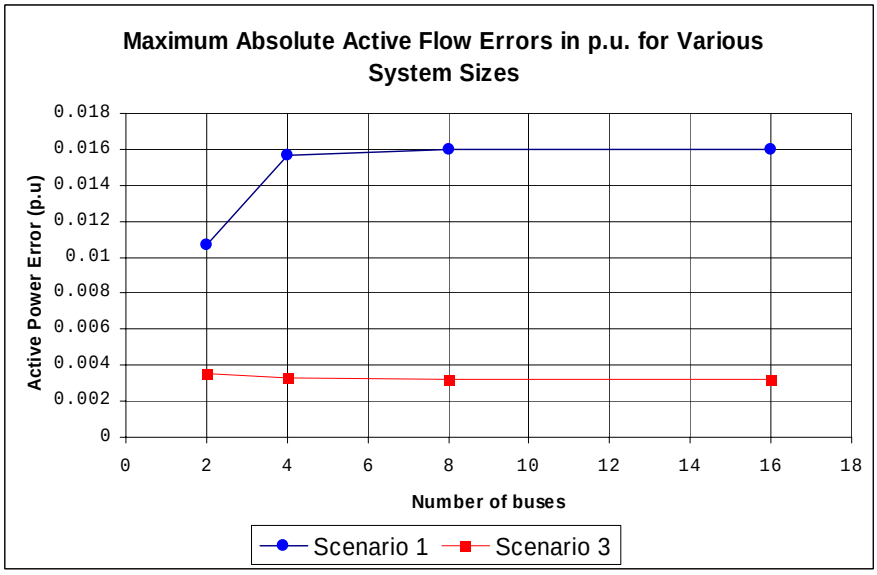

Figure 14 Maximum absolute active power flow error vs. system size.

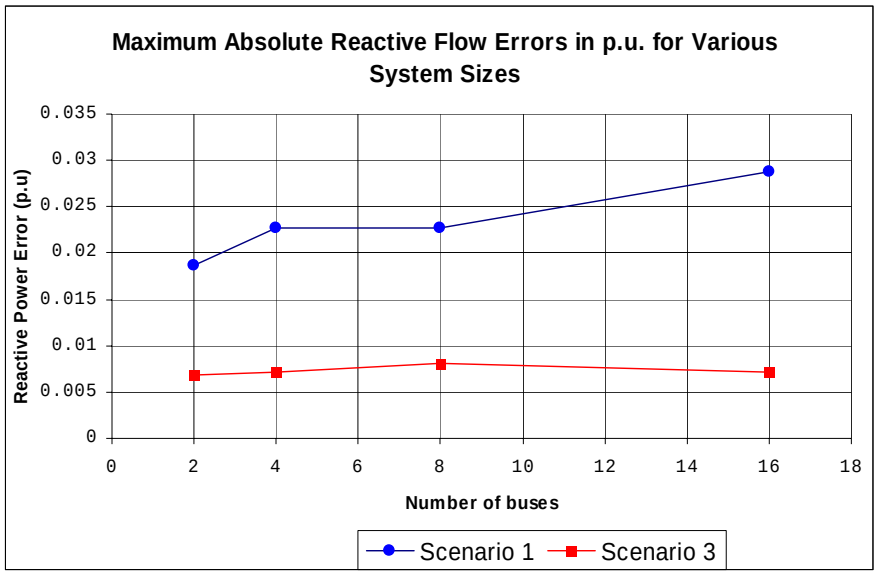

Figure 15 Maximum absolute reactive power flow error vs. system size.

To further investigate the issue the confidence level of the estimation is calculated for every case. The results are produced parametrically for various values of standard deviation σ of the measurements. Every measurement is assumed to follow Gaussian distribution with the same variance σ^2. All the measurements are assumed to have the same weight.

The confidence level of the estimation for various system sizes is presented in Fig. 16, for the measurement data of scenario 1. The plot is parametric, for various values of standard deviation.

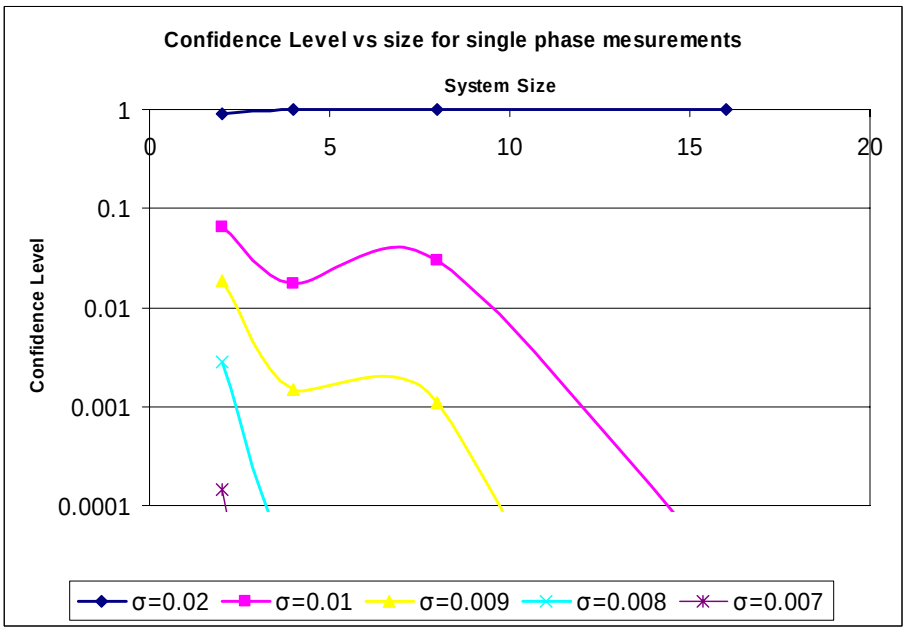

Figure 16 Confidence level of estimation vs. system size for different values of standard deviation, for scenario 1.

It can be concluded base on the plot that for values of σ lower than 0.02 the confidence level of the estimation is low and decreases very rapidly as the system size increases, and the estimation becomes unreliable. However, for values of σ greater than 0.02 the confidence of the estimation is very high and increases with the system size, approaching 1.00. This can be explained based on the chi-square distribution used to calculate the values of the confidence level. More specifically the value of the objective function $J(\hat{x}) = \sum_{j=1}^{M} \frac{\hat{e}_j^{\,2}}{\sigma_j^2}$, is increasing with the system size, but as explained previously the measurement redundancy which is equal to the degrees of freedom also increases linearly with the system size. So, as the system grows the redundancy of measurements also increases and this provides a better confidence level of the estimation. However, since the redundancy index tends to stabilize quickly as n increases, this behavior may not continue to be the same for extremely large systems and the confidence level may start to deteriorate for very large numbers of buses.
The confidence levels for scenario 3, for the same values of measurement variance, are presented in Fig. 17.

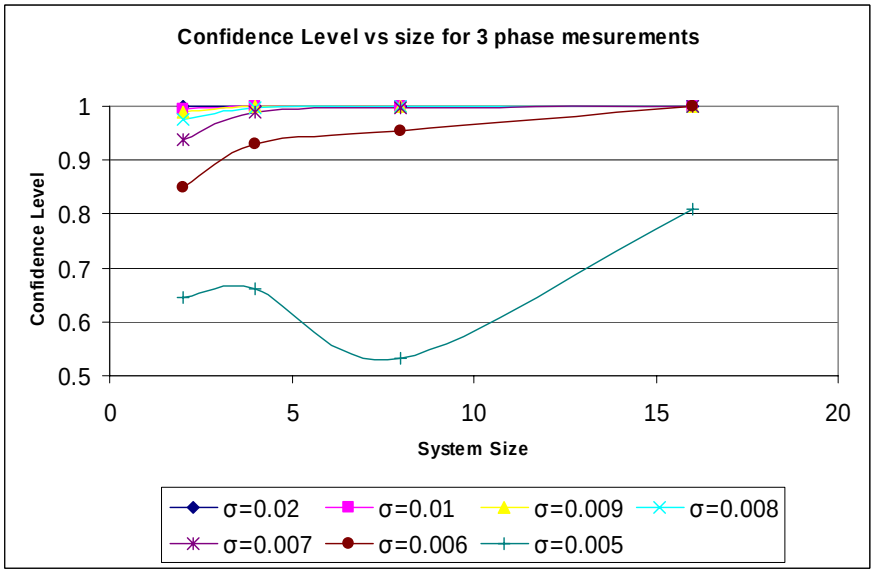

Figure 17 Confidence level of estimation vs. system size for different values of standard deviation, for scenario 3.

The behavior in this case is similar; however the confidence level is much higher for the same values of σ than in the previous case. This indicates that using measurement from all the three phases for the power flows a high confidence level of estimation can be achieved for lower values of measurement variance, which may be approximately as low as 0.006, while in the single phase measurements case the best that could be achieved was a standard deviation of approximately 0.02.

4. Effects of Bias Error on Bad Data Detection

The value of the SE is its promise to detect and identify bad data. This ability is best when the system model is not biased. In the presence of model bias, the ability to detect and identify bad data is compromised. Again we know very little on a theoretical or practical basis on the subject, i.e. how the performance of the bad data detection and identification will be affected in mega systems.

5. Effects of Time Skewness on SE Accuracy

The traditional SE is based on measurements that do not need to be fully synchronized. Specifically, it relies on measurement of quantities that are constant under the assumption of steady state operation, i.e. V (magnitude), P and Q. In practice, each measurement is taken by non-synchronized data acquisition systems, i.e. at different times within a short time interval, and transmitted to a central location. Thus the measurements (data) are not all taken at the same time. Since the system is always in transition, there will be a discrepancy between the system model and the collected data resulting from the time skewness of the data [9]. It is very difficult to quantify this discrepancy which is dependent upon the system and on how fast the system transits from one operating condition to another. This issue can be resolved with present technology (GPS) that provides practically absolute time (precision better than one microsecond).

6. Effects of System Size on Computational Effort

The traditional SE problem is based on a quasi-Newton algorithm. The direction of the Newton method is computed by inverting a matrix with size equal to the number of states. Sparsity techniques provide efficient algorithms for the solution and update for the state variables at each iteration. Numerical experiments for medium size power systems indicate that the computational effort depends on the system topology and is proportional to a factor of n.exp(a), where n is the number of states and a is an exponent that is system dependent (that is, it depends on the level of sparsity of the system model). If we assume that the exponent is approximately 1.7 then one can project the computational effort for mega systems, assuming that the observations for medium systems are valid for mega systems as well. The fear is that for mega systems, the sparsity properties of the equations may deteriorate (number of fill-ins may increase disproportionately with system size). The last issue not withstanding, a ten-fold increase in system size will result in a fifty-fold increase in computational effort. Another issue that we do not have data for is the number of iterations that the SE will need for convergence, in case of mega systems. All of this, point to the need for proper numerical experiments that will provide information for this topic.

The above discussion assumes that we simply apply the traditional SE to the mega systems. There are alternative approaches while we maintain the traditional SE formulation. For example, the system may be partitioned and diakoptical techniques could be applied for the solution. Computational issues and convergence issues will remain the same but this approach will allow scheduling the computations on a distributed computer system.

7. Proposed Direction to Meet the Challenges

To alleviate the sources of error, new measurement systems and estimation methods are needed. For example the first assumption can be met by utilizing synchronized phasor measurements [10,11]. Synchronization is achieved via a GPS (Global Positioning System) which provides the synchronizing signal with accuracy of 1 μsec. Assumption 2 can be met by utilizing three phase measurements. Finally assumption 3 can be met by employing full three phase models [6].

As shown from the numerical examples even by simple using three phase measurements of the power flows the improvement in the estimation quality is substantial, even though the model remained the same, and only the measurement set was improved, using data from all three phases. It is therefore expected that if, in addition to three phase measurement sets, synchronized measurements and three phase models are used, the performance of the state estimation algorithm will be very sufficient and reliable even for extremely large systems.

The state estimation based on the previous assumptions is not subject to the usual biases of the traditional state estimation. The state estimation can be formulated as a linear state estimation problem that has a direct solution. This take care of the uncertainty of how many iterations will be needed for convergence in case of mega systems. It is expected that this system, because of lack of biases will have better bad data detection and identification. It is important, however, to add that the proposed system will need a new infrastructure that presently is not there. It is recognized that the industry is moving towards the sensorless technology at least in new substations. The step to go from sensorless technology to synchronized measurements is economically very short. Thus we believe that it may happen in the near future.

It is important to recognize that quantification of the errors from the various sources of error in a control center environment with actual systems is very difficult due to the simultaneous presence of all errors. In addition other systematic errors may be present such as modeling errors, instrument calibration, etc. We propose a test-bed that is based on a high fidelity power system simulation tool. This tool is based on detailed representation of the system, for example all phase conductors, shield wires and grounding of transmission lines are explicitly modeled. The solution of this model represents a realistic operating condition of the system, including imbalances, asymmetries, etc. From this operating condition any measurement set can be generated with appropriately injecting measurement error. Single phase measurements, three phase (total) measurements, three-phase individual measurements, traditional set of measurements, phasor measurements, etc. can be generated or any combination of above list. The state estimation algorithm can be based on the three phase model or the positive sequence model, etc. In this way any possible approach to state estimation can be simulated and studied. By varying only one parameter in the scenario we can quantify the error from this parameter. The next sections present this approach. For flexibility the test-bed is based on a hybrid state estimation algorithm that permits the simulation of several approaches. The hybrid state estimator is described next. Typical numerical experiments with this test-bed are discussed later in the report.

8. Hybrid State Estimation

The proposed test-bed is based on a flexible hybrid SE formulation. This is a combination of the traditional state estimation formulation and the GPS-synchronized measurement formulation, which uses an augmented set of available data. This set comprises of (a) traditional, non-synchronized measurements (voltage magnitude, active and reactive line flows and bus injections, and other standard SCADA data) and (b) GPS-synchronized measurements of voltage and current phasors for each phase. Additionally, the hybrid state estimator can use a full three-phase system model or a positive sequence model of the system. The measurement set may include any combination of three phase measurements and single phase measurements. Typical measurements are illustrated in Fig. 18 and Table 1.

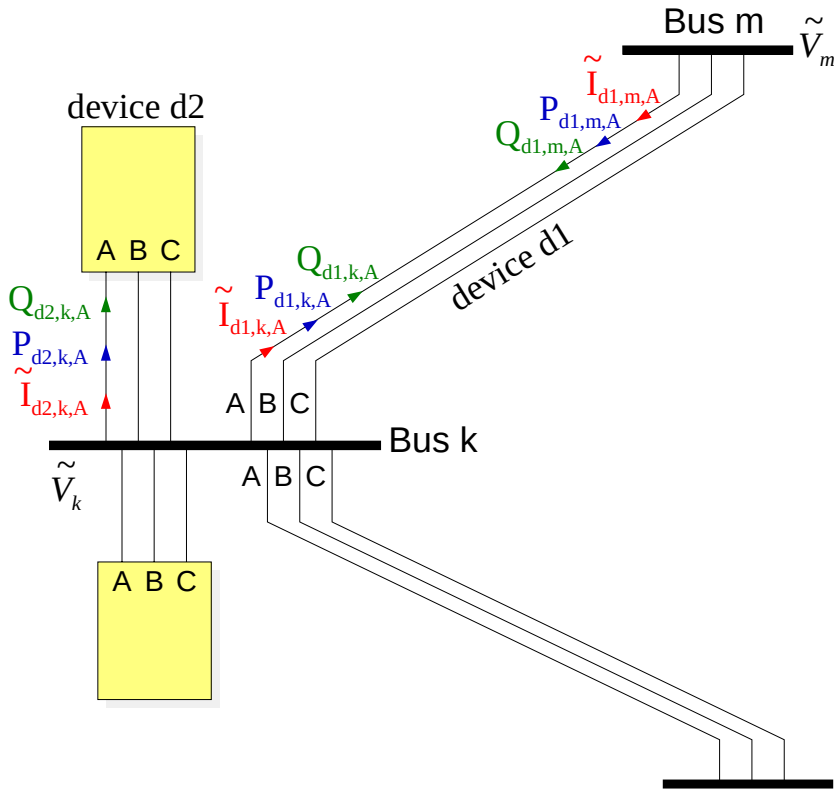

Figure 18 Measurement definition for hybrid QPF-SE approach – three phase model.

The state of the system is defined as the phasors of the phase voltages at each phase of a bus, including the neutral node. A bus k may have three to five nodes, phases A, B and C, possibly a neutral (N) and possibly a ground node (G). The state of the system at this bus is the node voltage phasors. The system model is a three phase model with explicit representation of the neutral nodes and ground nodes if present. A typical representation of a transmission line is shown in Fig. 19. For a four node bus, we use the symbols A, B, and C for the phase nodes and N for the neutral node. The states are defined as:

$$\begin{aligned}\tilde{V}_{k,A} &= V_{k,A,r} + jV_{k,A,i}\\ \tilde{V}_{k,B} &= V_{k,B,r} + jV_{k,B,i}\\ \tilde{V}_{k,C} &= V_{k,C,r} + jV_{k,C,i}\\ \tilde{V}_{k,N} &= V_{k,N,r} + jV_{k,N,i}\end{aligned} \tag{16}$$

In compact form, the state for a four node bus k will be:

$$\tilde{V}_k = \begin{bmatrix}\tilde{V}_{k,A}\\ \tilde{V}_{k,B}\\ \tilde{V}_{k,C}\\ \tilde{V}_{k,N}\end{bmatrix} = \begin{bmatrix}V_{k,A,r} + jV_{k,A,i}\\ V_{k,B,r} + jV_{k,B,i}\\ V_{k,C,r} + jV_{k,C,i}\\ V_{k,N,r} + jV_{k,N,i}\end{bmatrix} \tag{17}$$

The voltages of all buses of the system form the system state. We will refer to this as the system state x.

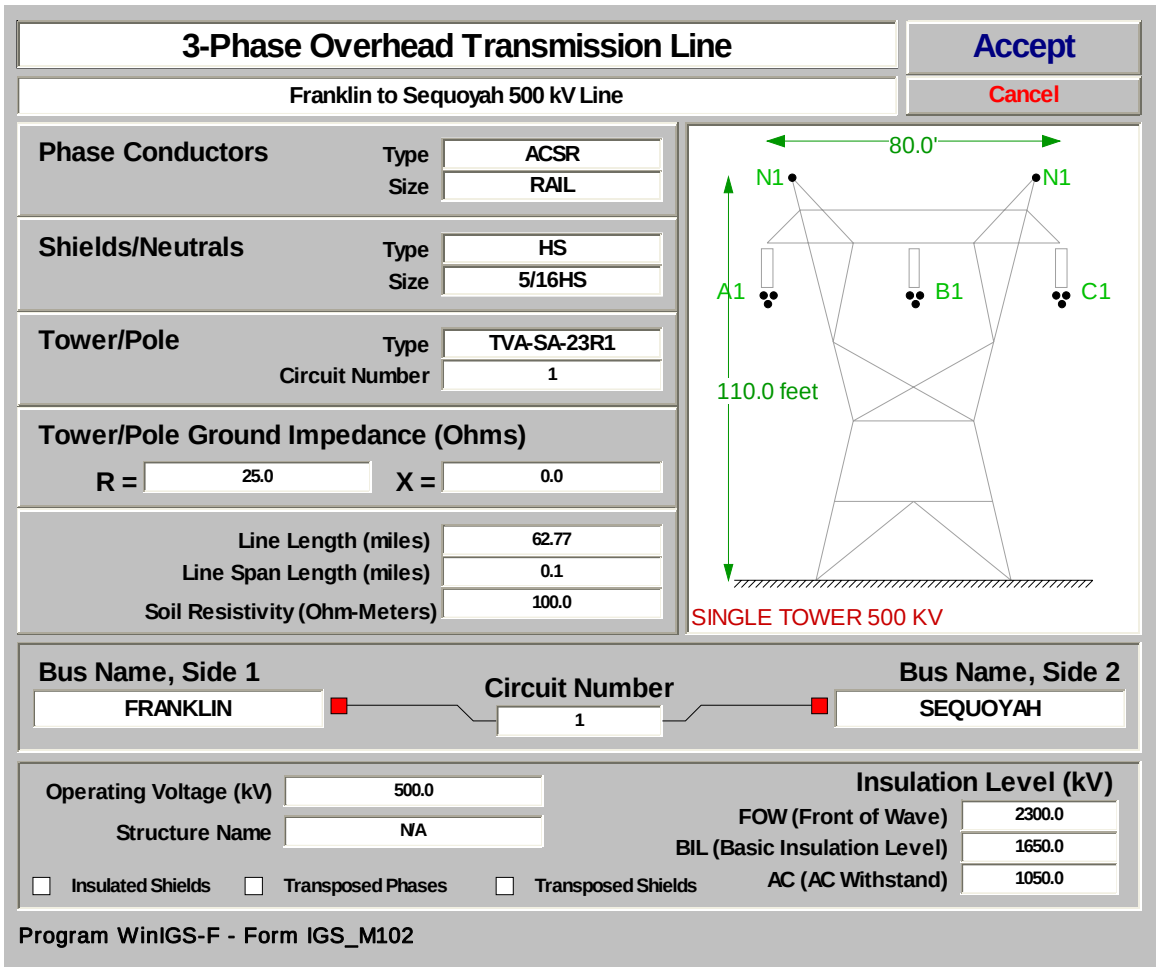

Figure 19 Physically-based, three-phase transmission line model.

Table 1 List of available data for hybrid QPF-SE approach.

GPS-Synchronized Measurements	
Description	**Type Code**
Voltage Phasor, $\tilde{V}$	1
Current Phasor, $\tilde{I}$	2
Current Injection Phasor, $\tilde{I}_{inj}$	3
Non-Synchronized Measurements	
Description	**Type Code**
Voltage Magnitude, V	4
Real Power Flow, P_f	5
Reactive Power Flow, Q_f	6
Real Power Injection, P_{inj}	7
Reactive Power Injection, Q_{inj}	8

The measurements are related to the state of the system via the "model" equations and they are assumed to have an error that is statistically described by the meter accuracy. It is also important to note that normally measurements of neutral or ground voltages are not available. On the other hand, these voltages are very small under normal operating conditions. For this reason, we introduce one pseudo-measurement of voltage phasor for each neutral and ground node in the system. The value of this measurement is exactly zero. The "meter accuracy" for this measurement is assumed to be low. Typically a value of 10% is used. The measurement model equations for phase A are given below. Similar equations are given for phases B and C.

Phasor measurements:

$$\tilde{z}_v = \tilde{V}_{k,A} - \tilde{V}_{k,N} + \tilde{\eta}_v \tag{18}$$

$$\tilde{z}_v = \tilde{I}_{d1,k,A} + \eta_v = C^T_{d1,k,A} \begin{bmatrix} \tilde{V}_{k,A} \\ \tilde{V}_{k,B} \\ \tilde{V}_{k,C} \\ \tilde{V}_{m,A} \\ \tilde{V}_{m,B} \\ \tilde{V}_{k,C} \end{bmatrix} + \tilde{\eta}_v \tag{19}$$

Pseudo-measurements for neutrals and grounds:

$$\tilde{z}_v = 0 + j0 = \tilde{V}_{k,N} + \tilde{\eta}_v \tag{20}$$

Non-synchronized measurements:

$$z_\nu = \left|\tilde{V}_{k,A} - \tilde{V}_{k,N}\right|^2 + 2\eta_\nu = \\ = \left(V_{k,A,r} - V_{k,N,r}\right)^2 + \left(V_{k,A,i} - V_{k,N,i}\right)^2 + 2\eta_\nu \tag{21}$$

$$z_\nu = P_{d1,k,A} + \eta_\nu = \mathrm{Re}\left\{\tilde{V}_{k,A}\left(C^T_{d1,k,A}\begin{bmatrix}\tilde{V}_{k,A}\\ \tilde{V}_{k,B}\\ \tilde{V}_{k,C}\\ \tilde{V}_{m,A}\\ \tilde{V}_{m,B}\\ \tilde{V}_{k,C}\end{bmatrix}\right)^*\right\} + \eta_\nu \tag{22}$$

$$z_\nu = Q_{d1,k,A} + \eta_\nu = \mathrm{Im}\left\{\tilde{V}_{k,A}\left(C^T_{d1,k,A}\begin{bmatrix}\tilde{V}_{k,A}\\ \tilde{V}_{k,B}\\ \tilde{V}_{k,C}\\ \tilde{V}_{m,A}\\ \tilde{V}_{m,B}\\ \tilde{V}_{k,C}\end{bmatrix}\right)^*\right\} + \eta_\nu \tag{23}$$

The hybrid estimation process minimizes the following objective function which includes all the available measurement data:

$$Min \quad J = \sum_{\nu \in phasor} \frac{\tilde{\eta}^*_\nu \tilde{\eta}_\nu}{\sigma^2_\nu} + \sum_{\nu \in non-syn} \frac{\eta_\nu \eta_\nu}{\sigma^2_\nu} \tag{24}$$

It is noted that if all measurements are synchronized, the state estimation problem becomes linear and the solution is obtained directly. In the presence of non-synchronized measurements and in terms of the above formulation, the problem is quadratic, consistent with the quadratized power flow. Specifically, using the quadratic formulation, the measurements can be separated into phasor and non-synchronized measurements with the following form:

$$z_s = H_s x + \eta_s \tag{25}$$

$$z_n = H_n x + \left\{x^T Q_i x\right\} + \eta_n \tag{26}$$

In the above equations, the subscript s indicates phasor measurements while the subscript n indicates non-synchronized measurements. The best state estimate is given by:

Case 1: Phasor measurements only.

$$\hat{x} = \left(H_s^T W H_s\right)^{-1} H_s^T W z_s \tag{27}$$

Case 2: Phasor and non-synchronized measurements.

$$\hat{x}^{\nu+1} = \hat{x}^{\nu} + \left(H^T W H\right)^{-1} H^T W \begin{bmatrix} z_s - H_s \hat{x}^{\nu} \\ z_n - H_n \hat{x}^{\nu} - \left\{\hat{x}^{\nu T} Q_i \hat{x}^{\nu}\right\} \end{bmatrix} \tag{28}$$

where:

$$W = \begin{bmatrix} W_s & 0 \\ 0 & W_n \end{bmatrix} \text{ and } H = \begin{bmatrix} H_s \\ H_n + H_{qn} \end{bmatrix}.$$

9. Visualization and Animation

The data available from SCADA, GPS-synchronized measurements and state estimation results are overwhelming to system operators in the usual tabular reports of numerical values on a single line diagram. Recent efforts resulted in displaying power flow data in 2-D or 3-D visualizations of the data [12], [13]. Visualization methods are powerful in enhancing the comprehension of system operating conditions for users and system operators. It is important to use the same technology for the results of state estimators for the purpose of enhancing the information transfer. An effective visualization method will help users and system operators to identify problems with one glance at the displays. The types of information that is important are (but not limited to this list):

1. Are all measurements good? Are there any bad data?
2. Can I trust the computed real time model of the system?
3. What is the true operating condition of the system?

The answer to these questions can be quickly assessed with a number of displays. At the research level, we have generated a matrix of useful information. The selection matrix is shown in Figure 2. Note that the user may select from a variety of quantities included the measurements, estimated values, residuals or normalized residuals. The quantities may be voltage magnitudes at any phase (or neutral), real or reactive power flow at any phase as well as electric current magnitude or phase at any phase of the system. The user may select a single quantity or multiple quantities and generate a visualization of this information in a 3-D or 2-D display.

Figure 20 Illustration of the selection matrix for visualizations.

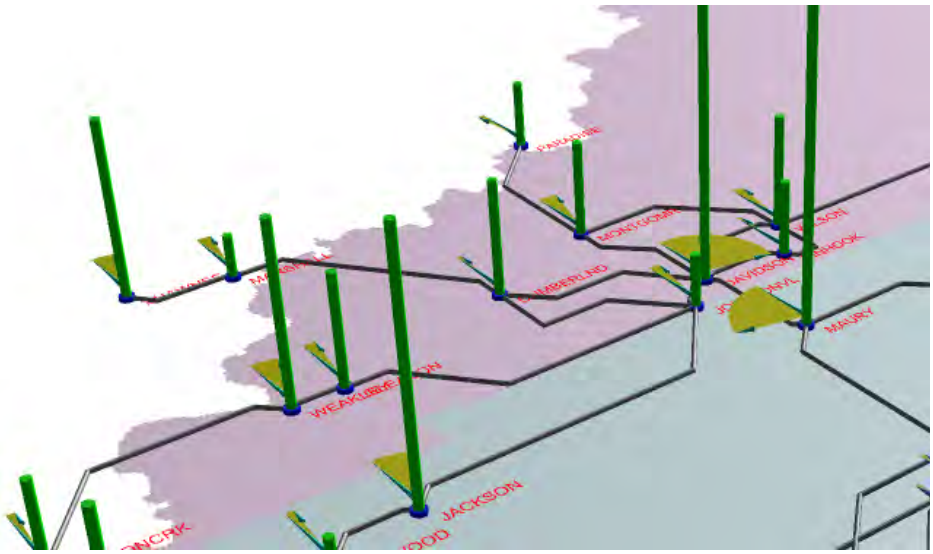

Figure 21 Example of visualization – Voltage magnitude (tubes) and phase (pies) errors.

10. Hybrid State Estimation Approach – Numerical Experiments

The proposed SE test-bed had been implemented and tested on the 500 kV TVA system shown in Fig. 22. The model includes the entire TVA 500 kV system and the transformers and autotransformers to the lower kV levels (mainly 161 kV and some 230 kV). The remaining system (beyond the secondary of the included transformers) is represented by equivalents. The system has 53 high voltage buses. The total number of nodes for this system is 1167 nodes. Visualization techniques are used in the implementation to facilitate the presentation and understanding of the results.

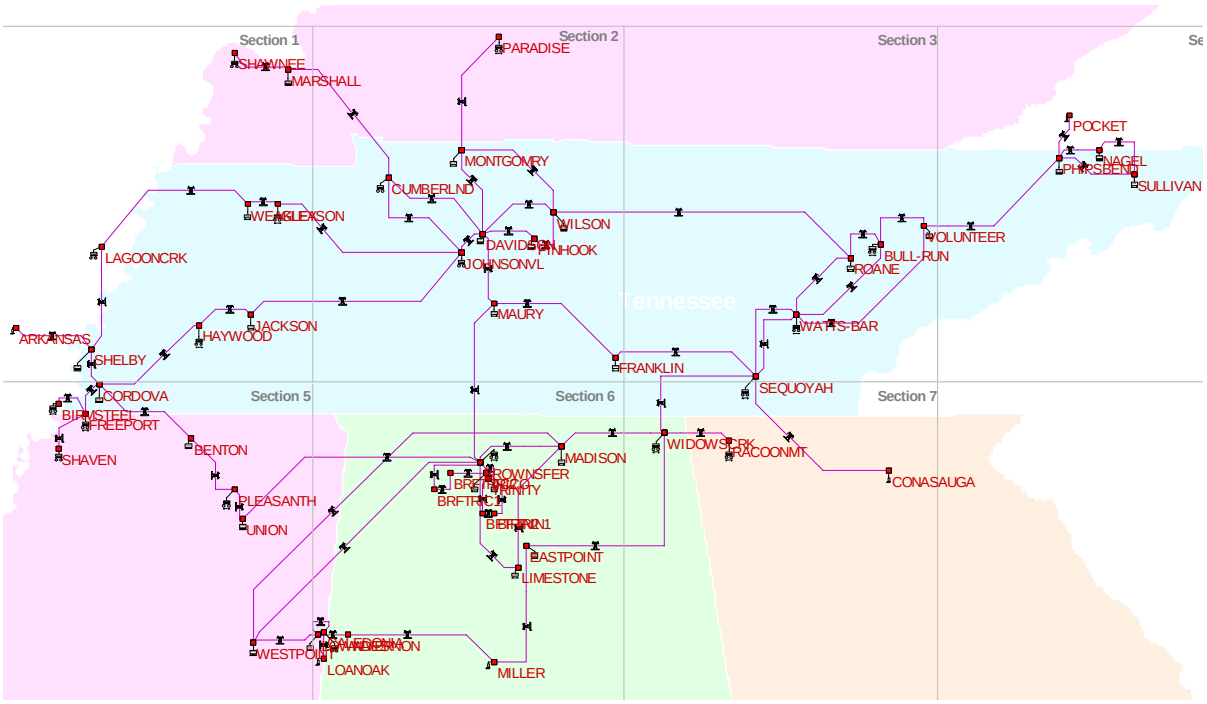

Figure 22 500 kV transmission system, TVA.

Several scenarios have been studied via numerical experiments. Here we present three simple scenarios:

Scenario 1: In this scenario it is assumed that the following measurements are available: (a) real and reactive power flow at the terminals of all circuits, all phases, and (b) voltage phasors of each phase at all buses.

Scenario 2: In this scenario it is assumed that the following measurements are available: (a) real and reactive power flow at the terminals of all circuits, phase A only, and (b) voltage phasors of phase A at all buses.

Scenario 3: In this scenario it is assumed that the measurement data are identical to those of scenario 1 except that a large error has been added to one datum (100 MW in one flow measurement).

The measurement data for the above scenarios were generated numerically using a load flow program and stored in data files. Random errors were added to the generated data to simulate typical measurement errors. The added errors were uniformly distributed with a specified range (for this data a standard deviation of 0.5% was used for flow measurements and 0.02 degrees for phase of synchronized measurements). Subsequently the estimator was executed with the numerically generated measurement data in order to evaluate its performance. In all tested scenarios the estimator converged within two to four iterations with excellent results.

Results of scenario 1 are illustrated in Figures 23, 24, and 25 in a visualization form. The visualization shows the phase residuals as pie-charts (magnified 100 times) and the voltage

magnitude residuals as tubes (magnified 10 times). Note that the errors are uniformly distributed and of very low magnitude for all phases A, B and C. The range of the errors is reported at the upper left corner of the display.

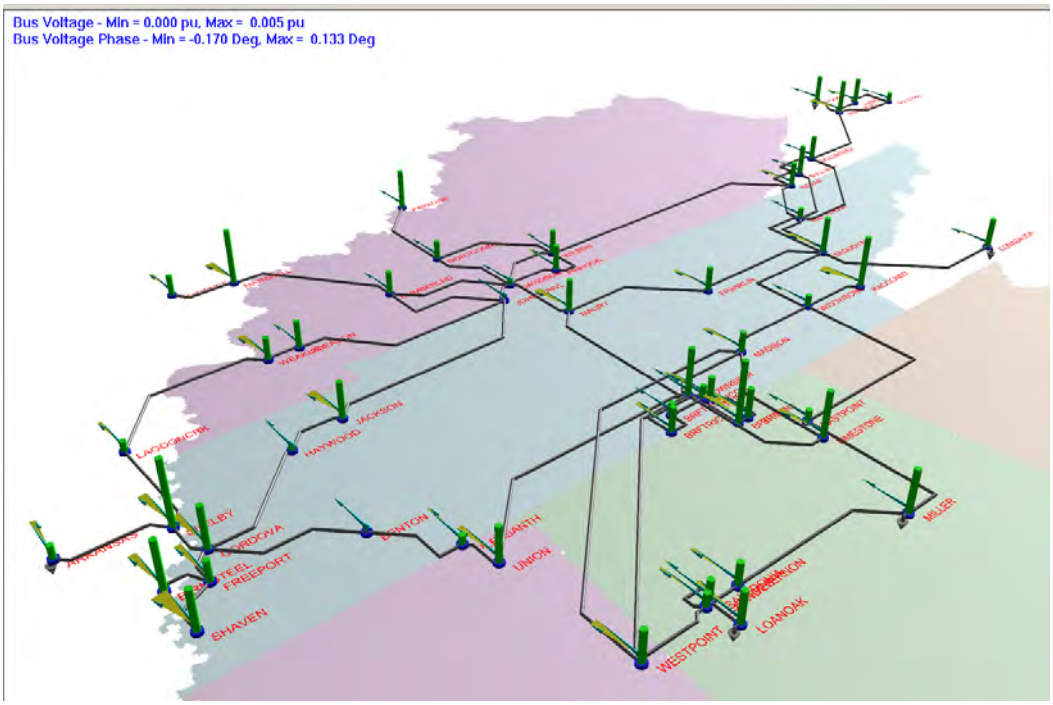

Figure 23 Residuals of bus voltage magnitude and phase – Scenario 1, Phase A.

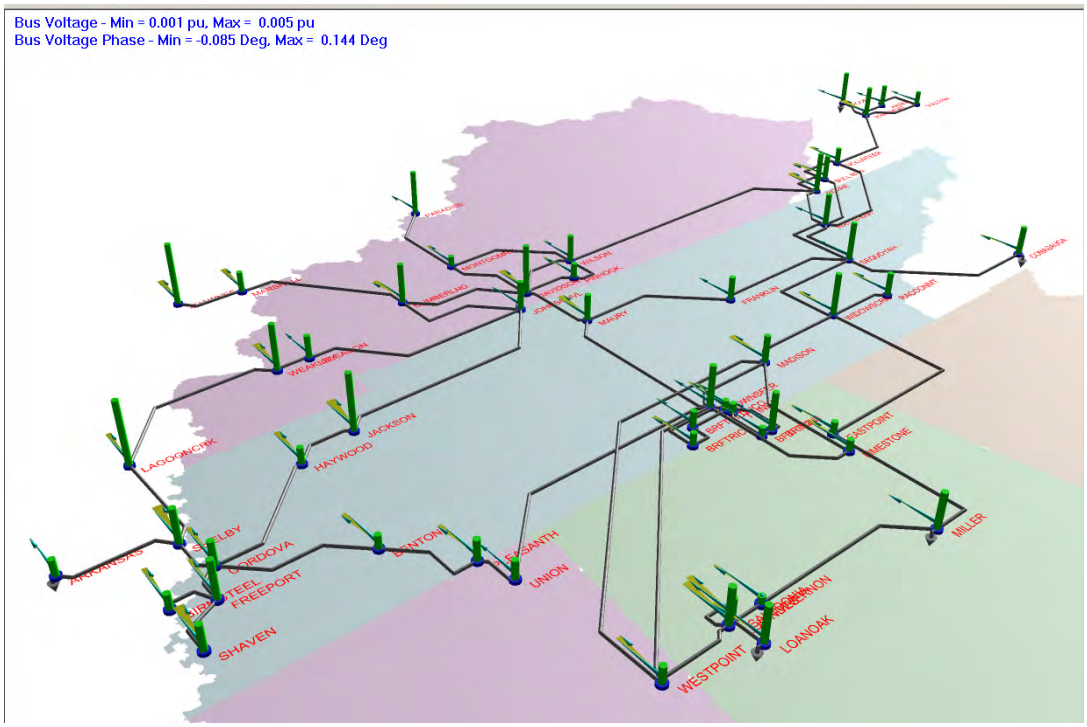

Figure 24 Residuals of bus voltage magnitude and phase – Scenario 1, Phase B.

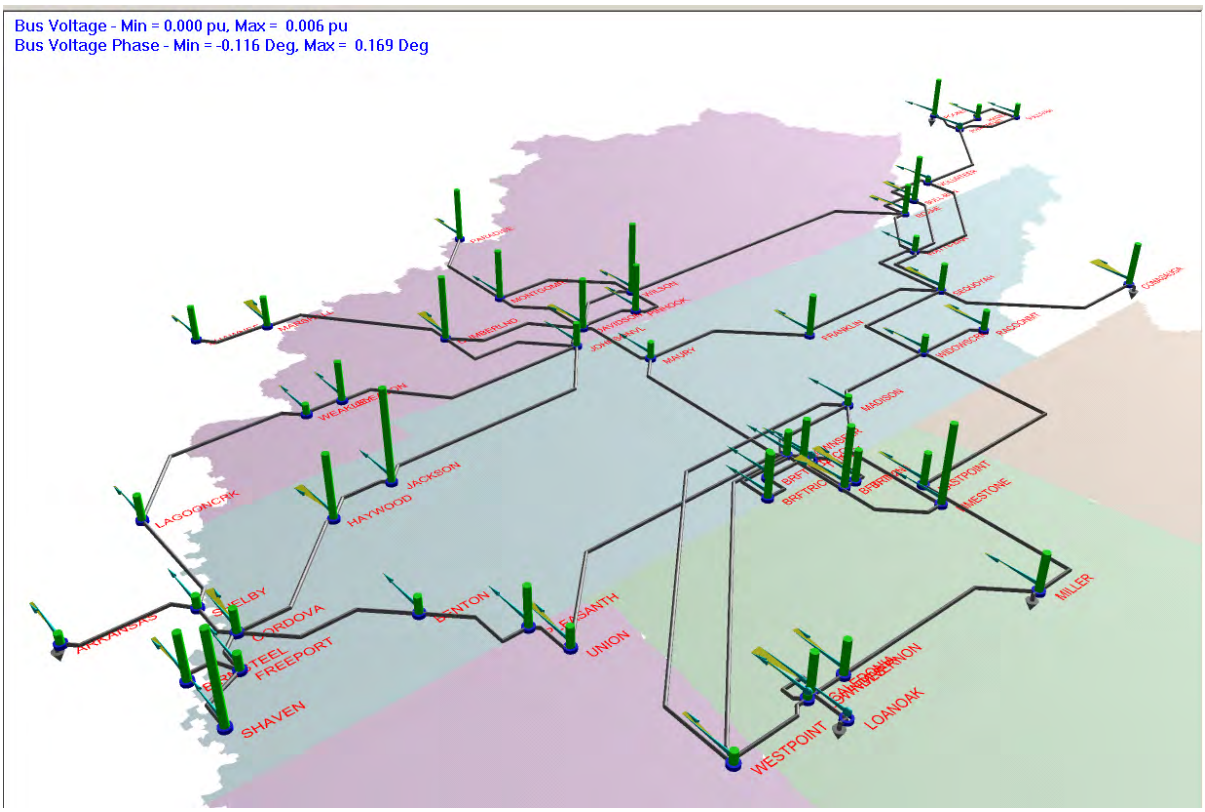

Figure 25 Residuals of bus voltage magnitude and phase – Scenario 1, Phase C.

The results of scenario 2 are illustrated in Figures 26 to 28. Note that the errors for phase A are uniformly distributed and of relatively low magnitude. The errors for phases B and C (Figures 27 and 28) are substantially greater. The source of these errors is the asymmetry of the system. It is important to point out that if the system was symmetric and balanced, there should not be any statistical difference in the residuals of phases A, B and C. Because of the imbalance and system asymmetries there is substantially greater (several times) residuals for the phases for which measurements are not available.

Figure 29 illustrates the estimation results for the same measurement data set, but with an arbitrary error of 100 MW introduced in the MW flow measurement of one circuit. The visualization display shows both magnitude and phase errors. Note that at one location of the network both magnitude and phase errors are much higher than anywhere else. These increased errors clearly identify the two ends of the circuit with the “bad data”. It is important to note that 100 MW for a 500 kV circuit is not a very large error. Yet the three phase state estimator with the visualization of Figure 29 clearly identifies the location of the bad datum.

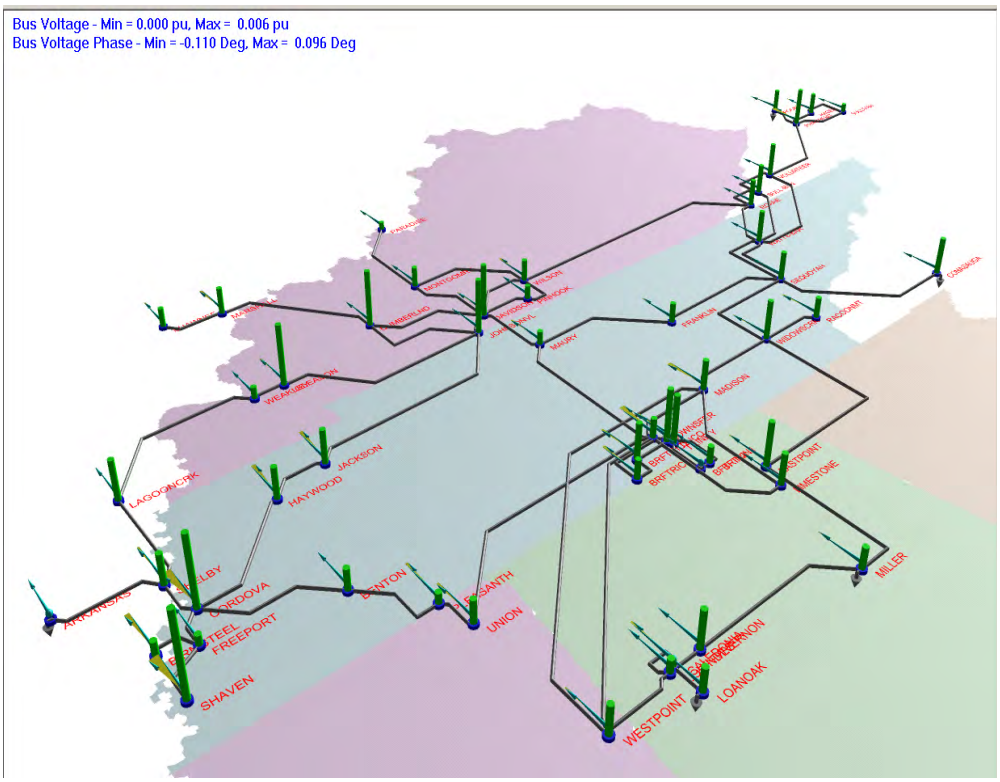

Figure 26 Residuals of bus voltage magnitude and phase – Scenario 2, Phase A.

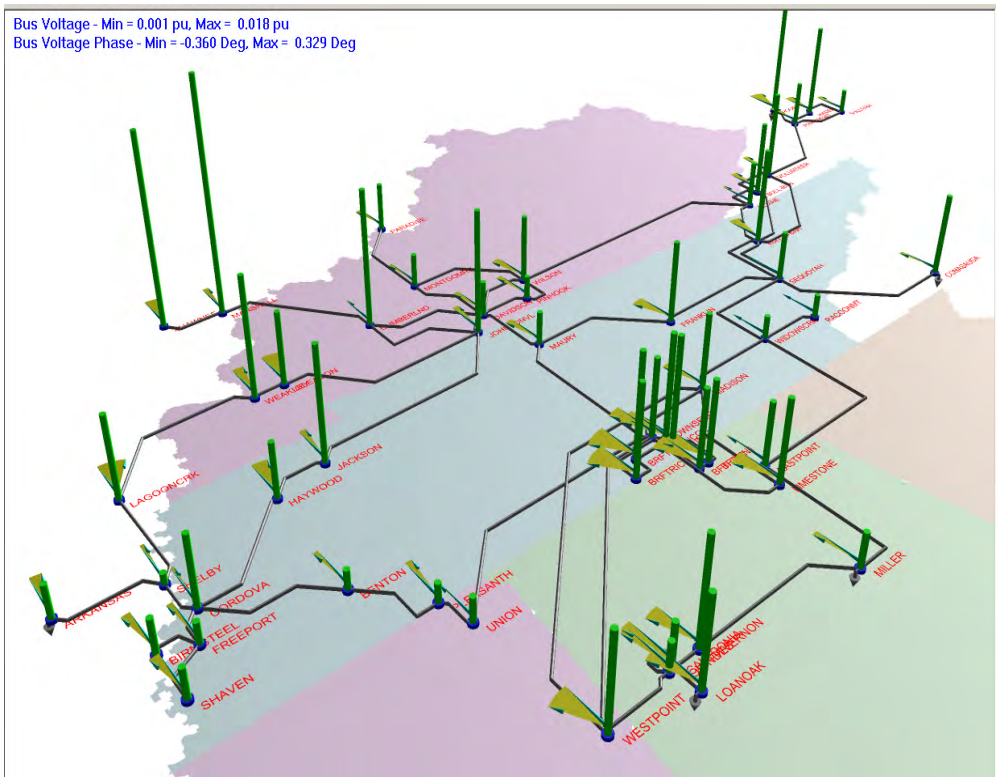

Figure 27 Residuals of bus voltage magnitude and phase – Scenario 2, Phase B.

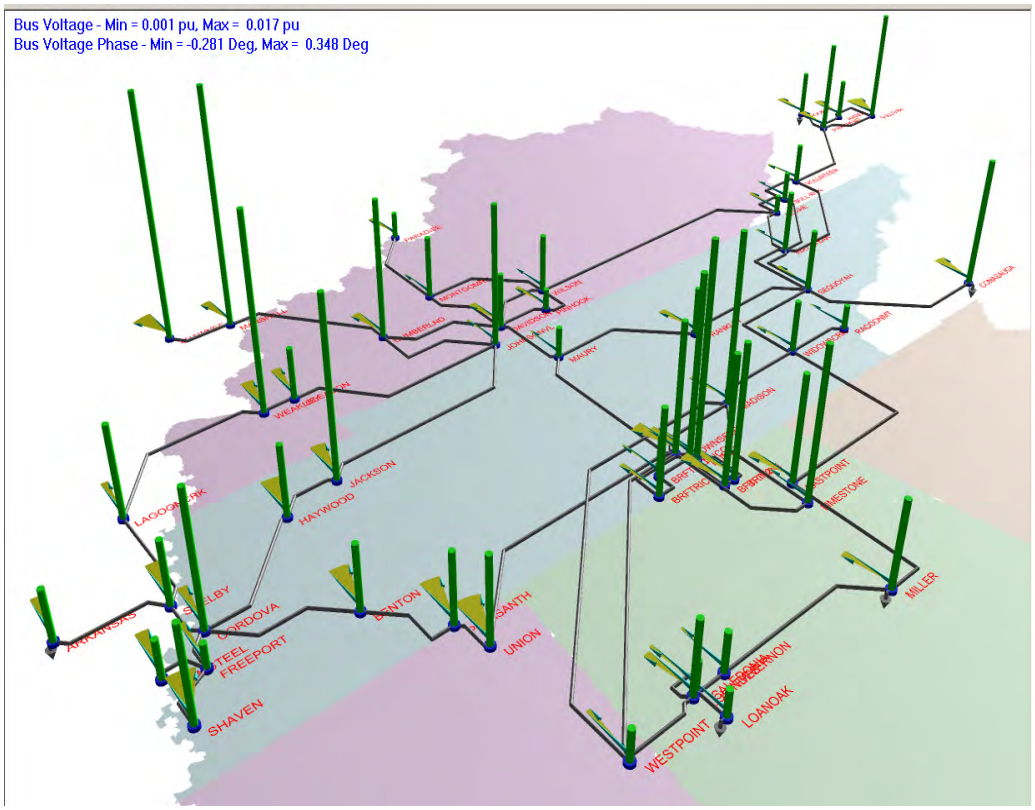

Figure 28 Residuals of bus voltage magnitude and phase – Scenario 2, Phase C.

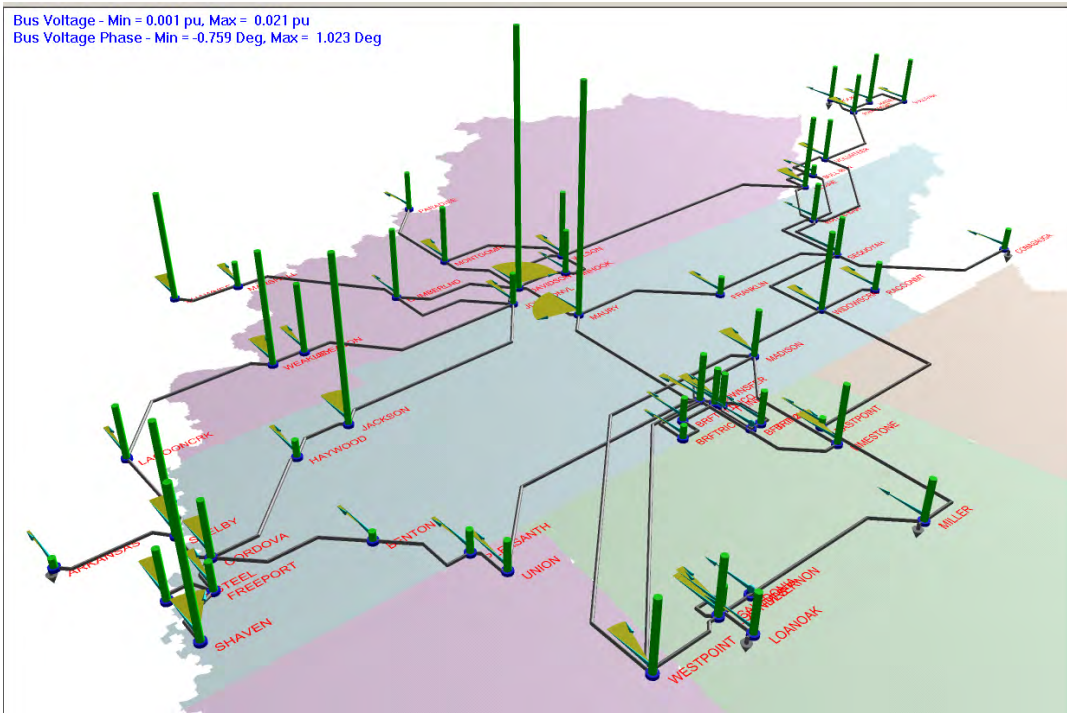

Figure 29 Residuals of bus voltage magnitude and phase – Scenario 3, Phase B.

11. Conclusions

The conventional State Estimation (SE) has inherent biases resulting from biases in the measurements and biases in the power system model (imbalance and asymmetry of component models). We presented a discussion of the various sources of errors. We have not included the errors resulting from human errors in calibrating instruments or human errors in setting up the system model. We propose a test-bed based on a flexible hybrid state estimator and a high fidelity three phase power system simulator. The test-bed allows numerical experiments that identify and quantify the errors from the various inherent sources of error.

Numerical examples have shown that just the use of segregated phase measurements of voltage and power flow (instead of total 3-phase flows) and a three phase model with the traditional state estimation approach results in substantial improvement in the estimate quality. Numerical experiments have also shown that additional GPS-synchronized measurements improve the performance of the state estimator. It is therefore expected that if, in addition to three phase measurement sets, synchronized measurements and full three-phase models are used, the performance of the state estimation algorithm will be sufficient and reliable even for extremely stressed large systems.

The state estimation based on these enhancements is not subject to the biases of the traditional state estimation. If all measurements are GPS-synchronized, the SE problem can be formulated as a linear state estimation problem that has a direct solution. This will be a great advantage especially for very large systems. It is expected that this system, because of lack of biases, will have better bad data detection and identification. It is important, however, to add that the proposed system will need a new infrastructure that is not presently available. However, the industry is moving towards this direction. Today, many meters and monitoring equipment are GPS-synchronized and it is a matter of time that all power system equipment will have this capability.

References

[1] Fred C. Schweppe and J. Wildes, "Power system static-state estimation, Part I, II, and III," *IEEE Transactions Power App. Syst.*, vol. PAS-89, No.1, pp.120-135, January 1970.

[2] A. P. Sakis Meliopoulos, Power System Grounding and Transients, Marcel Dekker Inc., 1988.

[3] A. P. Sakis Meliopoulos and A. D. Papalexopoulos, "Interpretation of Soil Resistivity Measurements: Experience with the Model SOMIP," *IEEE Transactions on Power Delivery*, vol. PWRD-1, no. 4, pp. 142-151, October 1986.

[4] A. P. Sakis Meliopoulos, G. C. Cokkinides, and R. P. Webb, "Multiphase Power Flow Analysis," *Proceedings of Southeastcon*, Destin, Florida, pp. 270-275, April 4-7, 1982.

[5] A. Semlyen and A. Deri, "Time Domain Modeling of Frequency Dependent Three-Phase Transmission Line Impedance," *IEEE Transactions on Power Apparatus and Systems*, Vol. PAS104, No. 6, pp.1549-1555, June 1985.

[6] A. P. Sakis Meliopoulos and Fan Zhang, "Multiphase Power Flow and State Estimation for Power Distribution Systems," *IEEE Transactions on Power Systems*, Vol. 11, No. 2, pp. 939-946, May 1996.

[7] A. P. Meliopoulos, F. Zhang, S. Zelingher, G. Stillmam, G. J. Cokkinides, L. Coffeen, R. Burnett, J. McBride, "Transmission Level Instrument Transformers and Transient Event Recorders Characterization for Harmonic Measurements," *IEEE Transactions on Power Delivery*, Vol. 8, No. 3, pp 1507-1517, July 1993.

[8] A. Arifian, M. Ibrahim, S. Meliopoulos, and S. Zelingher, "Optic Technology Monitors HV Bus", *Transmission and Distribution*, Vol. 49, No. 5, pp. 62-68, May 1997.

[9] K. A. Clements, O. J. Denison, and R. J. Ringlee, "The Effects of Measurement Non-Simultaneity, Bias, and Parameter Uncertainty on Power System State Estimation," *1973 PICA Conference Proceedings*, pp. 327-331, June 1973.

[10] A. P. Sakis Meliopoulos, F. Zhang, and S. Zelingher, "Hardware and Software Requirements for a Transmission System Harmonic Measurement System," *Proceedings of the Fifth International Conference on Harmonics in Power Systems (ICHPS V)*, pp. 330-338, Atlanta, GA. September 1992.

[11] A. G. Phadke, J. S. Thorp and K. J. Karimi, "State estimation with phasor measurements," *IEEE Transactions on Power Systems*, Vol. PWRS-1, No.1, pp. 233-241, February 1986.

[12] T. J. Overbye, D. A. Wiegmann, A. M. Rich, Y. Sun, "Human factors aspects of power system voltage contour visualizations," *IEEE Trans. on Power Systems*, pp. 76-82, February 2003.

[13] A. P. Sakis Meliopoulos, George. J. Cokkinides and Thomas J. Overbye, "Component Monitoring and Dynamic Loading Visualization from Real Time Power Flow Model Data", *Proceedings of the 37st Annual Hawaii International Conference on System Sciences*, p. 58 (pp. 1-6), Big Island, Hawaii, January 5-8, 2004.

Project Publications

1. A. P. Sakis Meliopoulos, “State estimation for mega RTOs,” presented at the 2002 IEEE Power Engineering Society Winter Meeting, New York, NY, Jan. 27-31, 2002.

2. A. P. S. Meliopoulos and G. K. Stefopoulos, “Characterization of state estimation biases,” Proceedings of the 2004 International Conference on Probabilistic Methods Applied to Power Systems, pp. 600-607, Ames, IA, Sept. 12-16, 2004.

3. A. P. Sakis Meliopoulos, G. J. Cokkinides, Mike Ingram, Sandra Bell, and Sherica Matthews, “Visualization and animation of state estimation performance,” Proceedings of the 38th Annual Hawaii International Conference on System Sciences, Big Island, Hawaii, January 3-6, 2005.

4. A. P. Meliopoulos, G. J. Cokkinides and G. K. Stefopoulos, “Numerical experiments for three-phase state estimation performance and evaluation,” Proceedings of the 2005 PowerTech, pp. 601-607, St. Petersburgh, Russia, June 27-30, 2005.

5. A. P. Sakis Meliopoulos and G. K. Stefopoulos, “Characterization of state estimation biases,” Probability in the Engineering and Informational Sciences, Cambridge University Press, 20, 2006, pp. 157-174.